

UNCLASSIFIED

AD NUMBER
ADB004062
NEW LIMITATION CHANGE
TO Approved for public release, distribution unlimited
FROM Distribution authorized to U.S. Gov't. agencies only; Test and Evaluation; MAY 1975. Other requests shall be referred to Aeronautical Systems Div., Attn: ASD/YHT, Wright-Patterson AFB, OH 45433.
AUTHORITY
USAF Aeronautical Systems Div. ltr dtd 16 Aug 1977

THIS PAGE IS UNCLASSIFIED

AEDC-TR-75-57

AD B004085



**RESULTS OF 0.2-SCALE B-1 PRODUCTION INLET
DEVELOPMENT AND VERIFICATION TESTS AT
SUBSONIC AND SUPERSONIC MACH NUMBERS**

R. F. Lauer, Jr.
ARO, Inc.

PROPULSION WIND TUNNEL FACILITY
ARNOLD ENGINEERING DEVELOPMENT CENTER
AIR FORCE SYSTEMS COMMAND
ARNOLD AIR FORCE STATION, TENNESSEE 37389

May 1975

Final Report for Period July 8 - December 17, 1975

Distribution limited to U.S. Government agencies only; this report contains information on test and evaluation of military hardware; May 1975; other requests for this document must be referred to Aeronautical Systems Division (ASD/YHT), Wright-Patterson AFB, OH 45433.

Prepared for

AERONAUTICAL SYSTEMS DIVISION (ASD/YHT)
and

AIR FORCE FLIGHT DYNAMICS LABORATORY (AFFDL/FXM)
WRIGHT-PATTERSON AFB, OH 45433

DDC
RECEIVED
MAY 28 1975
D

NOTICES

When U. S. Government drawings specifications, or other data are used for any purpose other than a definitely related Government procurement operation, the Government thereby incurs no responsibility nor any obligation whatsoever, and the fact that the Government may have formulated, furnished, or in any way supplied the said drawings, specifications, or other data, is not to be regarded by implication or otherwise, or in any manner licensing the holder or any other person or corporation, or conveying any rights or permission to manufacture, use, or sell any patented invention that may in any way be related thereto.

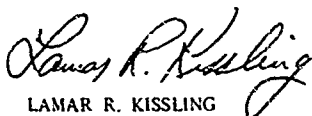
Qualified users may obtain copies of this report from the Defense Documentation Center.

References to named commercial products in this report are not to be considered in any sense as an endorsement of the product by the United States Air Force or the Government

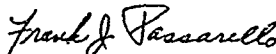
APPROVAL STATEMENT

This technical report has been reviewed and is approved for publication.

FOR THE COMMANDER



LAMAR R. KISSLING
Lt Colonel, USAF
Chief Air Force Test Director, PWT
Directorate of Test



FRANK J. PASSARELLO
Colonel, USAF
Director of Test

UNCLASSIFIED

REPORT DOCUMENTATION PAGE		READ INSTRUCTIONS BEFORE COMPLETING FORM
1. REPORT NUMBER AEDC-TR-75-57	2. GOVT ACCESSION NO.	3. RECIPIENT'S CATALOG NUMBER
4. TITLE (and Subtitle) RESULTS OF 0.2-SCALE B-1 PRODUCTION INLET DEVELOPMENT AND VERIFICATION TESTS AT SUBSONIC AND SUPERSONIC MACH NUMBERS		5. TYPE OF REPORT & PERIOD COVERED Final Report, July 8 - December 17, 1974
7. AUTHOR R. F. Lauer, Jr., ARO, Inc.		6. PERFORMING ORG. REPORT NUMBER
9. PERFORMING ORGANIZATION NAME AND ADDRESS Arnold Engineering Development Center (XO), Arnold Air Force Station, TN 37389		8. CONTRACT OR GRANT NUMBER(s)
11. CONTROLLING OFFICE NAME AND ADDRESS Aeronautical Systems Division (ASD/YHT) Wright-Patterson AFB, OH 45433		10. PROGRAM ELEMENT PROJECT TASK AREA & WORK UNIT NUMBERS 64215F-139A-01 63202F-668A-02
14. MONITORING AGENCY NAME & ADDRESS (if different from Controlling Office)		12. REPORT DATE May 1975
		13. NUMBER OF PAGES 148
		15. SECURITY CLASS (of this report) UNCLASSIFIED
		15a. DECLASSIFICATION/DOWNGRADING SCHEDULE N/A
16. DISTRIBUTION STATEMENT (of this Report) Distribution limited to U.S. Government agencies only; this report contains information on test and evaluation of military hardware; May 1975; other requests for this document must be referred to Aeronautical Systems Division (ASD/YHT), Wright-Patterson AFB, OH 45433.		
17. DISTRIBUTION STATEMENT (of the abstract entered in Block 20, if different from Report)		
18. SUPPLEMENTARY NOTES Available in DDC.		
19. KEY WORDS (Continue on reverse side if necessary and identify by block number) B-1 aircraft scale model jet engine inlets inlets wind tunnels distortion tests performance		
20. ABSTRACT (Continue on reverse side if necessary and identify by block number) Results are presented for a wind tunnel investigation of the 0.2-scale B-1 aircraft inlet/forebody model during which a pro- duction version of the inlet configuration was defined and the performance characteristics verified. The test was conducted at Mach numbers from 0 to 2.3, at angles of attack from -2 to 13 deg, and at yaw angles from -6 to 6 deg. Performance data are presented primarily in the form of engine-face total-pressure		

DDC
RECEIVED
MAY 28 1975
REGISTERED
D

UNCLASSIFIED

UNCLASSIFIED

20, Continued

recovery, turbulence index, and various distortion indices as a function of engine-face mass-flow ratio. For the development test phase, results are given that show the effects of reducing the inlet diffuser ramp length, varying the inlet cowl lip contours, changing the inlet bleed porosities, and reducing the inlet bleed discharge area. The performance characteristics of the selected inlet configuration are documented over the Mach number range with inlet geometry as controlled by the individual inlet control sensor schedules as well as by a free-stream Mach number schedule. The effects of control system errors and the aircraft takeoff inlet performance characteristics are also presented.

444
A-10-1000-1000

UNCLASSIFIED

PREFACE

The work reported herein was conducted by the Arnold Engineering Development Center (AEDC), Air Force Systems Command (AFSC), at the request of the Aeronautical Systems Division (ASD/YHT) and the Air Force Flight Dynamics Laboratory (AFFDL), under Program Elements 64215F and 63202F, Systems 139A and 668A, respectively. The test results presented were obtained by ARO, Inc. (a subsidiary of Sverdrup & Parcel and Associates, Inc.), contract operator of AEDC, AFSC, Arnold Air Force Station, Tennessee. The work was done under ARO Project Nos. P41T-63A and -95A, and the data reduction was completed on January 15, 1975. The manuscript (ARO Control No. ARO-PWT-TR-75-30) was submitted for publication on March 12, 1975.

CONTENTS

	<u>Page</u>
1.0 INTRODUCTION	7
2.0 APPARATUS	
2.1 Test Facilities	8
2.2 Test Article	8
2.3 Instrumentation	10
3.0 PROCEDURES	
3.1 Test Operating Procedure	11
3.2 Precision of Measurement	12
4.0 RESULTS AND DISCUSSION	
4.1 Production Configuration Development	12
4.2 Inlet Control Schedules	16
4.3 Proposed Production Inlet Performance	18
4.4 Transonic Inlet Drag Characteristics	23
5.0 CONCLUSIONS	23
REFERENCES	25

ILLUSTRATIONS

Figure

1. Sketches of Model Installation	27
2. Installation Photographs	28
3. Inlet Geometry	31
4. Duct Area Distribution	33
5. Inlet Boundary-Layer Bleed Porosity Configuration	34
6. Production Configuration Bleed Zone Discharge Doors	35
7. Cowling Lip Contours	36
8. Crosswind Generator Installation	37
9. Bypass Door Schematic	38
10. EVS Pod Installation	39
11. MA/ML Probe Calibration Plate	40
12. Instrumentation Locations	41
13. Variation of Corrected Engine Airflow with Free-Stream Mach Number	45
14. Inlet Performance Effects of Shortened Inlet Fourth Ramp at $M_0 = 2.20$	46

Figure	Page
15. Effects of Shortened Inlet Fourth Ramp on Engine-Face Total Pressure Contours	53
16. Effects of Bleed Porosity Configurations on Inlet at $M_0 = 2.20$	56
17. Effects of Cowl Lip Contours on Inlet Performance at $M_0 = 2.20$	59
18. Effects of Reduced BLCI and II Discharge Areas on Inlet Performance at $M_0 = 2.20$	62
19. Effects of Reduced BLCI and II Discharge Areas on the BLCI and II Plenum Pressures	66
20. Effects of Reduced Fourth Ramp Length on Inlet Performance at $M_0 = 0$	67
21. Effects of Crosswind on Inlet Performance at Takeoff Conditions	69
22. MA/ML Local Mach Number Data Matrix	70
23. 0.2-Scale/Full-Scale Local Mach Sensor Correlation	76
24. Full-Scale AICS Schedules	79
25. Effects of Airflow on Sensed Local Mach Numbers at $M_0 = 1.40$, $\psi = 0$	82
26. Inlet Performance Effects of Extreme Ramp Geometry	83
27. Bypass Door Effectiveness at $\alpha = 2.7^\circ$ deg, $\psi = 0$	89
28. Effects of Airflow Variations on Inlet Performance with Inlet Operated under Simulated AICS Control, $\psi = 0$	93
29. Effects of Airflow Variations on Inlet Performance with Inlet Operated under Simulated AICS Control, $\alpha = 2.5^\circ$ deg	97
30. Inlet Performance Characteristics with Inlet Operated under Simulated AICS Control and at Engine Intermediate Airflows	101
31. Effects of Mispositioned Inlet Geometry on Inlet Performance at $M_0 = 2.2$	105
32. Inlet Performance Characteristics with MG Scheduled Geometry at $M_0 = 2.2$	111
33. Transonic Inlet Performance Characteristics at $\psi = 0$	115
34. Transonic Inlet Performance Characteristics at $\alpha = 3.0^\circ$ deg	119
35. Effects of Opened Weapons Bay Doors and EVS Pods at $M_0 = 0.85$	123
36. Effects of Cruise and Takeoff Cowl Lip Positions on Subsonic Inlet Performance	129
37. Subsonic Inlet Performance Characteristics as a Function of Mach Number	133

<u>Figure</u>	<u>Page</u>
38. Simulated Takeoff Transient	135
39. Inlet Spillage Drag Characteristics	136
40. Effects of Opened BLCII Discharge Doors on Inlet Drag Characteristics at $M_0 = 1.40$, $\alpha = 2.5$ deg	139

TABLE

1. Precision of Measurement	140
---------------------------------------	-----

APPENDIXES

A. EQUATIONS FOR CALCULATING DISTORTION PARAMETERS: IDC, IDR, AND IDL	141
B. METHOD OF CALCULATION FOR INLET SPILLAGE AND BLEED DRAG TERMS	143
NOMENCLATURE	145

1.0 INTRODUCTION

At the request of the Aeronautical Systems Division (ASD), Air Force Systems Command (AFSC), a series of inlet development and verification tests was performed in the 16-ft Propulsion Wind Tunnels (16T, Transonic, and 16S, Supersonic) for the Rockwell International Corporation (RI) on a 0.2-scale model representing the forebody and left-hand nacelle of the B-1 Air Vehicle (A/V). The primary objective of the first test series, in Tunnel 16S, was to develop an inlet configuration for the production B-1 A/V that would maintain the performance and stability characteristics of the prototype configuration as reported in Ref. 1 but would be lighter in weight and have reduced drag. The second test series was devoted to verifying and documenting the inlet performance and stability characteristics of the production inlet configuration that resulted from the first test series.

Data were obtained at Mach numbers from 0 to 1.5 in the 16T tests and at $M_0 = 0$ and from 1.8 to 2.3 in the 16S tests. Typical data obtained during the developmental test phase are presented herein showing the effects of shortening the inlet fourth ramp, changing the inlet bleed porosities, altering the cowl lip contours, and reducing the BLC bleed exit areas. From the production inlet verification test phase, results are presented which show the inlet control system schedules, the scheduled inlet performance characteristics, off-schedule performance characteristics, interference effects of opened weapons bay doors and electro-optical visual systems (EVS) pods, and the takeoff inlet performance characteristics. Representative data are generally presented in the form of engine-face total-pressure recovery, various total-pressure distortion indices, and turbulence index as a function of engine-face mass-flow ratio, corrected airflow rate, or other applicable parameters.

In addition to the tests described above, a test was conducted in Tunnel 16T at the request of the Air Force Flight Dynamics Laboratory (AFFDL), AFSC, using the same model as above configured to represent the prototype B-1 A/V. Pressure data were obtained at Mach numbers from 0.70 to 1.40 to determine the inlet drag characteristics of the 0.2-scale model inlet system. The primary objective of this test was to obtain data that will later be compared with flight test data and used to develop wind tunnel/flight test correlations in the AFFDL Airframe Propulsion Subsystem Integration (APSI) program.

2.0 APPARATUS

2.1 TEST FACILITIES

Tunnels 16T and 16S are closed-circuit, continuous flow tunnels with Mach number capabilities from 0.2 to 1.6 and from 1.5 to 2.3, respectively. A complete description of the facilities, including operating characteristics, is presented in Ref. 2.

2.2 TEST ARTICLE

The test article was a 0.2-scale model of the Rockwell International Corporation B-1 Air Vehicle. The location of the model and support system is shown in Figs. 1a and b for Tunnels 16T and S, respectively. Photographs of the installations are given in Fig. 2.

The model simulated the A/V fuselage forebody with fixed-position structural mode control vanes, various sweep angle left-hand stub wings, and the dual inlet, left-hand engine nacelle. The nacelle external lines simulated the A/V lines, with minor exceptions, to within approximately 4 in. of the engine-face station. Both the inboard and outboard inlets simulated A/V internal surfaces to the engine-face station as described below.

The variable ramp system for both inlets consisted of a fixed ramp (RA) and three movable ramps (see Figs. 3a and b). The second ramp (RB) and the ramp train, consisting of the third and fourth ramps (RC and RD), were remotely controlled using servo loop hydraulic systems for each inlet. The first three ramps (RA, RB, and RC) simulated prototype A/V geometry, but the fourth ramp (RD) tested was 16 and then 32 in. (full-scale dimensions) shortened from the prototype configuration (Ref. 1). The effects of these fourth ramp changes on the diffuser duct area distribution may be seen in Fig. 4.

Boundary-layer control for both inlets was provided by porous surfaces on the third and fourth ramps and on the sideplates as shown in Fig. 5. The sideplate porosity was eliminated during the course of the test program (solid sideplates were used), and the ramp porosity was varied slightly (the 11-percent porosity areas were briefly changed to 12.5-percent porosities) but finally remained as shown. Bleed air from the third ramp and side plates went into the bleed zone I (BLCI) compartment. Initially the BLCI air discharged through fixed area doors with a total area of 1.92 in.² per inlet on the bottom of the nacelle; however, during the course of the program the discharge area was varied and the forward two doors eliminated so that the final model configuration had a total BLCI discharge area of 1.2 in.² per inlet (Fig. 6). Bleed air from the fourth ramp went into the bleed zone II (BLCII) compartment and discharged through the remotely operable BLCII doors (Fig. 6). The position (and consequently the discharge area) of these

four doors was varied from the simulated prototype value of 13 deg (3.36 in.² for the four doors) during the early test period. Later the fourth door was sealed and the door positions adjusted so that the final total exit area was 2 in.² with the doors in the open position.

During the first test period, the effects of cowl leading-edge contours were investigated. The cowl shapes tested are shown in Fig. 7. Also during that test period at $M_0 = 0$ and during portions of the Tunnel 16T testing, the simulated takeoff (T/O) cowl was installed on the model. The T/O cowl lip contours simulated that of the prototype A/V.

During the $M_0 = 0$ portion of the July 1974 test period, the effects of crosswinds 90 deg relative to the model centerline were determined. The crosswinds were simulated at velocities of 20, 30, and 40 knots by an AEDC-designed, fabricated, and calibrated crosswind generator which was supplied with high-pressure air at flow rates up to 40 lbs/sec. A photograph of the crosswind-generator/model installation may be seen in Fig. 8.

Inlet/engine airflow matching was provided for each inlet by means of a remotely variable bypass door controlled by a servo-loop hydraulic actuator. The difference between the bypass doors tested and the prototype configuration doors may be seen in Fig. 9. The bypass doors were closed and sealed for all testing except those where the effects of bypass flow were investigated and during the scheduled performance portions of the testing in the second 16S entry.

Both inlets had an environmental control system (ECS) air duct subinlet in the subsonic diffuser (Fig. 3a). Air from each subinlet was ducted to a flow-measuring section with one remotely variable plug valve used to simulate aircraft airflow demand from both inlets.

Simulated engine airflow was controlled with flow-throttling, remotely operable vanes located downstream of the engine-face station to provide a choke point at the vanes so that the acoustic properties of the engine could be approximated. Downstream of the vanes, a transition section with flow-straightening screens led to an ASME-type airflow-metering section. At $M_0 = 0$ testing in Tunnel 16S and during all 16T testing, the discharge of the airflow-metering duct was connected to a suction system to ensure choked flow at the vanes.

In Tunnel 16T, the effects of electro-optical visual system (EVS) pods (Fig. 10) and opened weapons bay doors were determined, and the left-hand stub wing was manually positioned at sweep angles of 15, 25, and 67.5 deg to ensure adequate simulation of the inlet flow field.

During a portion of the latter Tunnel 16S test period, a flat plate with full-scale and 0.2-scale local Mach number pitot-static probes was installed 27 in. above the tunnel floor (Fig. 11) for a 0.2-scale/full-scale probe calibration.

Additional test article details may be found in Refs. 3 and 4.

2.3 INSTRUMENTATION

Up to 379 steady-state pressure measurements were made on wing surfaces, internal and external cowl surfaces, internal and external bypass door surfaces and ramp surfaces, in boundary-layer bleed compartment plenums and metering sections, on upper and lower sideplate surfaces and flow-diverter surfaces, at the engine-face station, in the primary flow-metering ducts, and on the local Mach number calibration probes and plate. Unsteady-state pressure measurements were made on the wing, ramps, upper and lower side plates and cowl surfaces, in the boundary-layer bleed plenums, and at the engine-face station. (See Figs. 12a-d for pressure orifice locations.)

Engine-face steady- and unsteady-state pressures were measured with dual purpose probes. Each engine-face array consisted of 40 probes in eight 5-probe rakes, as may be seen in Fig. 12d.

Complete model instrumentation details may be found in Refs. 3 and 4.

All steady-state transducer outputs were sequentially input to an on-line computer system in which the data were reduced to engineering units. From the engineering unit data all desired weight flows, Mach numbers, engine-face total-pressure recovery and distortion parameters, and other requested parameters were computed and tabulated in the control room. Selected parameters were also plotted and displayed on a cathode-ray tube in the control room. The immediate availability of the tabulated and plotted data permitted continual on-line monitoring of the test results, which aided in the test direction, particularly in the early configuration development phase of the test. Facility instrumentation and data reduction capabilities are given in Ref. 2.

Outputs of the 65 unsteady-state pressure transducers per inlet were recorded by constant bandwidth, multiplexed FM recording systems on magnetic tapes. The signals from the 40 engine-face probes on each inlet were paralleled to rms-to-dc converters to obtain the rms magnitude of engine-face turbulence; the signals were also paralleled to the RI-furnished Analog Distortion Analyzer (ADA). The ADA calculated the various distortion parameters for both inlets in real time, digitally sampled the 40 engine-face pressures at each instant of successively higher peak distortion (engine fan stall margin ratio allowable for engine-face distortions, IDL—see Appendix A), and transferred the end results to the facility data acquisition system.

Model angle of attack was determined by means of a strain-gaged pendulum-type angle sensor. Model yaw angle and the positions of all remotely operable model component positions were sensed by potentiometers.

For the inlet drag portion of the testing in Tunnel 16T, 140 additional pressure orifices were installed on the inlet cowl external surfaces, outboard inlet ramp surfaces, and wing surfaces, at the outboard inlet cowl lip station (inlet total-pressure rakes), and at the outboard bypass door exit station (bypass discharge total-pressure rakes). A complete description of these additional instrumentation locations may be found in Ref. 4, Appendix A.

3.0 PROCEDURES

3.1 TEST OPERATING PROCEDURE

After the desired tunnel free-stream conditions had been established, the model was positioned to the desired pitch and yaw attitude. Model variables such as second ramp angle, inlet lip height, bypass door angle, BLCII door angle, mass flow control vane angle, etc., were systematically varied to study the desired effect. At most test conditions, steady-state data and 30 sec of unsteady-state data were obtained over a range of simulated engine airflow-rates. Airflow variations were obtained by positioning the flow control vanes from values causing supercritical inlet operation to those causing subcritical or inlet instability. Onset of inlet instability and/or inlet buzz was determined by observation of inlet duct and engine-face unsteady-state pressure transducer signals on oscilloscopes.

The flow-control vanes were normally operated under AEDC-designed automatic computer control, whereby the vanes were moved to set a specific requested engine-face corrected airflow rate. Real-time sampling of the flowmeter pressure transducer outputs and engine-face total-pressure recovery from the ADA permitted this mode of operation, which resulted in desired engine-face airflows being set more accurately and faster than could be accomplished by manual operation. The exception to this mode of operation was in definition of inlet instability, where manual vane control operation was employed.

During portions of the latter Tunnel 16S test program, simulated inlet/engine airflow matching was achieved by controlling the bypass door positions with an AEDC-developed analog system to maintain a specific duct control pressure ratio, the normal shock parameter (NSP). NSP is the ratio of a static pressure (orifice No. X703 located in each inlet throat on the upper sideplate at NS 16.98, NWL 5.2, Fig. 12b) to a total pressure (orifice No. X702 located in each inlet throat on the cowl surface at NS 19.00, NWL 1.28, Fig. 12a). Using NSP and a schedule of NSP versus MA or ML (see Section 4.2), the A/V Air Inlet Control System (AICS) causes the bypass door to open if a value of NSP is sensed that is greater than scheduled, and to close if NSP is less than scheduled. In addition, at some

supersonic A/V maneuvering attitudes or on cold-day operation where engine airflow demand would tend to cause supercritical inlet operation (low NSP value) even with the bypass door closed, the AICS sends a signal to the engine control causing a fan speed rollback (and reduction in airflow) to maintain inlet operation on the NSP schedule. The AEDC controller simulated the action of the AICS in controlling the bypass door position as a function of NSP. However, the fan speed rollback (airflow reduction) feature of the AICS was simulated by the operational procedures; as a condition was approached where the bypass door was closed and NSP was less than scheduled for a given airflow, the airflow was reduced until NSP was again on schedule.

3.2 PRECISION OF MEASUREMENT

Listed in Table 1 are estimates of the precisions of measurement for selected parameters. The uncertainties in these parameters include the inaccuracies in the tunnel reference systems, the recording systems, and the measuring devices themselves. The errors presented are combined errors (the square root of the sum of the squares of the individual errors) and were derived for a 95-percent confidence level using the Taylor series expansion method. Any errors contributed by the user-provided ADA are not included in these calculations.

4.0 RESULTS AND DISCUSSION

4.1 PRODUCTION CONFIGURATION DEVELOPMENT

The first test period was primarily devoted to developing a production A/V inlet configuration that would have lower weight and drag penalties while maintaining the performance characteristics of the prototype inlet reported in Ref. 1. The major investigation to effect a weight savings involved reducing the length of the fourth (diffuser) inlet ramp up to 32 in. (full-scale dimension), thus reducing the structural requirements for the ramps and actuators. Also, the length of the bypass door was reduced and the height increased, thereby reducing the moment arm of the aerodynamic loads on the door and hence allowing a lighter weight actuator. However, the bypass door changes were not critical to the inlet performance characteristics with the bypass doors sealed closed, and the revised bypass door effectiveness will be shown in Section 4.3. Drag reduction investigations involved reducing the boundary-layer bleed discharge areas and changing to a sharper cowl lip contour. Also investigated were the effects of eliminating the inlet side plates bleed and the possible inlet stability improvements that might be achieved by increasing the ramp bleed porosities or using a blunter cowl lip contour.

Data were obtained only at $M_0 = 2.2$ and at selected combinations of angles of attack and yaw where suspected effects would be most significant. All data presented

herein were obtained with the inlet ramps in the same MA/ML schedule positions as for the prototype testing (Ref. 1) and with the bypass door sealed so that effects are noted on a one-for-one basis. The performance data are presented in terms of engine-face total-pressure recovery (R_2), steady-state maximum-minus-minimum-over-average total-pressure distortion (D_2), the average engine-face root-mean-square value of total pressure fluctuations ratioed to engine-face total pressure (T_{I2}), the peak values of the circumferential (IDC_8) and radial (IDR_8) distortion indices, and the peak values of stall-margin ratio (IDL_8) as a function of engine-face mass-flow ratio (MFR_2). The value of IDL_8 is particularly critical to inlet/engine compatibility because it is the ratio of engine-face distortion-caused fan stall-margin deterioration to the maximum distortion-caused fan stall-margin deterioration allowable for stall-free engine operation. Thus, as IDL_8 exceeds 1.0 the probability of a distortion-induced engine stall increases beyond a value presumed to be tolerable. The peak distortion indices are those values recorded from the Analog Distortion Analyzer (ADA) within a 30-sec period at each data point and have been corrected for the zero shift of each of the dynamic transducers that was measured during the data point. (It should be noted that the constants used in the computations for the stall margin parameter, IDL , for this test series are as in Ref. 5, and have been changed since the Ref. 1 test phase; see Appendix A. All Ref. 1 data presented herein have been appropriately modified.) Noted on the plots are the values of engine airflow; a plot of the engine intermediate and idle power corrected airflow as a function of free-stream Mach number is presented in Fig. 13.

4.1.1 Effect of Reduced Fourth Ramp Length

At supersonic Mach numbers, the prime concern in reducing the fourth ramp length lay in the possibility of having separated flow in the subsonic diffuser because of the changed flow area distribution as seen in Fig. 4. The increased diffusion angle becomes more significant at the higher free-stream Mach numbers and attitudes where the value of HL and throat area is reduced. Inlet performance characteristics are presented in Figs. 14a through c at $M_0 = 2.20$ for configurations having fourth ramp lengths simulating the prototype A/V (data from Ref. 1) as well as two reduced length fourth ramps. At the worst cases of $\alpha = -2$ deg, $\psi = 0$ (Fig. 14a) and $\alpha = 9$ deg, $\psi = -3.0$ deg (Fig. 14c), where the respective inboard and outboard inlet HL values are reduced from the cruise attitude condition, there appears to be no significant difference in the inlet performance characteristics because of reduced diffuser ramp length. (The difference in supercritical mass-flow ratio noted in Fig. 14a for the inboard inlet is attributed to a difference in lip height, and therefore throat area, rather than to the diffuser ramp length.) Engine-face total-pressure contours obtained at the same conditions for the prototype and 32-in. shortened ramp and presented in Figs. 15a through c give no indications of separation. The slight difference in contours may be attributed as much to the differences in airflow as to the difference in configuration.

Because of these test results, the 32-in. shortened fourth ramp configuration was used for the remainder of the development testing and was selected for use in the production inlet.

4.1.2 Effects of Inlet Bleed Porosities

From previous tests of the prototype inlet configuration, pressure measurements on either side of the porous inlet sideplates indicated that there was minimal, if any, sideplate bleed flow. Therefore, the effects of solid (nonporous) sideplates on inlet performance were investigated. Also, in an effort to improve the inlet stability at some of the α/ψ attitudes where the inlet stability was marginal, the effect of increasing the 11-percent porous bleed area of the third (RC) and fourth (RD) ramps to 12.5-percent porosity was investigated. Typical inlet performance data are presented in Fig. 16a at the nominal cruise attitude and in Fig. 16b for the inboard inlet at $\alpha = 0$, $\psi = 3$ deg where the inboard inlet stability is marginal. It is readily seen that these bleed changes had no significant effect on the performance characteristics of either inlet. Similarly, no stability improvement (or loss) was obtained with any of the changes. Consequently, the solid sideplate and prototype RC and RD porosity configurations were maintained for the remainder of the development testing and were selected for the production A/V.

4.1.3 Effects of Cowl Lip Shape

The effects of the cowl lip contours on inlet performance are shown in Fig. 17a for both inlets at the $MO = 2.20$ cruise attitude and in Fig. 17b for the inboard inlet at $\alpha = 2.5$ deg, $\psi = 3.0$ deg, another attitude where inlet stability is marginal. The only significant performance difference between the three configurations is the reduced inboard inlet stability margin displayed by the sharp lip cowl configuration at the yawed attitude. The slight change in the stability point indicated in Fig. 17b is significant because of its proximity to the operating point; the change in stability noted in Fig. 17a for the outboard inlet is insignificant because of the adequate margin between the operating point and the instability point. (The difference in supersonic mass-flow ratio for the configurations is not deemed significant, as the data were computed using the referenced prototype capture area, and the cowl lip stagnation points for the other configurations were not precisely determined.) Because of the slight loss in stability attributable to the sharp lip cowl, and the lack of stability increase with the blunt lip cowl, the simulated prototype cowl lip was used for the further development testing.

4.1.4 Effects of Reduced Boundary-Layer Bleed Exit Area

Throughout the attitudes tested, there was no significant effect noticed on the inlet performance or stability characteristics because of reducing the bleed zone II discharge

area to 60 percent of the simulated prototype A/V or because of reducing the bleed zone I discharge area to 40 percent of the prototype. Typical data, obtained at the cruise attitude, are shown in Fig. 18a for zone II area variations with zone I at the simulated prototype A/V exit area, and in Fig. 18b for zone I variations with zone II at 60 percent of the simulated prototype valve.

For all subcritical inlet mass flow ratios, and most supersonic ratios, the bleed flows were choked at the discharge doors, never at the ramp surfaces. However, bleed flow rates were not reduced proportionally to the exit area reduction because of the increase in bleed plenum pressure as the exit area was reduced (see Fig. 19). Therefore, a slight drag reduction was obtained in that the total bleed door area (including forward-facing areas) was reduced, and the unit energy of the bleed discharge air was increased. As a result, bleed exit areas equal to about 60 percent of the prototype A/V were selected for the production A/V inlet.

4.1.5 $M_0 = 0$ Effects

During the development test period, the effects of the reduced length fourth ramps were determined also at $M_0 = 0$. This investigation was conducted because of the high distortion levels associated with the $M_0 = 0$ conditions as reported in Refs. 1 and 5; any increase in distortion at $M_0 = 0$ associated with the reduced length ramps would eliminate them as candidates for use in the production A/V inlet. The basic inlet performance characteristics are presented for the two shortened ramp configurations in Fig. 20, and the outboard inlet prototype configuration data from Ref. 1 are also presented. All data were obtained with the cowl lip in the takeoff position.

As is seen in Fig. 20, the inboard and outboard performance characteristics are very similar at the $M_0 = 0$ conditions, as would be expected. Also, there is no significant difference between the configurations. Considering the time-dependent nature and the inherent uncertainty associated with the peak distortion parameters, the variations between the IDL8 values for the different ramp configurations are not felt to be significant. This opinion is reinforced by consideration of the similarity of the steady-state distortion (D_2) values and the average root-mean-square (TI2) values of pressure fluctuations at the engine face.

The effects of sealing the gap between the cowl lip and sideplates when the cowl is in the takeoff position and the effect of opening the bleed zone II discharge doors were also investigated in this test phase. Summarizing the results of these investigations, it was seen that installing the cowl lip seals produced about a 1-percent increase in total-pressure recovery at the design engine airflow rate but had virtually no effect on the steady-state or peak distortion parameters. Opening the BLCII discharge doors appeared

to effect a marginal improvement in the peak distortion parameters, but insufficient data were obtained to be conclusive.

Because of the high distortion values attendant with the $MO = 0$ condition and the question of whether or not a crosswind would cause a further deterioration in inlet performance characteristics, the sensitivity of the inlet to crosswinds was investigated. Crosswind velocities were simulated up to 40 knots at 90 deg to the nacelle axis with the crosswind coming from the outboard side. The lack of sensitivity of both the outboard and inboard inlets to the simulated crosswinds is shown in Fig. 21 for the 32-in. shortened ramp configuration. Similar results were obtained for the 16-in. shortened ramp configuration.

4.2 INLET CONTROL SCHEDULES

The later test periods in Tunnels 16S and 16T were devoted to defining the performance characteristics of the selected production inlet configuration, but before this could be accomplished it was first necessary to prepare the inlet control schedules.

The logic used in the selection of the ML sensor (located on the bottom of the engine nacelle) for control of the inboard inlet and the MA sensor (located on the outboard inlet first ramp) for control of the outboard inlet is given in Ref. 1. Briefly, these control sensors were selected for the respective inlets as the single indicators that would allow development of ramp position schedules in which an acceptable compromise could be achieved between engine airflow demand and inlet local-flow conditions that resulted in stable inlet operation and satisfactory inlet performance characteristics throughout the A/V flight and maneuvering envelope. Selection of other possible sensors (e.g., MO , MA for the inboard inlet, and ML for the outboard inlet) would have restricted the A/V maneuvering envelope because of inlet instability (buzz) or extremely supercritical inlet operation and attendant excessive engine-face distortion levels.

The ML/MA data matrix obtained for the proposed production configuration is presented in Figs. 22a through f. It is quite apparent that the outboard inlet sensor, MA , is sensitive to yaw angle, but relatively insensitive to pitch angle. Conversely, the ML sensor is quite sensitive to angle of attack and less sensitive to yaw angle (except at yaw angles greater than ± 3 deg). This occurs because, at supersonic free-stream conditions, the Mach number over the lower fuselage decreases as angle of attack increases and the magnitude of the flow outwash angle increases with angle of attack. For a given angle of attack, the under-fuselage Mach number does not change greatly with yaw angle, but the flow outwash angle on the leeward side of the fuselage is proportional to the magnitude of the yaw angle. Thus, the measured ML value is fairly insensitive to yaw angle because

the probe is located in a position which makes it relatively insensitive to local flow angle. However, the measured MA value, being the outboard first ramp local Mach number, is quite sensitive to the local flow angle approaching the first ramp leading edge and the resultant expansion (or compression) around the leading edge. Consequently, the effect of reduced under-fuselage Mach number as a function of angle of attack is cancelled by the increased flow outwash and expansion around the first ramp leading edge. The consistency of these phenomena is not evident at the transonic free-stream conditions. As may be seen in Figs. 22c and f, ML and MA values near 1.0 are not stable and may present a problem which will be described below.

Presented in Figs. 23a to c are the 0.2-scale/full-scale local Mach sensor correlation data obtained during the parasite flat-plate test in Tunnel 16S. Presented are data for the ML and MA probes used in this test series (Figs. 23a and b) as well as the MA probe used for the test series reported in Ref. 1 (Fig. 23c). The data from that test were used to schedule the prototype A/V Air Inlet Control System (AICS). Using these correlation data and inlet ramp position schedules defined in Ref. 1 and previous tests, the schedules presented in Figs. 24a through c were constructed.

Concerning these schedules and the MA/ML data in Fig. 22, there are several points of special interest. As is seen in Fig. 24b, the AICS controls the lip height position for sensed local Mach numbers greater than approximately 0.85. As stated above, it is apparent that MA and ML are not stable near 1.0. Therefore, at the low supersonic free-stream Mach numbers, A/V pitch or yaw oscillations, or transients, could lead to abrupt movements or a slight instability in the positioning of the aft inlet ramp. As this discontinuity, or instability, may result only in an A/V HL movement up to $\pm 1/2$ in., it is not felt that this would significantly affect inlet performance (see Section 4.3.1).

Another peculiarity may be observed in Fig. 25 where the effect of engine, and therefore inlet, airflow on the measured local Mach numbers is shown. Data presented in Fig. 25 were obtained at $M_0 = 1.4$, but the effect of inlet airflow on the inlet static pressure field, and consequently on MA and ML, occurs at all lower free-stream Mach numbers. Because of these phenomena, it may be inferred that MA, and probably ML, are also functions of RB and HL, which affect the static pressure field. But once again, the instabilities that might be created by engine transients or ramp position changes would be small and not deleterious to the propulsion system performance. It also should be noted that any instability would to a large extent be dependent upon the gains and threshold error signals programmed into the AICS and are thus beyond the scope of this report.

In Fig. 24c, the decrease in the inboard inlet NSP schedule above $ML = 1.8$ should be noted. For a given flight condition, NSP is very sensitive to inlet flow and therefore

is an ideal parameter to use for inlet/engine airflow matching. Using this characteristic, the AICS controls the bypass doors in a closed-loop system as a function of NSP, as described in Section 3.1. For most conditions, an NSP value of about 0.68 to 0.72 yields high recovery, low distortion inlet characteristics. However, at some conditions (e.g., $M_0 = 2.2$, $\alpha = 0$, $\psi = 3$ deg), flow conditions and the scheduled inboard ramp positions are such that inlet instability occurs at values as low as 0.61. Therefore, the schedule must be reduced below that value to ensure stable operation for these conditions at some sacrifice in total-pressure recovery while maintaining inlet distortions less than the prescribed maximum allowable value of $IDL8 = 1.0$.

4.3 PROPOSED PRODUCTION INLET PERFORMANCE

After the inlet control schedules had been constructed, the inlet performance characteristics of the proposed production inlet configuration were verified and documented. Mach numbers of 2.2, 1.8, 1.4, 0.85, and the takeoff condition were of primary interest. Representative data and comments defining the effects of ramp positioning, bypass door effectiveness, scheduled inlet performance characteristics, interference effects of the weapons bay doors and EVS pods, and takeoff performance are given below.

4.3.1 Ramp Positioning Effects

At the nominal cruise attitude the effects of ramp positions are presented in Figs. 26a through c for $M_0 = 2.2$, 1.8, and 1.4, respectively. These data were obtained with the bypass doors sealed. At $M_0 = 2.2$ and 1.80 the desirability of the scheduled ramp position at the matched engine airflow is seen as the inlet is operating at about 95 percent of the supercritical mass-flow ratio with adequate inlet stability margin. In these cases, the matched airflow $IDL8$ value is below 1.0. At $M_0 = 1.40$ (Fig. 26c) it is seen that the effects of HL for values above 4.9 in. are negligible; however, at the lower HL values, the inlet becomes choked at the matched engine airflow point, and performance deteriorates.

In a failed geometry situation as is represented by the cases of $HL = 5.45$ in. or 2.95 in., engine operation and inlet stability become questionable at $M_0 = 2.20$ and 1.80. For the $HL = 5.45$ -in. case, at $M_0 = 2.20$, excessive distortion would preclude stall-free engine operation even if the bypass doors could pass enough airflow to maintain stable inlet operation. At $M_0 = 1.80$, stable inlet operation would be possible, but engine operation would be marginal as the $IDL8$ values at matched engine airflows are about 20 percent greater than allowable (1.0). At $M_0 = 1.40$ and below, the failed-open inlet presents no operational problems. As would be expected, an inlet failed at the minimum HL position presents the opposite problem; in this case $M_0 = 2.20$ would be

possible, but deceleration to lower Mach numbers would cause supercritical inlet operation until an engine stall occurred because of excessive distortion.

4.3.2 Bypass Door Effectiveness

The effect of the bypass doors on the control parameter, NSP, is seen in Figs. 27a and b for Mach numbers 2.20 and 1.80, respectively. These data were obtained at the scheduled ramp position and cruise attitude. Noted on the figures are the inlet stability limits, the excessive supercritical ($IDL8 > 1.0$) limits, and the engine intermediate and idle power airflow rates. The doors are capable of handling the equivalent of about 100 to 125 lb/sec of engine airflow at these supersonic speeds.

As the bypass doors are opened at a constant engine airflow, or as engine airflow is increased at a constant door angle, NSP decreases and the inlet tends to operate more supercritically. This process increases until $IDL8$ exceeds 1.0, at which point engine operation becomes marginal.

Of particular note in these figures is the uniformity of the inlet stability limit with NSP for all cases except the outboard inlet at $M0 = 2.20$. The apparent inconsistency in defining the $M0 = 2.20$ outboard inlet stability limit was also observed during the cold-pipe testing of the full-scale inlet/engine test reported in Ref. 5. In that test, and the test reported herein, there appeared to be some inlet/duct airflow resonance created at certain combinations of bypass door openings and simulated engine airflows. This is believed to be a function of the ramp oblique shock waves coalescing with the inlet normal shock inboard of the cowl lip buttock plane, the resultant shock strength (and consequently the NSP signal because of the location of the NSP total-pressure probe; see Section 3.1) thus being insensitive to small inlet airflow changes. The result of this phenomenon is a weak, localized instability.

4.3.3 MA/ML Scheduled Inlet Performance

The MA/ML scheduled inlet performance characteristics are presented for $M0 = 2.20$ and 1.80 as a function of corrected engine-face airflow rate in Fig. 28 for variations in angle of attack at $\psi = 0$ and in Fig. 29 for yaw variations at $\alpha = 2.5$ deg. These data were acquired with the bypass doors operating under automatic NSP control as given in the Fig. 24c schedule. Airflows that would have required NSP values less than the scheduled value (and thereby caused the bypass doors to be closed) were not obtained; similarly, stability limits were not defined. This mode of operation was followed to simulate the AICS/engine operation of the A/V as explained in Section 3.1.

There is one condition at which $IDL8$ exceeds a value of 1.0: $M0 = 1.80$, $\psi = -3.0$ deg, and the minimum airflow tested (Fig. 29b). However, since this airflow is less than the engine idle airflow, the high distortion level is of no consequence.

Data are presented in Fig. 30 which completely map the inlet operating characteristics over the $M_0 = 2.20$ and 1.80 maneuvering envelopes with simulated engine airflows representative of intermediate power settings having, if necessary, fan speeds rolled back as dictated by the AICS/NSP schedule. Satisfactory inlet performance characteristics are evident for both inlets at both Mach numbers for all attitudes presented. The only conditions where IDL8 is near 1.0 are at $M_0 = 2.20$ for the inboard inlet (Fig. 30a), where the ML values are in excess of 1.85 (see Fig. 22a) and NSP is reduced (Fig. 24c), thus forcing the inlet towards more supercritical operation.

4.3.4 Effects of Mis-Scheduled Ramp Positions

The effect on the inlet performance characteristics that would occur if the A/V AICS mispositioned the ramps enough to cause a 1-in. full-scale error in the value of HL was determined at $M_0 = 2.20$ for a few model attitudes. It is noteworthy that this much error can be caused by an MA or ML static-to-total pressure ratio error of only ± 0.011 at these flight conditions. Data are presented in Figs. 31a and b for two cases showing the effect of HL being too large, and in Fig. 31c for a case of HL being too small. These data for the scheduled and off-scheduled ramp positions were obtained with the bypass door sealed.

As is seen, the outboard inlet stability and performance characteristics are not severely affected for any of the three cases. However, the situation is different for the inboard inlet; in both situations where HL is greater than that scheduled, instability occurs at values of airflow greater than the engine demand. Although the instability could be eliminated by increasing inlet airflow by opening the bypass door, such action would also increase the peak stall margin ratio to a value greater than 1.0 . For the instance where the value of HL is less than scheduled, some gain in stability margin is achieved, but this is at the cost of a reduction in recovery, and an increase in IDL8.

Thus, it is seen that errors in the positioning of the ramps by the AICS or any other cause could result in rather serious inlet stability and performance problems, particularly for the inboard inlet.

4.3.5 M_0 Scheduled Inlet Performance

The data presented in Fig. 32 were obtained with the ramps positioned as a function of free-stream Mach number, i.e., the M_0 -scheduled positions. The values of RB and HL used for the M_0 schedule are the same as for the MA/ML schedule at the cruise attitude (i.e., $\alpha = 2.5$ deg, $\psi = 0$). They are not a function of the A/V attitude or inlet local Mach number; they are a function only of free-stream Mach number. All these data were obtained with the bypass sealed. The $\psi = 0$ data presented in Fig. 32a indicate that

satisfactory inlet performance and stability characteristics are obtainable for the outboard inlet; however, the inboard inlet is unstable at $\alpha = -2.0$ deg for the design engine airflow. Increasing the inboard inlet stability by opening the bypass doors would cause an increase in IDL8, which is already above the limit of 1.0. Hence, the minimum angle of attack at $M_0 = 2.2$ with this M_0 ramp schedule would be about zero. In the yaw data in Fig. 32b, a similar situation occurs for the outboard inlet at $\psi = -5.8$ deg and for the inboard inlet at $\psi = 3.2$ and 5.8 deg. Thus, it is readily seen that the A/V maneuvering envelope would be severely limited if M_0 inlet ramp scheduling was used.

4.3.6 Transonic Inlet Performance Characteristics

The inlet performance characteristics are presented as a function of mass-flow ratio for $M_0 = 1.4$ and 0.85 in Fig. 33 at $\psi = 0$ and various angles of attack, and in Fig. 34 for various yaw angles at $\alpha = 3.0$ deg. All these data were obtained with the ramps positioned as in the MA/ML schedule and with the bypass doors sealed. At and below the intermediate engine airflow operating points, the distortion values are well within the acceptable limits. Inlet stability is marginal at some of the near-idle airflow points for both Mach numbers. However, these instability points are only at maneuvering attitudes, and these maneuvering attitudes would not normally be attempted with an engine at reduced power or sub-idle. In addition, the bypass doors are presently scheduled to be active at the sensed local Mach numbers typical of the $M_0 = 1.4$ cruise conditions. This would eliminate any of the stability problems predicted by these data for the inboard inlet at $\alpha \leq 3.0$ deg and for the outboard inlet at $\psi \leq 0$ and $\alpha > 3$ deg.

Only minimal amounts of data were obtained on the M_0 ramp schedule in the Tunnel 16T tests. These data are not presented herein, but the inlet was shown to be insensitive to slight HL variations from the optimum which would result from an M_0 schedule at these Mach numbers in Section 4.3.1.

4.3.7 Interference Effects of the Weapons Bay Doors and EVS Pods

The inlet performance effects of opened mid and forward weapons bay doors and of the EVS pods were determined at $M_0 = 0.85$, $\alpha = 3$ deg, $\psi = -5$ to 5 deg. Data presented in Fig. 35 show that opened doors and installed EVS pods have no deleterious effect on the inlet performance characteristics. In fact, the inboard inlet peak stall margin ratio, IDL8, is improved with the opening of the doors or installation of the pods because of the reduction in the peak circumferential distortion parameter. This effect tends to be most significant at the negative yaw angles (nacelle leeward of the doors and pods) and is lessened at the positive yaw angles.

4.3.8 Subsonic and Takeoff Performance

The inlet performance characteristics for Mach numbers from 0 to 0.85 are presented as a function of engine-face airflow in Fig. 36a with the cowl lip in the cruise position and in Fig. 36b for the T/O cowl lip position. (The T/O cowl position is not realistic for $M_0 > 0.4$, as stated below, but the cowl could fail open, and therefore the data are presented herein.) These data have been crossplotted at the sea-level intermediate power airflow and are presented in Fig. 37 as a function of Mach number. It is evident that satisfactory inlet performance characteristics are obtainable at least up to $M_0 = 0.85$ with the cowl lip in the T/O position. Even though the T/O cowl lip position demonstrates superior engine-face total-pressure recovery and reduced distortion characteristics up to $M_0 = 0.8$, it also has higher drag penalties associated with it. Hence, determining the optimum Mach number at which to transition from the T/O to cruise cowl lip position is beyond the scope of this report. At present, however, the cowl lip positioning mechanism is linked to the A/V landing gear; i.e., if the landing gear is down, the cowl lip is in the T/O position, and if the gear is retracted, the cowl lip is in the cruise position. According to the peak fan stall margin ratio (IDL8) in Fig. 37, it appears landing gear retraction should be delayed until at least $M_0 = 0.30$ (approximately 200 knots on a standard day), presuming takeoff engine power setting will be intermediate or above. On landing approach, gear extension could take place at a lower Mach number if engine power and airflow are reduced.

During this test, as in the full-scale test (Ref. 5), data were obtained during a tunnel Mach number transient from $M_0 = 0$ to 0.20 with simulated engine airflow equivalent to the engine intermediate power setting. The instantaneous total-pressure recovery and distortion parameters as sensed and computed by the ADA are presented in Fig. 38 as a function of Mach number. Also shown in Fig. 38 are the loci of estimated peak fan stall margin ratio values based on the peak values obtained at $M_0 = 0$ and 0.20 steady-state conditions. (IDL8 values were not available from the ADA during these transients.)

As may be seen for both inlets, there is a decline in IDL which starts at about $M_0 = 0.04$ or 0.05 and is essentially complete by $M_0 = 0.10$ to 0.13. This is caused by a reduction of the radial distortion component, IDR; the change in the circumferential component, IDC, is not so definite. These data validate the questionable data obtained during the Mach number transients reported in Ref. 5. Therefore, it is evident that as the A/V approaches 80 knots (less than rotation velocity), inlet-created engine-face distortion will be reduced to the point where the probability of an engine stall because of distortion is minimal.

4.4 TRANSONIC INLET DRAG CHARACTERISTICS

The outboard inlet drag characteristics were determined over a small angle-of-attack range about the nominal cruise attitude. Typical data are presented in the form of spillage drag as a function of mass-flow ratio in Figs. 39a to c for $M_0 = 0.85$, 1.20, and 1.40, respectively. These data were obtained with the ECS closed, the bypass doors sealed, and the zone II BLC doors closed. The method of calculations for the inlet spillage drag term is given in Appendix B.

During the course of the test it became apparent that determination of inlet momentum by use of inlet total-pressure rakes and average static pressure would not yield valid answers, so the method of calculation was altered and the inlet momentum was determined by using the inlet airflows and the average inlet static pressure at the cowl lip plane.

The effects of opening the zone II BLC doors were determined at $M_0 = 1.40$, where the doors are nominally scheduled to be opened on the A/V. The bleed drag term is also defined in Appendix B and is the loss in momentum of the bleed airflow for both bleed zones from free-stream conditions to door exit stations, plus the pressure-drag term of the opened BLCII doors. Data are presented in Fig. 40 for the zone II doors opened and closed. With the BLCII doors closed, CDBLC is the bleed zone I drag, and with the doors open it is the BLCI plus BLCII drag. Observing the spillage drag term in Fig. 40, one notes that the increase in BLC drag with the BLCII doors open is offset by a decrease in spillage drag. At the highest mass-flow ratios the decrease in spillage drag is greater than the increase in BLC drag, but at the lower mass-flow ratios the reverse is true. At the matched airflow point, the increase in BLC drag appears to be slightly greater than the decrease in spillage drag, but not significantly so.

5.0 CONCLUSIONS

An investigation was conducted in tunnels 16T and 16S of the Propulsion Wind Tunnel Facility on the 0.2-scale B-1 forebody/inlet model to develop an inlet configuration for the production B-1 A/V and to verify and document the performance characteristics of that configuration.

From the results of the developmental phase of the test series, the following conclusions were reached:

1. Shortening the inlet fourth ramp by up to 32 in. full scale from the prototype configuration did not significantly affect the inlet performance or stability characteristics.

2. Eliminating the inlet sideplate boundary-layer bleed porous areas did not reduce the inlet stability margin nor affect the inlet performance characteristics.
3. Increasing the porosity of the third and fourth ramp boundary-layer bleed porous areas did not improve inlet stability nor affect the inlet performance characteristics.
4. Replacing the prototype cowl lip with one having more blunt contours did not improve the inlet stability or performance characteristics but could be expected to increase inlet drag.
5. Replacing the prototype cowl lip with a more sharp-lipped cowl caused a reduction in stability margin at model attitudes where stability was already marginal.
6. Reducing the boundary-layer bleed discharge areas to approximately 60 percent of the prototype configuration was accomplished at no loss to inlet stability or performance while effecting an inlet drag reduction.
7. At takeoff ($M_0 = 0$) conditions, the inlet performance characteristics were insensitive to crosswinds up to 40 knots velocity at 90 deg to the inlet.
8. At takeoff conditions, the use of seals to fill the gaps between the cowl lip in the takeoff position and the sideplates increased inlet total-pressure recovery by about 1 percent but did not affect the distortion parameters.
9. At takeoff conditions, opening the throat bleed discharge doors may effect a slight improvement in the inlet peak distortion parameters.

From the results obtained during the production inlet verification test phase, the following conclusions have been reached:

1. The outboard inlet control sensor is sensitive to yaw angles but relatively insensitive to angles of attack, while the reverse is true for the inboard inlet control sensor. ML.
2. Using the outboard and inboard inlet control sensor schedules presented herein, stable inlet operation with distortion parameters below the fan stall margin distortion limit were demonstrated for all conditions tested at representative engine airflows.

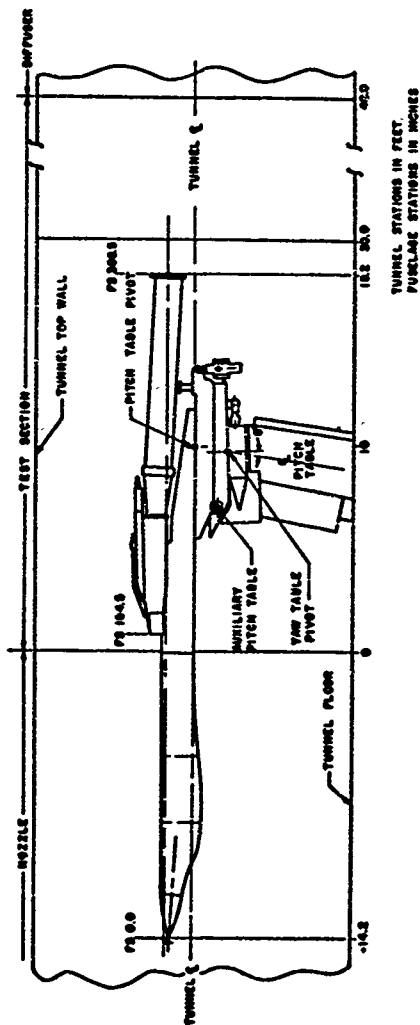
3. Above Mach number 1.8, with the inlet failed at maximum lip height position, inlet instability or excessive distortion will prevent stall-free engine operation. Conversely, with the inlet failed at minimum lip height, low supersonic and subsonic engine operation will be prevented by excessive engine-face distortion except at very low engine airflow rates.
4. Mis-positioning of the fourth ramp (i.e., lip height) up to 1 in. full scale will result in inboard inlet instability and/or excessive distortions at matched engine airflows for Mach number 2.20 maneuvering attitudes.
5. If free-stream Mach number rather than outboard and inboard inlet control sensors were used to control the inlet ramp positions, the air vehicle maneuvering envelope would be severely limited at the higher supersonic Mach numbers because of reduced inlet stability margin and/or excessive peak total-pressure distortion.
6. Neither the opened weapons bay doors nor the electro-optical visual system pods caused any significant effects on the inlet performance characteristics at the Mach number 0.85 condition tested.
7. Up to about Mach number 0.80, inlet total-pressure recovery is increased and distortion reduced with the cowl lip in the takeoff position. The cowl lip may be translated from the takeoff position to the cruise position and vice-versa at Mach numbers ≥ 0.3 with intermediate power engine airflow settings while maintaining the peak fan stall margin distortion parameter at less than 1.0.
8. During a Mach number transient simulating takeoff, the peak fan stall margin ratio decreases from about 1.0 at Mach number 0 to a value of about 0.70 at Mach number 0.12 with airflows representative of intermediate engine power setting.

REFERENCES

1. German, R. C. "0.2-Scale B-1 External-Compression Inlet Verification Model Test at Transonic and Supersonic Mach Numbers (Phase II)." AEDC-TR-74-52 (AD921416), August 1974.
2. Test Facilities Handbook (Tenth Edition). "Propulsion Wind Tunnel Facility, Vol. 4." Arnold Engineering Development Center, May 1974.

AEDC-TR-75-57

3. "B-1 Test Plan/Procedure, Inlet Verification Model PWT-16, Test 3." NA-70-550-2, Vol. VII, April 1974.
4. "Pretest Information for the 0.20-Scale B-1 Inlet Verification Model in the AEDC Propulsion Wind Tunnels - 16S, 16T (Test 4)." NA-70-550-2, October 1974.
5. McDill, H. E. "Results of a Full-Scale B-1 Inlet/Engine Compatibility Test at Subsonic and Supersonic Mach Numbers." AEDC-TR-75-3 (ADB001545L), January 1975.



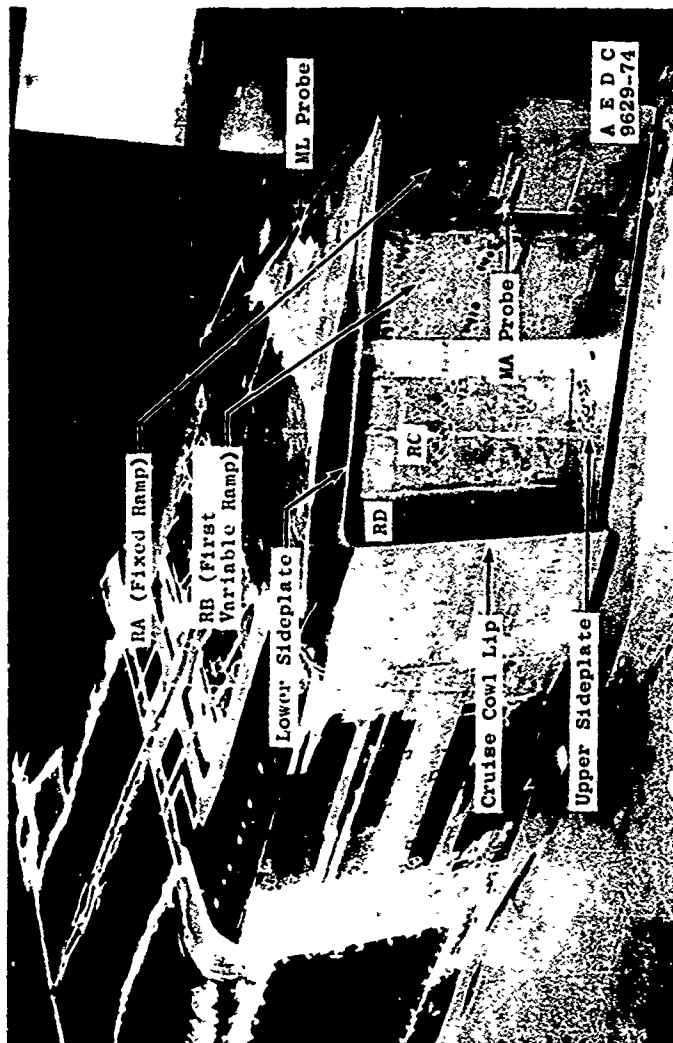
b. Tunnel 16S
Figure 1. Concluded.



a. Tunnel 16T
Figure 2. Installation photographs.



b. Tunnel 16S
Figure 2. Concluded.



b. Photograph
Figure 3. Concluded.

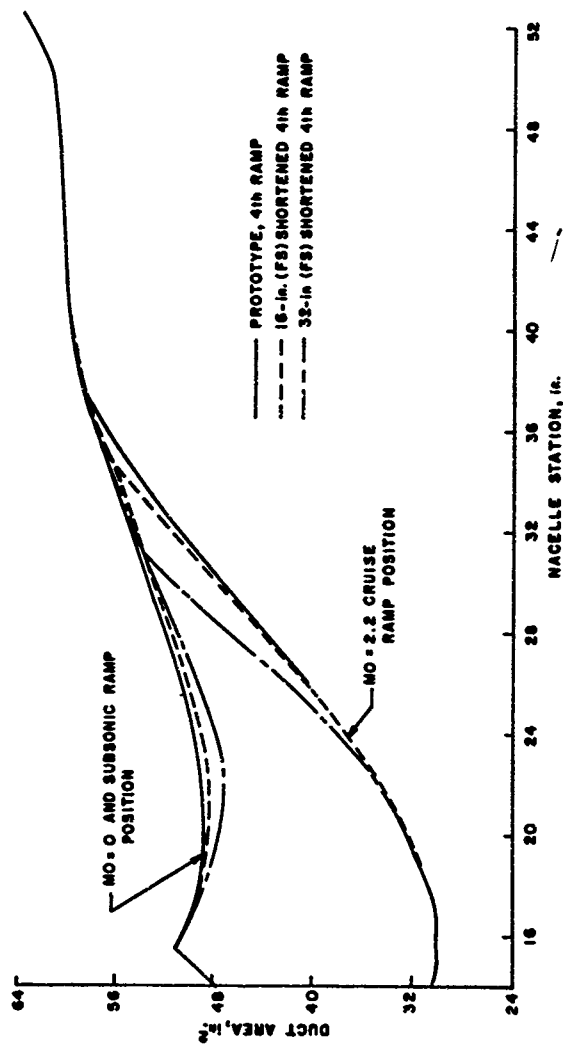


Figure 4. Duct area distribution.

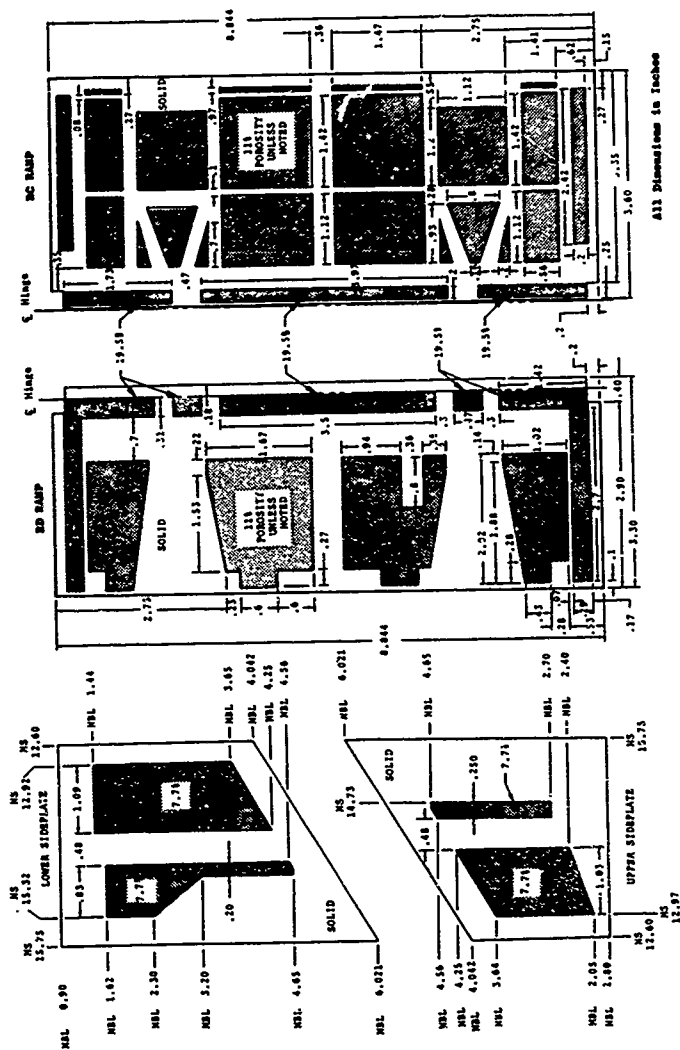


Figure 5. Inlet boundary-layer bleed porosity configuration.

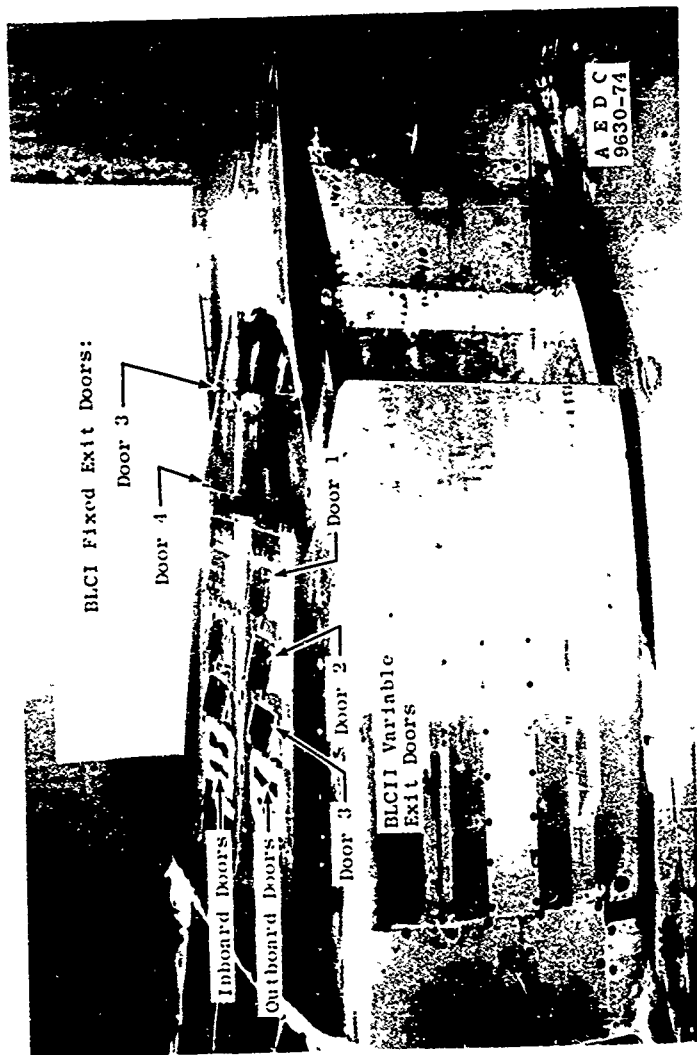
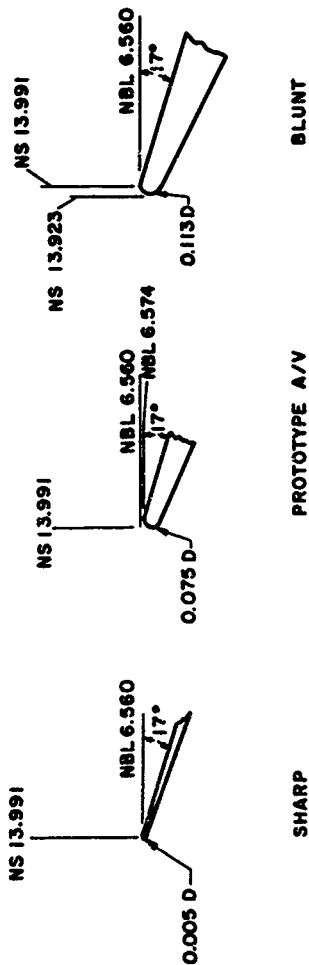


Figure 6. Production configuration bleed zone discharge doors.



DIMENSIONS IN INCHES

Figure 7. Cowl lip contours.

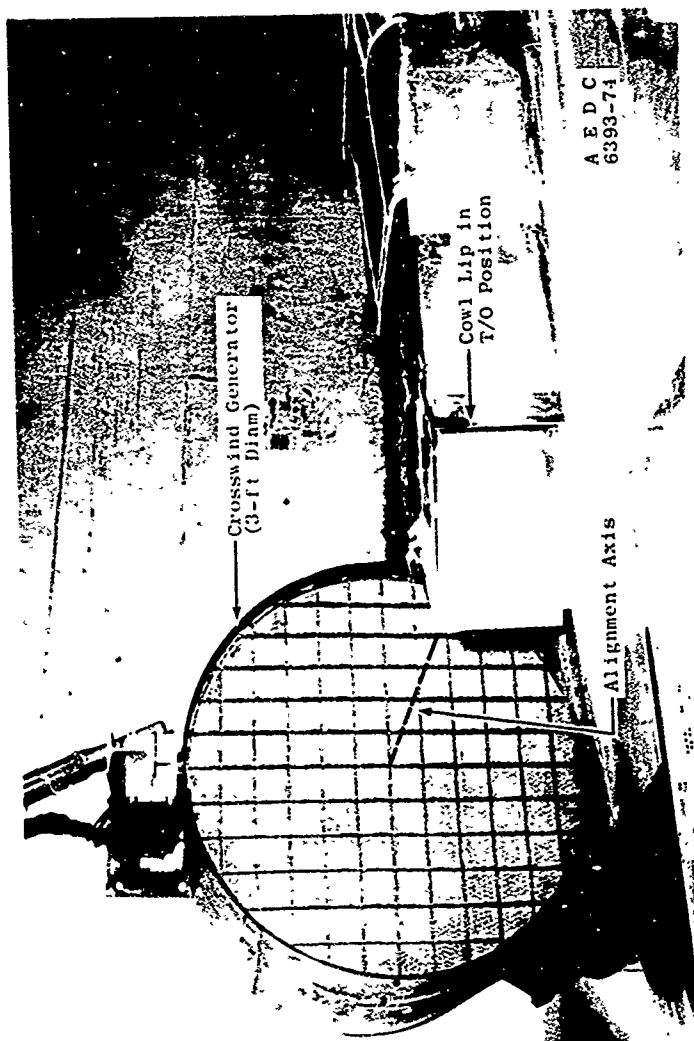
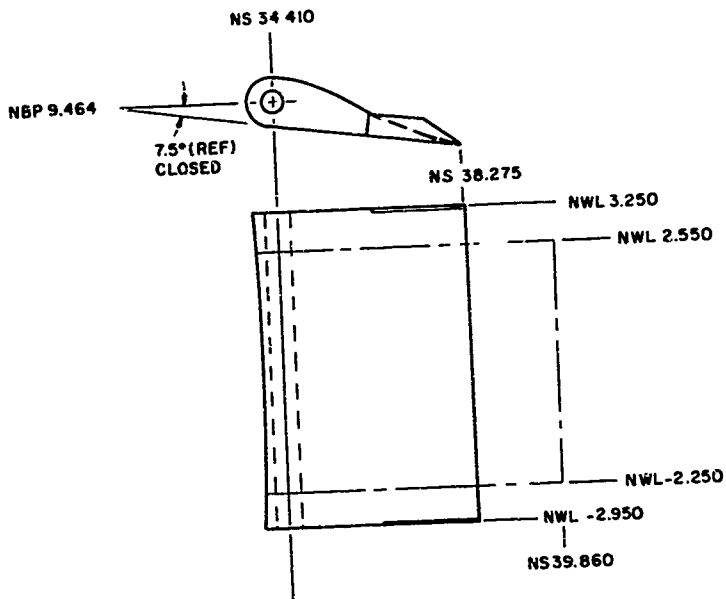


Figure 8. Crosswind generator installation.



(REF. PROTOTYPE DOOR IN
PHANTOM LINE)
DIMENSIONS IN INCHES

Figure 9. Bypass door schematic.

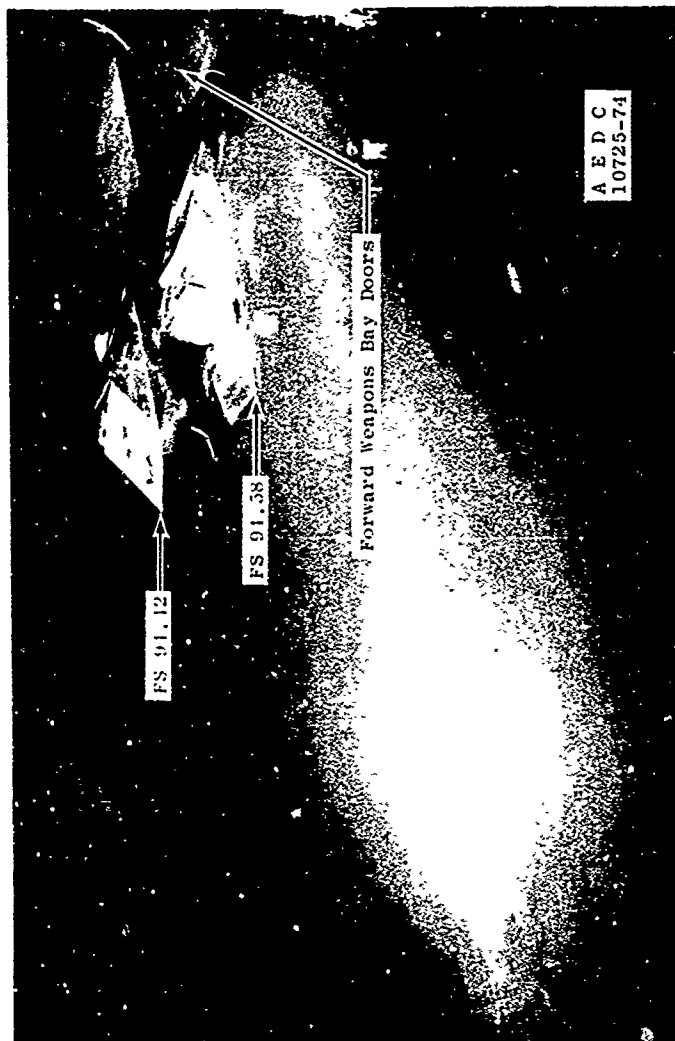


Figure 10. EVS pod installation.

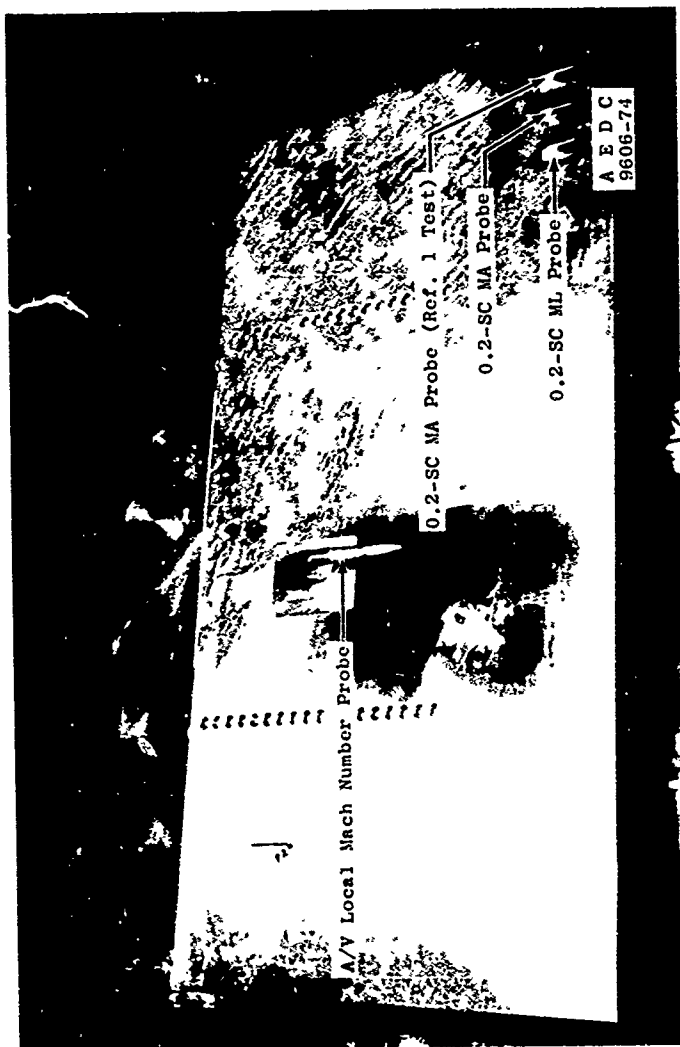
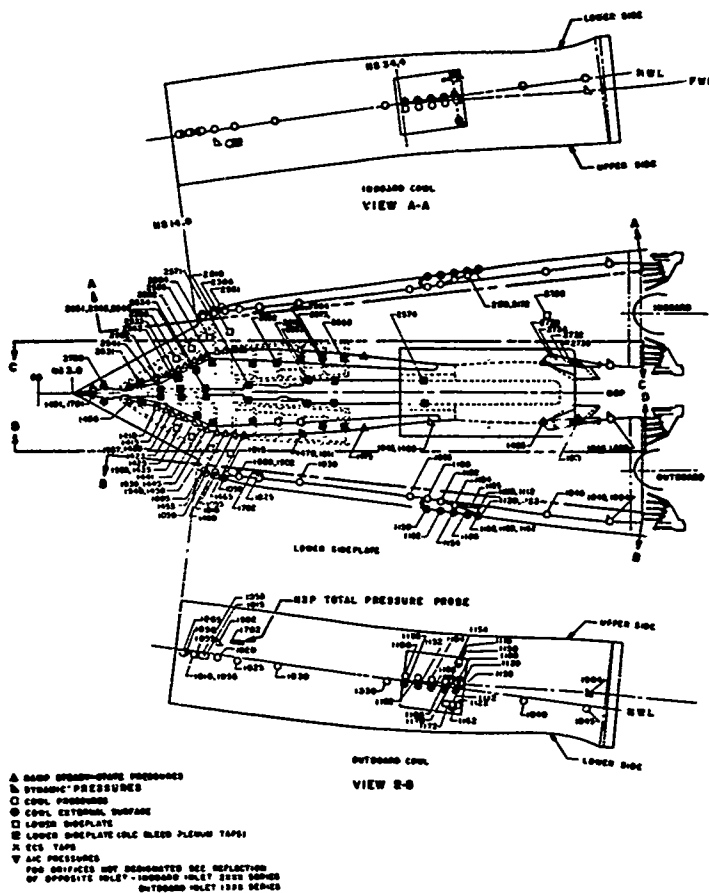
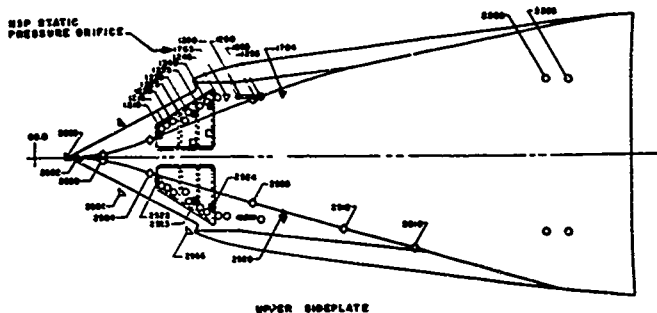


Figure 11. MA/ML probe calibration plate.

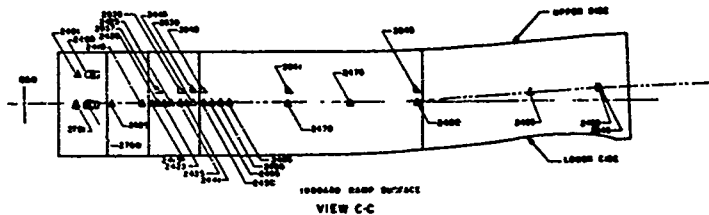


a. Inboard cowl, lower sideplate, outboard cowl
Figure 12. Instrumentation locations.

VIEW 0-0

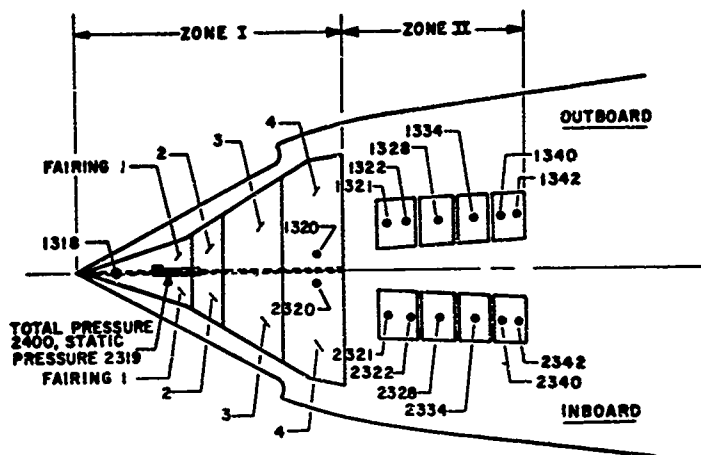


UPPER SIDEPLATE



VIEW C-C

42



TYPICAL ZONE I EXIT

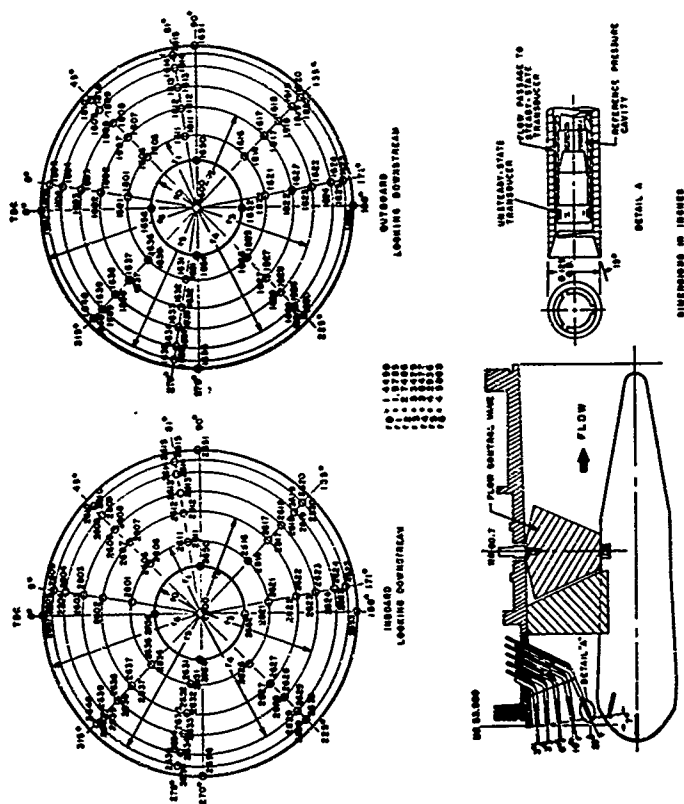


FAIRING	EXIT STATIC	EXIT TOTAL
1	X311	X310
2	X313	X312
3	X315	X314
4	X317	X316

X=1, OUTBOARD
X=2, INBOARD

DOOR	EXIT STATIC	EXIT TOTAL
1	X326	X324
2	X332	X330
3	X338	X336
4	X346	X344

c. Schematic of boundary-layer control system instrumentation
Figure 12. Continued.



d. Pressure instrumentation at compressor face
Figure 12. Concluded.

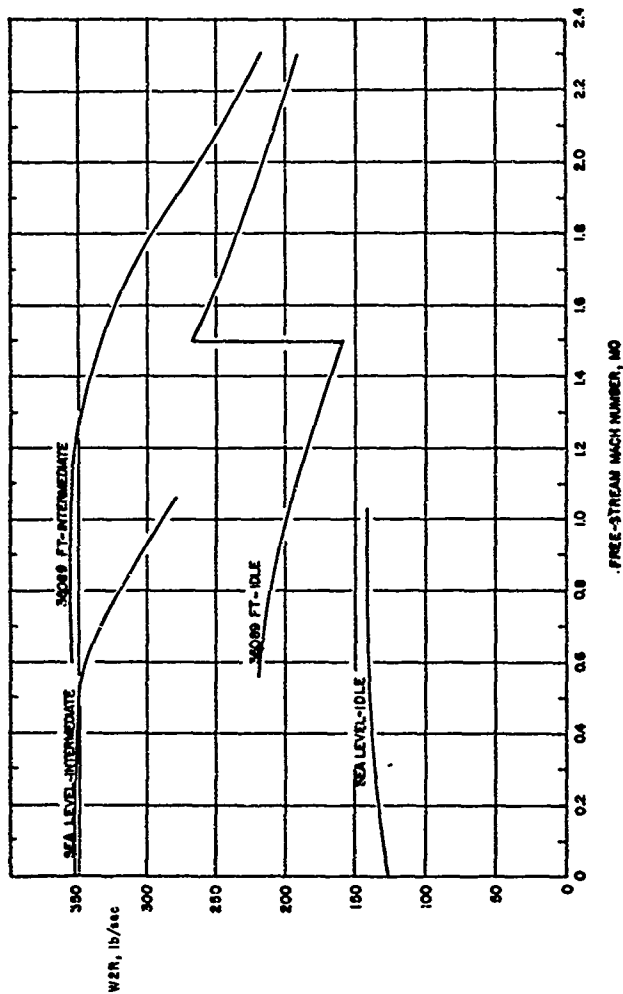
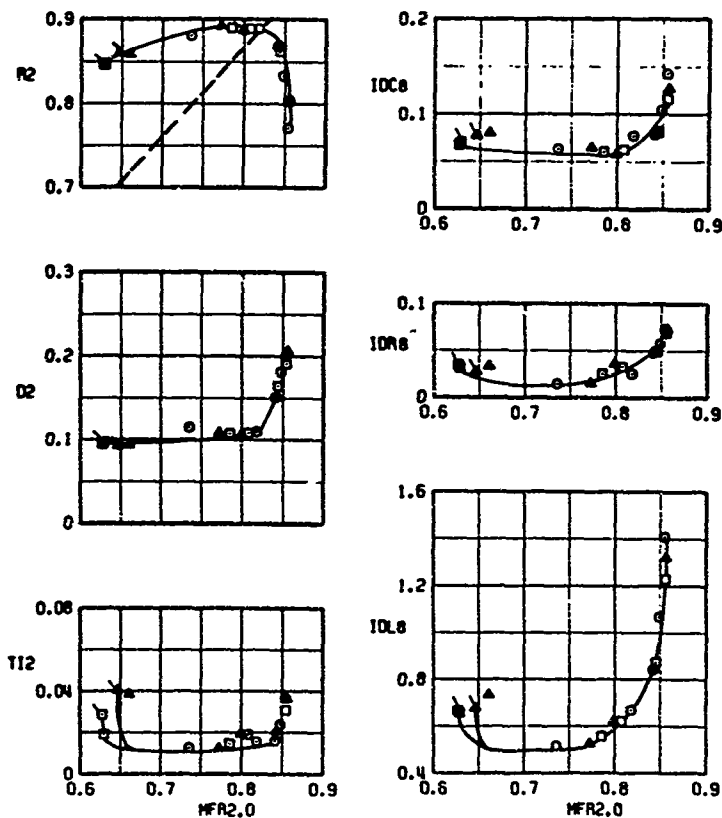


Figure 13. Variation of corrected engine airflow with free-stream Mach number.

SYMBOL α ψ M_0 H_L FOURTH RAMP
 ○ -2.1 0.0 14.0 3.37 PROTOTYPE 1015
 □ -2.0 0.0 14.0 3.30 16-in. SHORTENED 1562
 ▲ -2.0 0.1 14.0 3.30 32-in. SHORTENED 1593
 FLAGGED SYM - STABILITY LIMIT
 --- INTERMEDIATE POWER AIRFLOW, 36K (1)

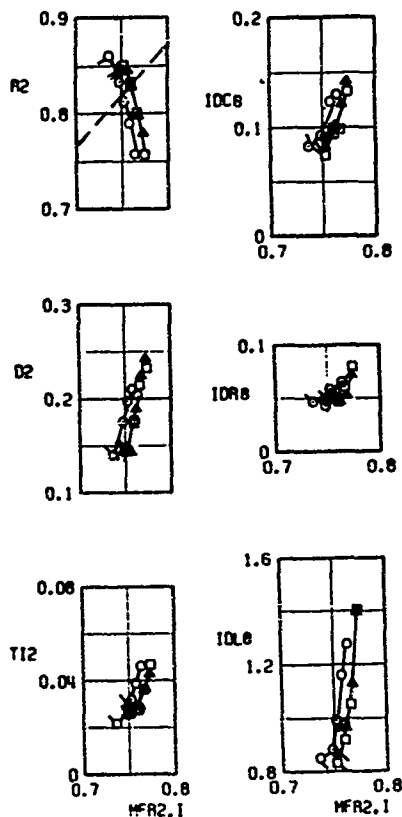


$\alpha = -2$ deg, $\psi = 0$, outboard

Figures 14. Inlet performance effects of shortened inlet fourth ramp at $M_0 = 2.20$.

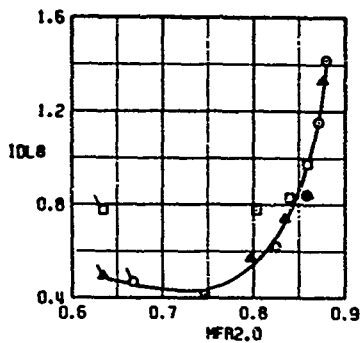
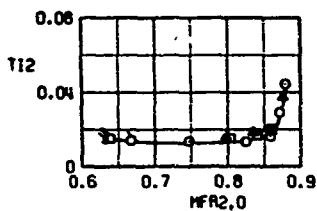
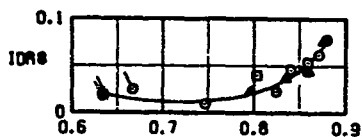
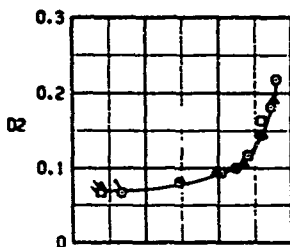
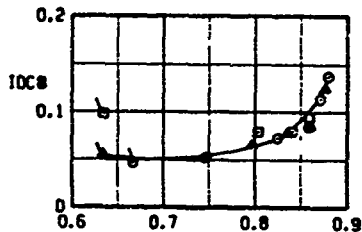
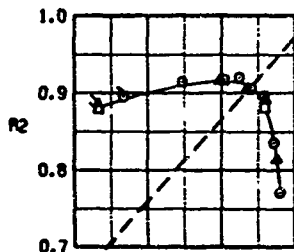
SYMBOL	α	ϕ	RB	HL	FOURTH RAMP	
O	-2.1	0.0	16.7	3.10	PROTOTYPE	1015
□	-2.0	0.0	16.7	3.14	16-in.SHORTENED	1562
△	-2.0	0.0	16.8	3.14	32-in.SHORTENED	1593

FLAGGED SYM - STABILITY LIMIT
 --- INTERMEDIATE POWER AIRFLOW, 36K ft



a. Concluded, inboard
 Figure 14. Continued.

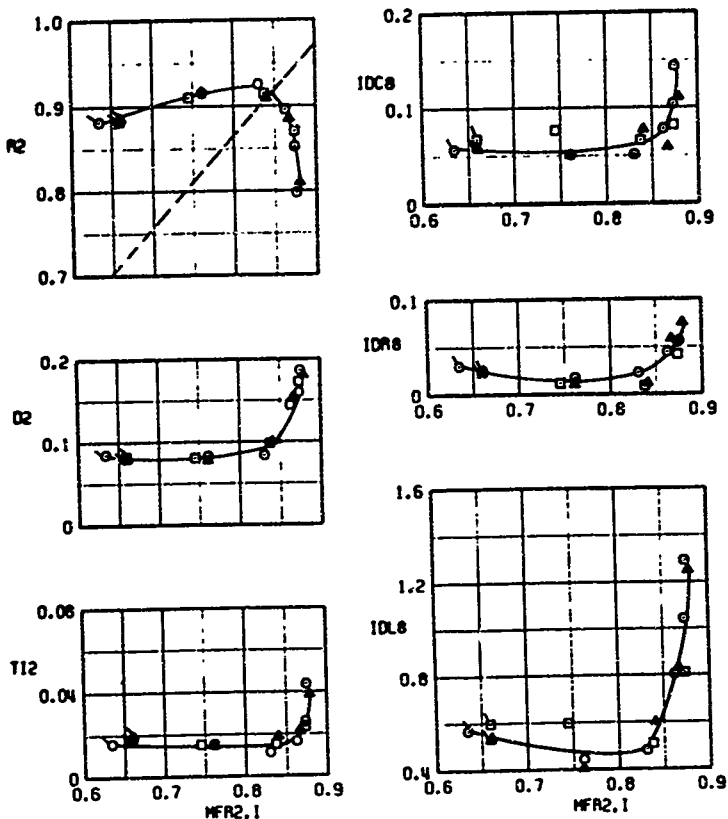
SYMBOL = ψ P3 HL FOURTH RAMP
 O 2.5 0.0 14.0 3.36 PROTOTYPE 1021
 □ 2.5 0.0 14.0 3.36 16-in. SHORTENED 1534
 ▲ 2.5 0.0 14.0 3.36 32-in. SHORTENED 1583
 FLAGGED SYM - STABILITY LIMIT
 --- INTERMEDIATE POWER AIRFLOW, 36K (1)



b. $\alpha = 2.5$ deg, $\psi = 0$, outboard
 Figure 14. Continued.

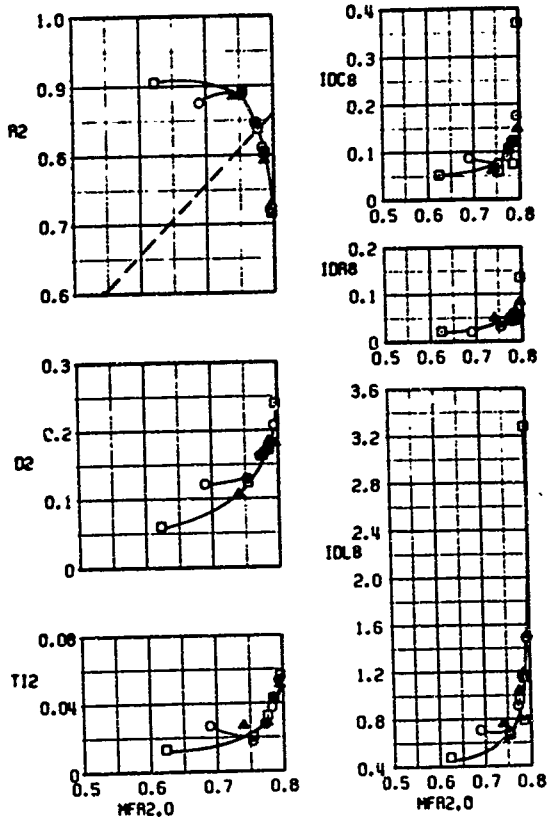
SYMBOL	α	ϕ	PR	HL	FOURTH RAMP	
○	2.5	0.0	14.0	3.36	PROTOTYPE	1021
□	2.5	0.0	14.0	3.36	16-in SHORTENED	1534
△	2.5	0.0	14.0	3.36	32-in SHORTENED	1583

LAGGED SYM STABILITY LIMIT
 --- INTERMEDIATE POWER AIRFLOW, 36K II



b. Concluded, inboard
 Figure 14. Continued.

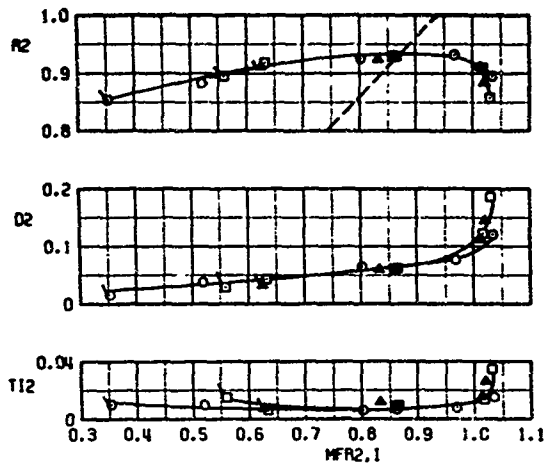
SYMBOL = ψ RB HL FOURTH RAMP
 O 9.0 -3.0 16.0 3.10 PROTOTYPE 1044
 □ 9.0 -2.9 16.0 3.10 16-IN. SHORTENED 1556
 ▲ 9.0 -2.9 16.0 3.10 32-IN. SHORTENED 1584
 FLAGGED SYM - STABILITY LIMIT
 --- INTERMEDIATE POWER AIRFLOW, 36K II



c. $\alpha = 9$ deg, $\psi = 5$ deg, outboard
 Figure 14. Continued.

SYMBOL	α	ψ	PS	HL	FOURTH RAMP	
O	9.0	-3.0	13.2	3.81	PROTOTYPE	1044
□	9.0	-2.9	13.2	3.81	16-in. SHORTENED	1356
▲	9.0	-2.9	13.2	3.81	32-in. SHORTENED	1384

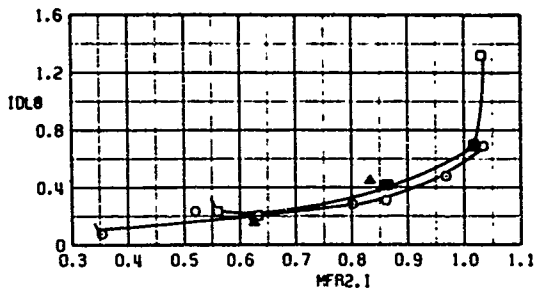
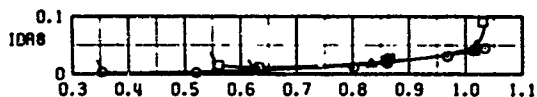
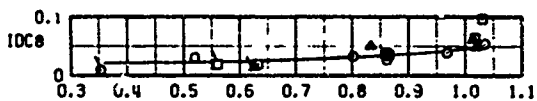
FLAGGED SYM - STABILITY LIMIT
 --- INTERMEDIATE POWER AIRFLOW, 36K II



c. Continued, inboard
 Figure 14. Continued.

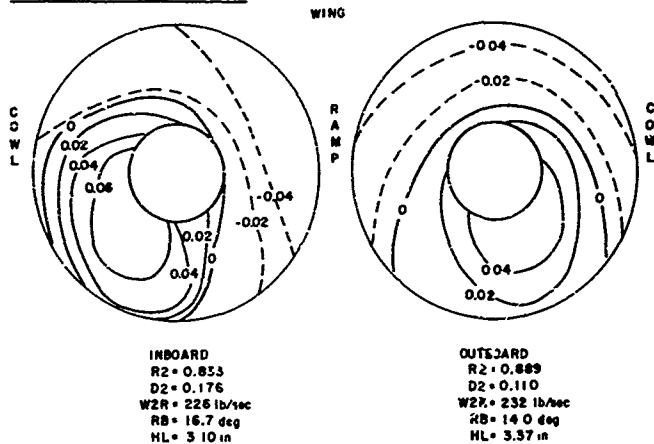
SYMBOL	α	ψ	RS	ML	FOURTH RAMP	
O	9.0	-3.0	13.2	3.81	PROTOTYPE	1044
□	9.0	-2.9	13.2	3.81	16-in. SHORTENED	1556
△	9.0	-2.9	13.2	3.81	32-in. SHORTENED	1584

FLAGGED SYM - STABILITY LIMIT
 --- INTERMEDIATE POWER AIRFLOW, 36K ft

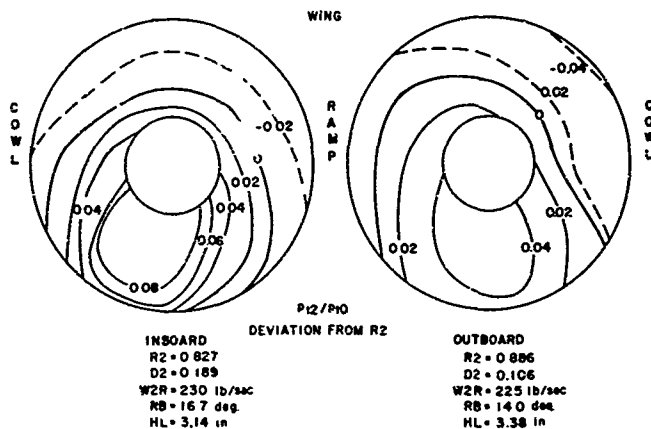


c. Concluded, inboard
 Figure 14. Concluded.

PROTOTYPE FOURTH RAMP



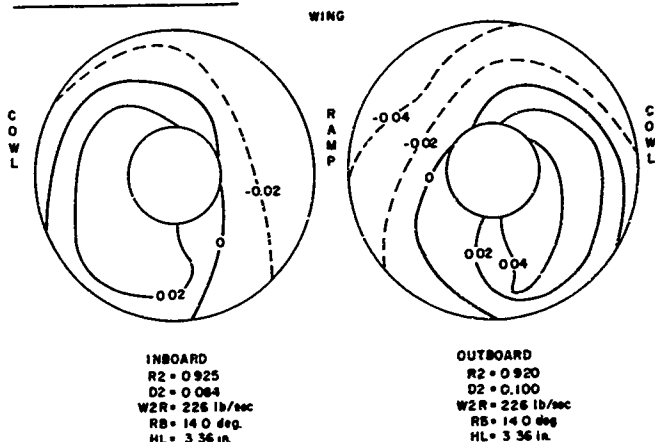
32-in SHORTENED FOURTH RAMP



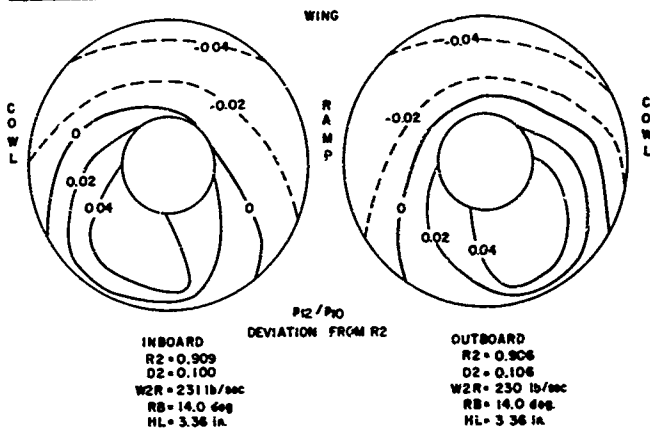
a. $\alpha = 2 \text{ deg}$, $\psi = 0$

Figure 15. Effects of shortened inlet fourth ramp on engine-face total pressure contours.

PROTOTYPE FOURTH RAMP



32-in SHORTENED FOURTH RAMP



b. $\alpha = 2.5$ deg, $\psi = 0$
Figure 15. Continued.

INBOARD

RZ = 0.930
D2 = 0.062
WZR = 233 lb/sec
RB = 13.2 deg.
HL = 3.81 in.

OUTBOARD

RZ = 0.847
D2 = 0.163
WZR = 230 lb/sec
RB = 16.0 deg.
HL = 3.10 in.

32-in. SHORTENED FOURTH RAMP

INBOARD

R2 = 0.924
 D2 = 0.060
 WZR = 225 ft/sec
 RB = 13.2 deg
 HL = 3.81 in.

OUTBOARD

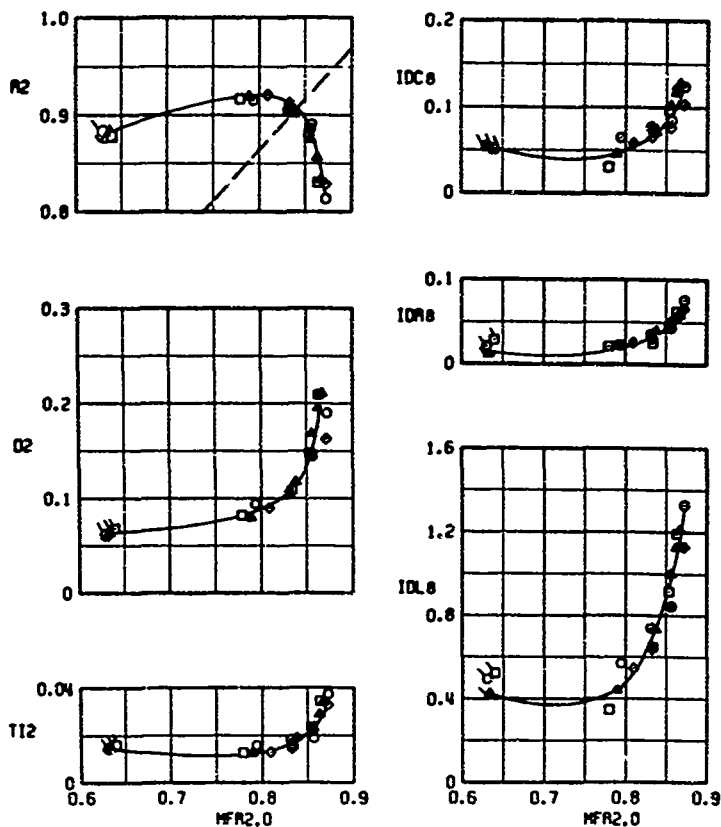
R2 = 0.844
 D2 = 0.167
 WZR = 230 ft/sec
 RB = 18.0 deg
 HL = 3.10 in.

55

SYMBOL	α	ψ	RB	HL	BLEED	
○	2.5	0.1	14.0	3.36	PROTYPE	1563
□	2.5	0.0	14.0	3.36	NO SIDE PLATE	1672
△	2.5	0.0	14.0	3.36	INCREASED RC	1712
◇	2.5	0.0	14.1	3.36	INCREASED RO	1693

FLAGGED SYM - STABILITY LIMIT

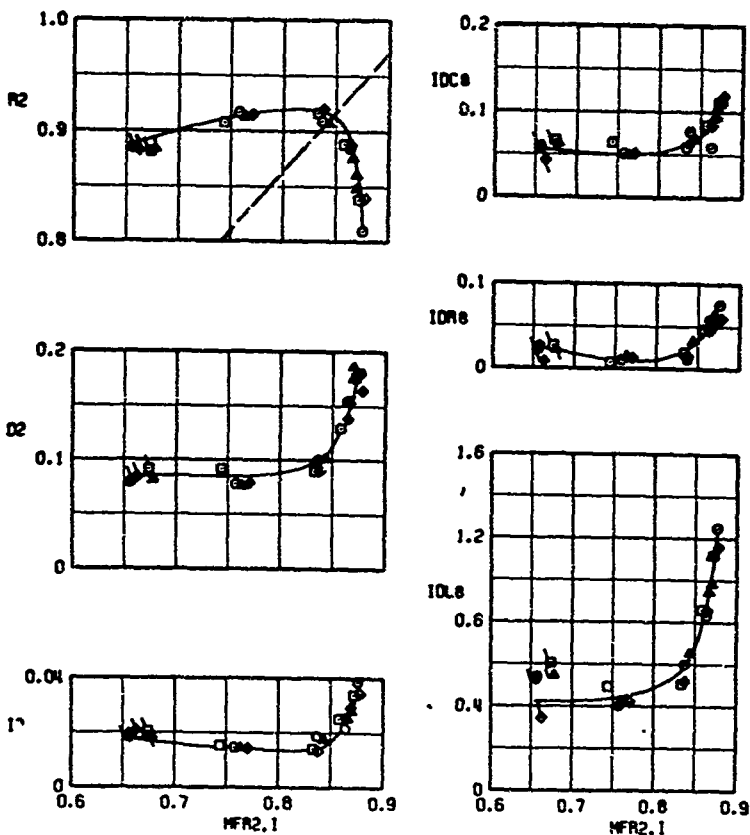
--- INTERMEDIATE POWER AIRFLOW, 36K II

a. $\alpha = 2.5$ deg, $\psi = 0$, outboardFigure 16. Effects of bleed porosity configurations on inlet at $M_0 = 2.20$.

SYMBOL	α	ϕ	PG	HL	BLEED	
○	2.5	0.1	14.0	3.36	PROTOTYPE	1583
□	2.5	0.0	14.0	3.36	NO SIDE PLATE	1672
△	2.5	0.0	14.0	3.36	INCREASED RC	1712
◆	2.5	0.0	13.9	3.37	INCREASED RD	1693

FLAGGED SYM - STABILITY LIMIT

--- INTERMEDIATE POWER AIRFLOW, 36K ft

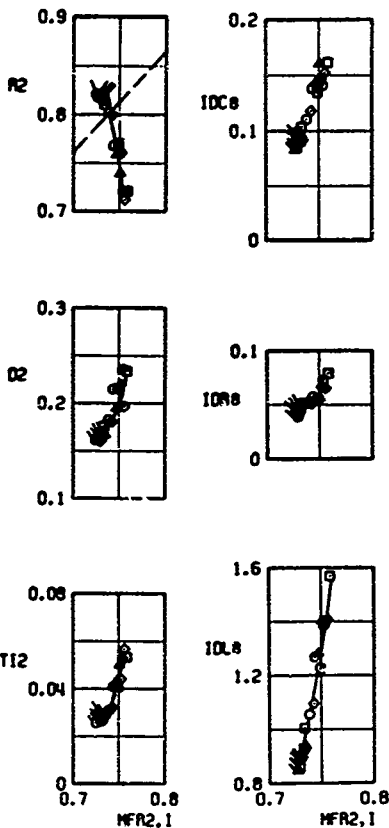


a. Concluded, inboard
Figure 16. Continued.

SYMBOL	α	ψ	RS	HL	BLEED	
○	0.0	3.0	15.2	3.13	PROTOTYPE	1585
□	0.0	2.9	15.2	3.13	NO SIDE PLATE	1673
▲	0.0	2.9	15.2	3.13	INCREASED RC	1713
◇	0.0	2.9	15.2	3.13	INCREASED RD	1695

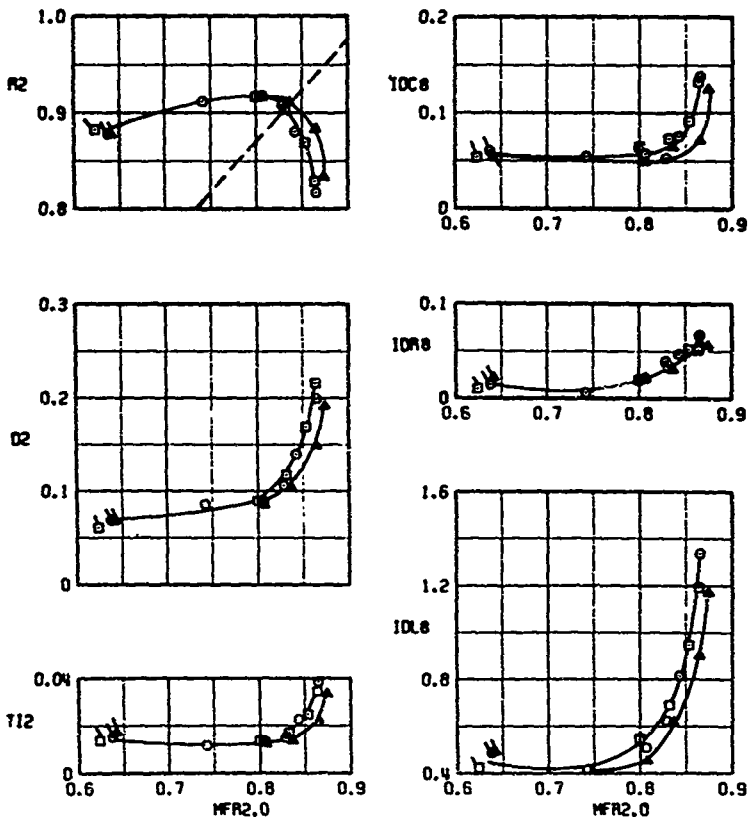
FLAGGED SYM - STABILITY LIMIT

--- INTERMEDIATE POWER AIRFLOW, 36K II



b. $\alpha = 0$, $\psi = 3$ deg, inboard
Figure 16. Concluded.

SYMBOL α ψ P_0 M_∞ COWL
 O 2.5 0.0 14.0 3.36 PROTOTYPE 1751
 □ 2.5 0.0 14.0 3.36 SHARP 1845
 ▲ 2.5 0.0 14.0 3.36 BLUNT 1854
 FLAGGED SYM-STABILITY LIMIT
 --- INTERMEDIATE POWER AIRFLOW, 36K #

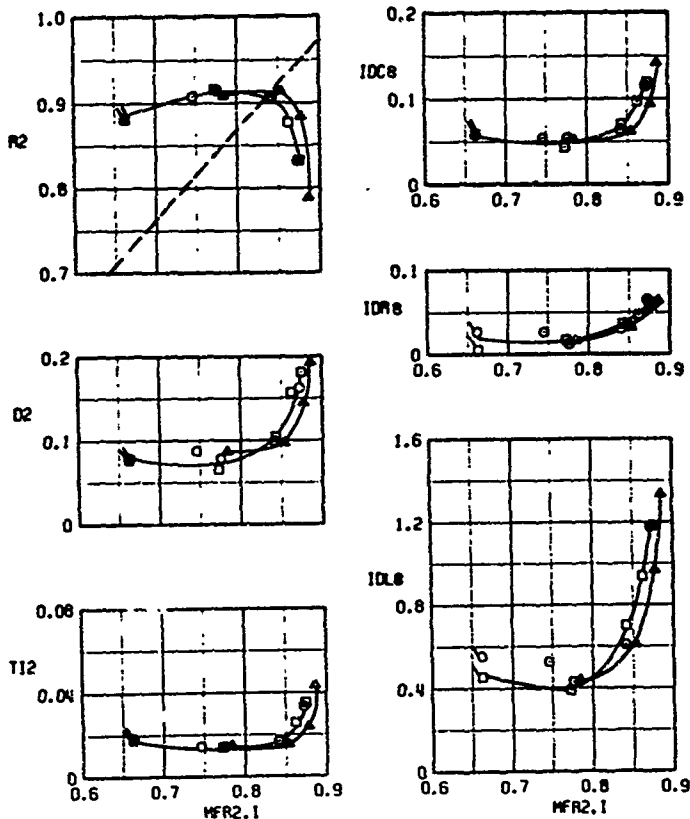


a. $\alpha = 2.5$ deg, $\psi = 0$, outboard

Figure 17. Effects of cowl lip contours on inlet performance at $M_0 = 2.20$.

SYMBOL	α	ψ	RS	HL	COWL
O	2.5	0.0	14.0	3.36	PROTOTYPE 1751
□	2.5	0.0	14.0	3.36	SHARP 1845
△	2.5	0.0	14.0	3.36	BLUNT 1854

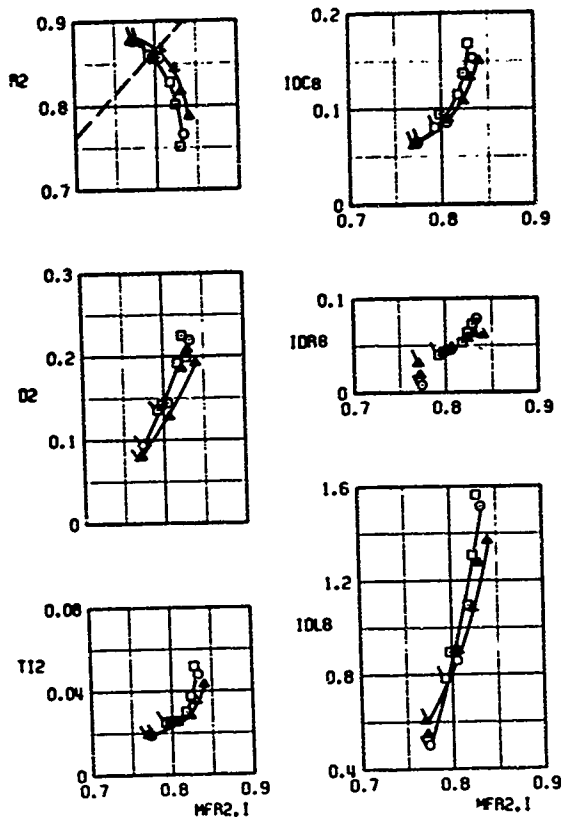
FLAGGED SYM-STABILITY LIMIT
 --- INTERMEDIATE POWER AIRFLOW, 36K #1



a. Concluded, inboard
 Figure 17. Continued.

SYMBOL	α	ψ	RE	HL	COWL	
O	2.5	3.0	14.0	3.33	PROTOTYPE	1752
□	2.5	3.0	14.0	3.33	SHARP	1846
△	2.5	3.0	14.0	3.33	BLUNT	1857

FLAGGED SYM-STABILITY LIMIT
 --- INTERMEDIATE POWER AIRFLOW, 36K #

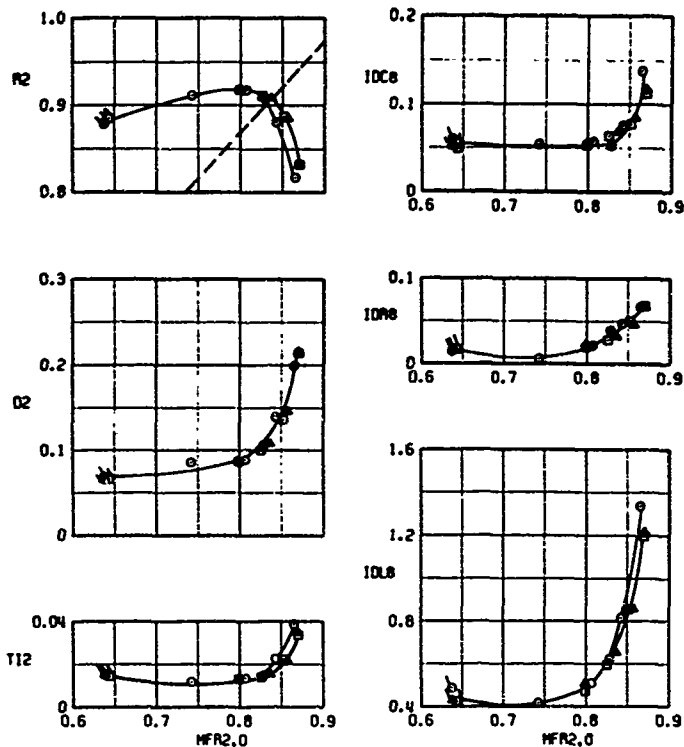


b. $\alpha = 2.5$ deg, $\psi = 3$ deg, inboard
 Figure 17. Concluded.

SYMBOL	α	ψ	PS	HL	ABLCL, in ²	
○	2.5	0.0	14.0	3.36	3.34	1751
□	2.5	0.0	14.0	3.36	2.68	1757
△	2.5	0.0	14.0	3.36	1.98	1763

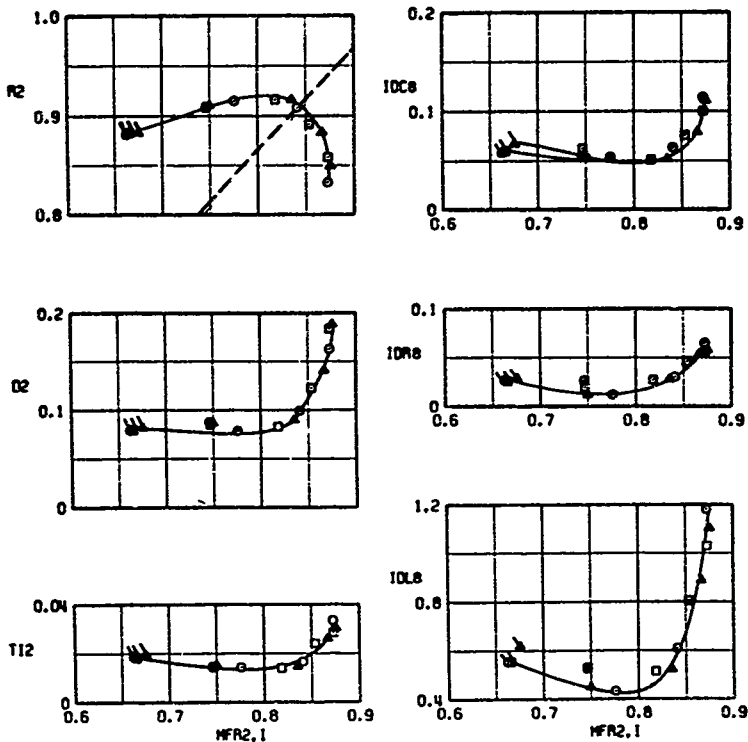
FLAGGED SYM - STABILITY LIMIT

--- INTERMEDIATE POWER AIRFLOW, 34K II

a. $\alpha = 2.5$ deg, $\psi = 0$, outboardFigure 18. Effects of reduced BLCI and II discharge areas on inlet performance at $M_0 = 2.20$.

SYMBOL	ϕ	PBI	MLI	ABLCE, in ²
○	2.5	0.0	14.0	3.36 3.34 1751
□	2.5	0.0	14.0	3.37 2.68 1757
△	2.5	0.0	14.0	3.36 1.98 1765

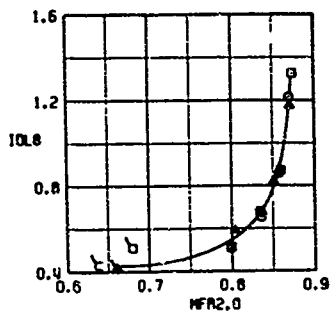
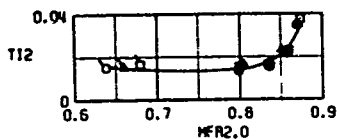
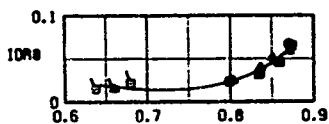
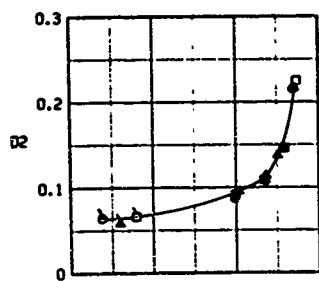
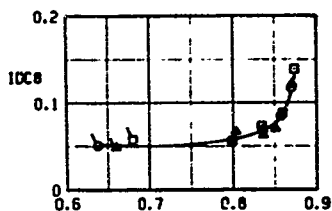
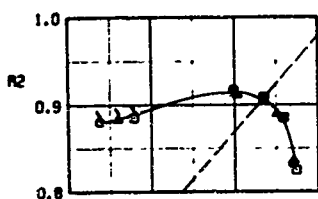
FLAGGED SYM - STABILITY LIMIT
 --- INTERMEDIATE POWER AIRFLOW, 36K II



a. Concluded, inboard
 Figure 18. Continued.

SYMBOL	α	ψ	PR	HL	18LCI, in ²
O	2.5	0.0	14.0	3.36	1.82 1765
□	2.5	0.0	14.0	3.36	1.11 1802
△	2.5	0.0	14.0	3.36	0.79 1820

FLAGGED SYM - STABILITY LIMIT
 --- INTERMEDIATE POWER AIRFLOW, 36K ft

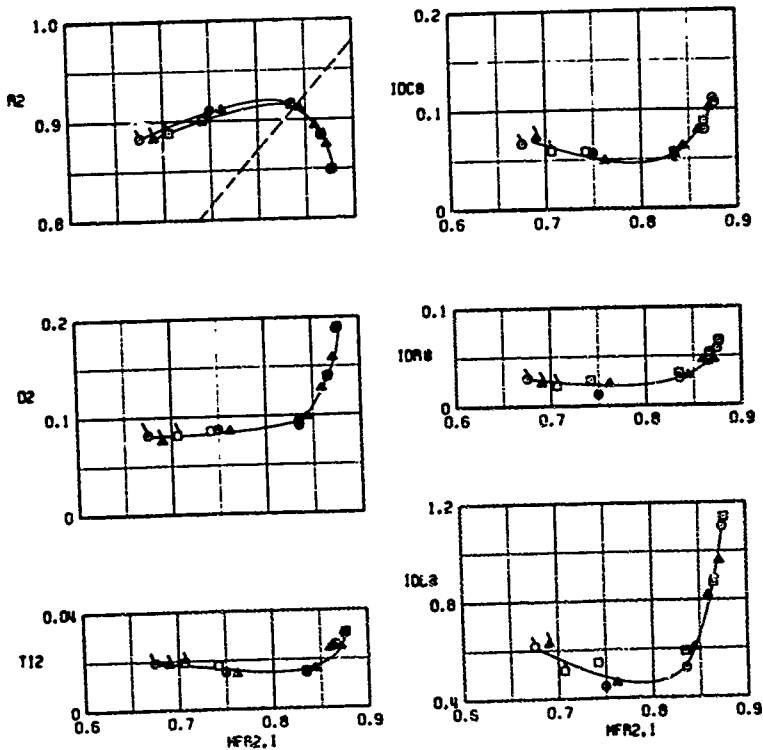


b. $\alpha = 2.5$ deg, $\psi = 0$, outboard
 Figure 18. Continued.

SYMBOL	#	ϕ	NOI	MLI	ABLCI, 10^2	
O	2.5	0.0	14.0	3.36	1.02	1765
□	2.5	0.0	14.0	3.36	1.11	1802
△	2.5	0.0	14.0	3.36	0.79	1820

FLAGGED SYM - STABILITY LIMIT

--- INTERMEDIATE POWER AIRFLOW, 36K ft



b. Concluded, inboard
Figure 18. Concluded.

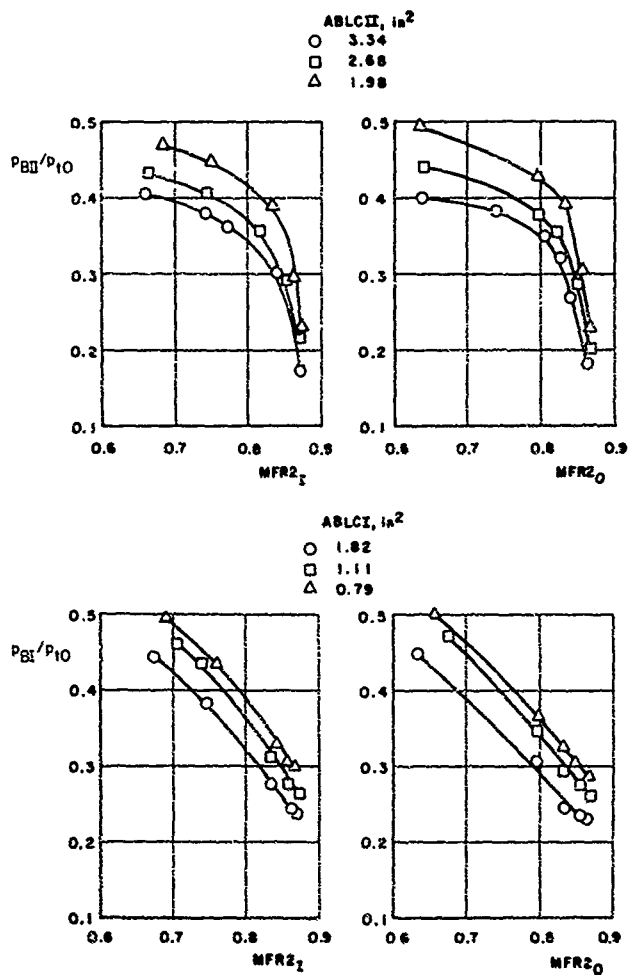
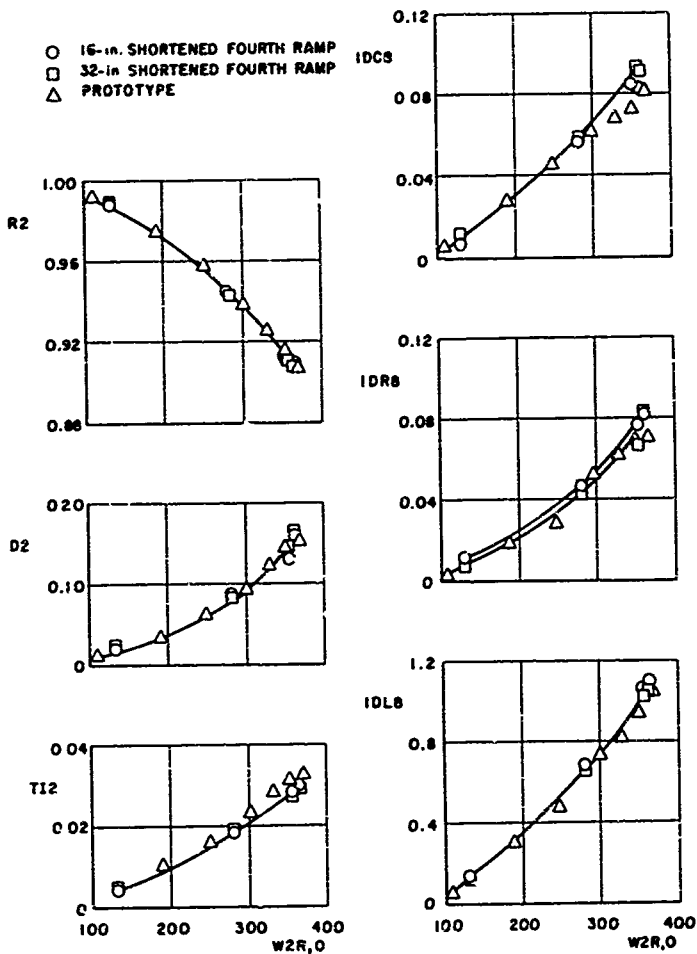
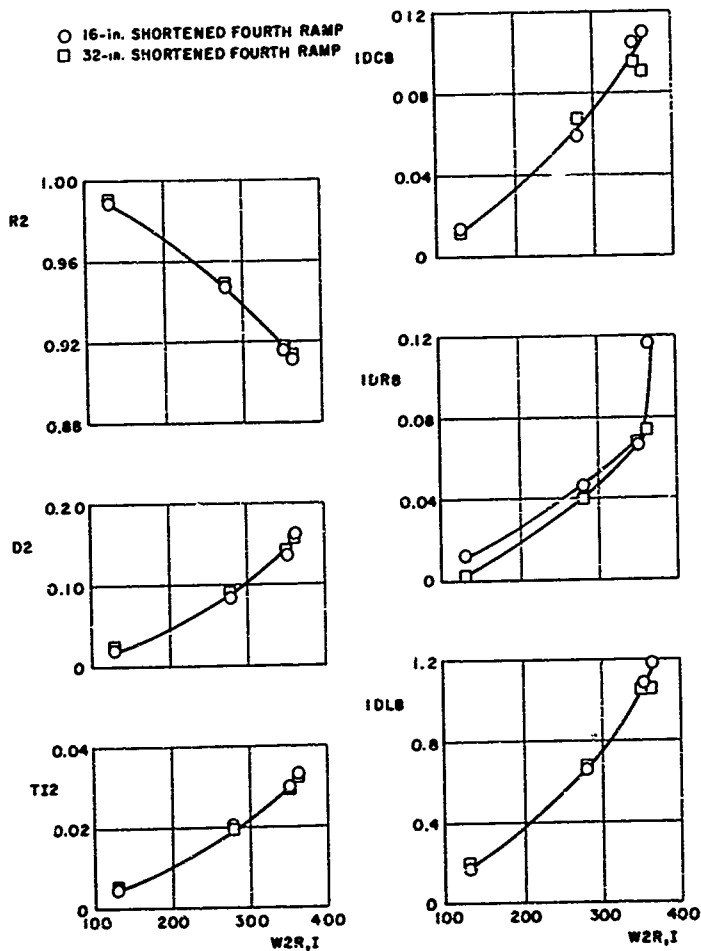


Figure 19. Effects of reduced BLCI and II discharge areas on the BLCI and II plenum pressures.



a. Outboard

Figure 20. Effects of reduced fourth ramp length on inlet performance at $M_0 = 0$.



b. Inboard
Figure 20. Concluded.

○ OUTBOARD INLET, $W2R \approx 356$ lb/sec
 □ INBOARD INLET, $W2R \approx 350$ lb/sec

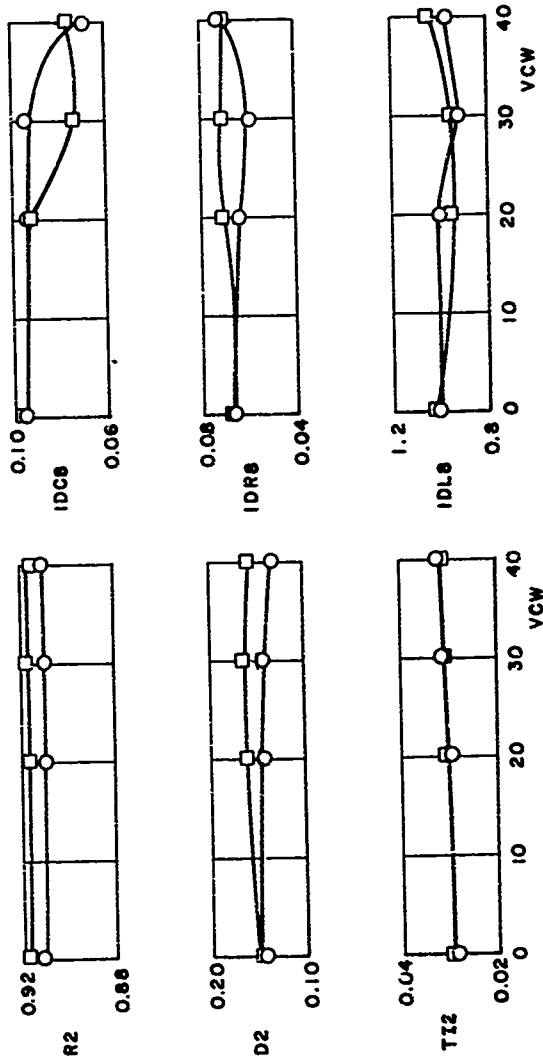


Figure 21. Effects of crosswind on inlet performance at takeoff conditions.

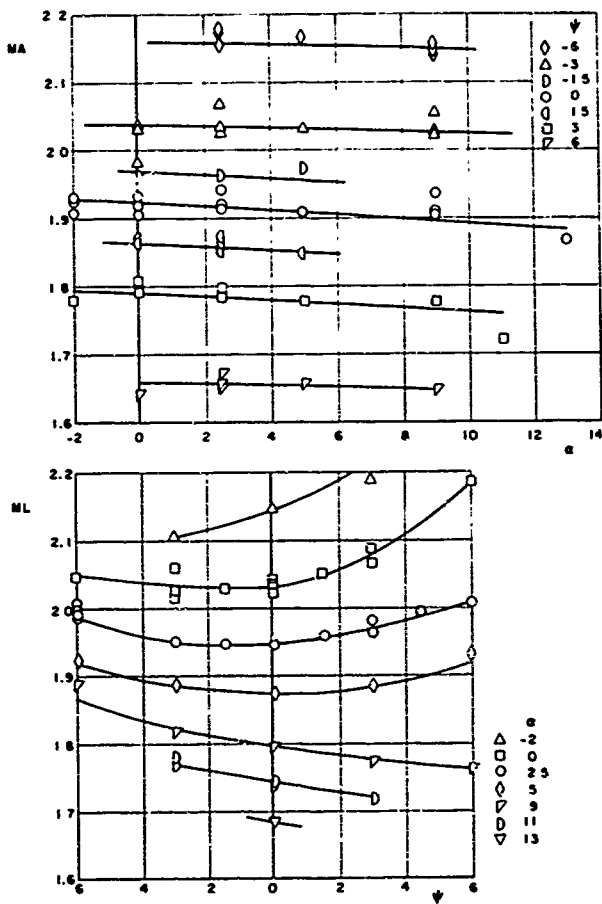
a. $M_0 = 2.2$

Figure 22. MA/ML local Mach number data matrix.

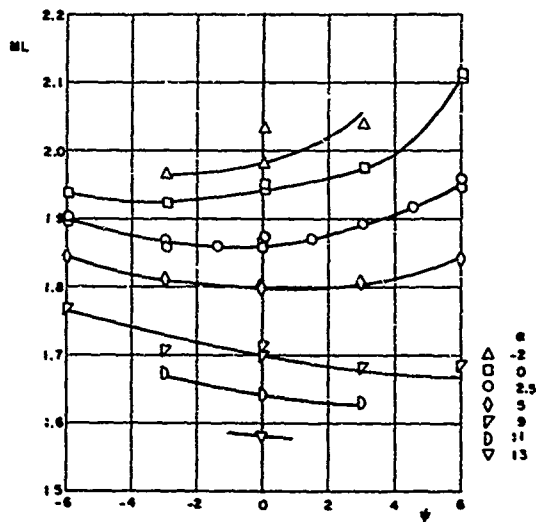
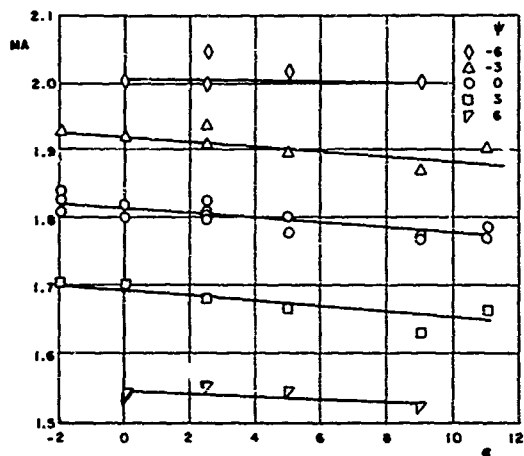
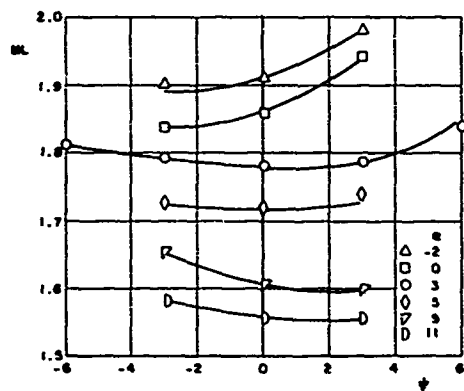
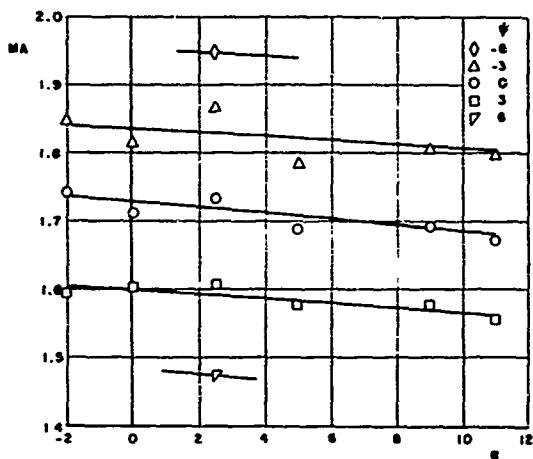
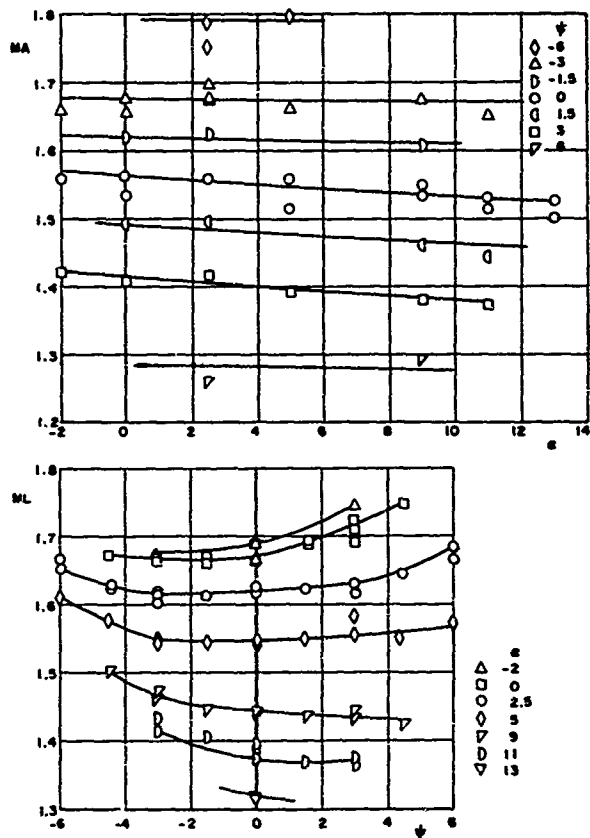
b. $M_0 = 2.1$

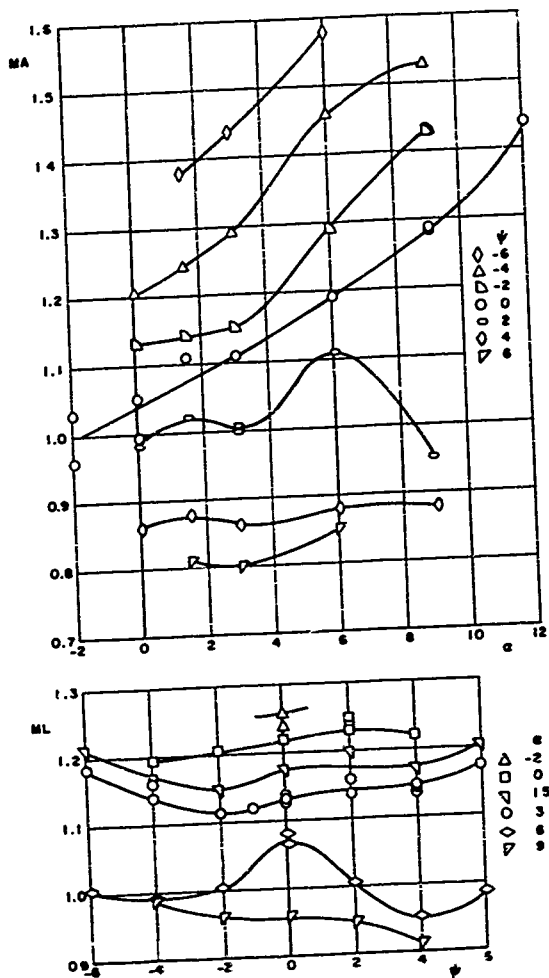
Figure 22. Continued.



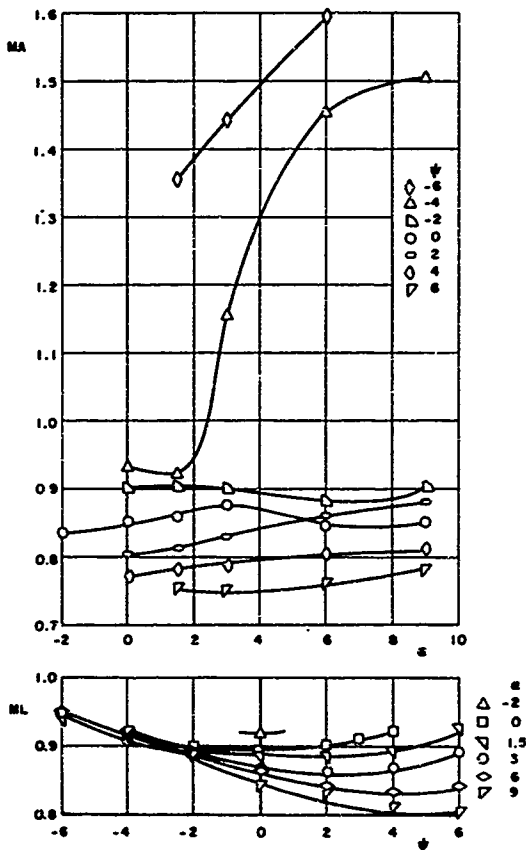
c. $M_0 = 2.0$
Figure 22. Continued.



d. $M_0 = 1.8$
Figure 22. Continued.

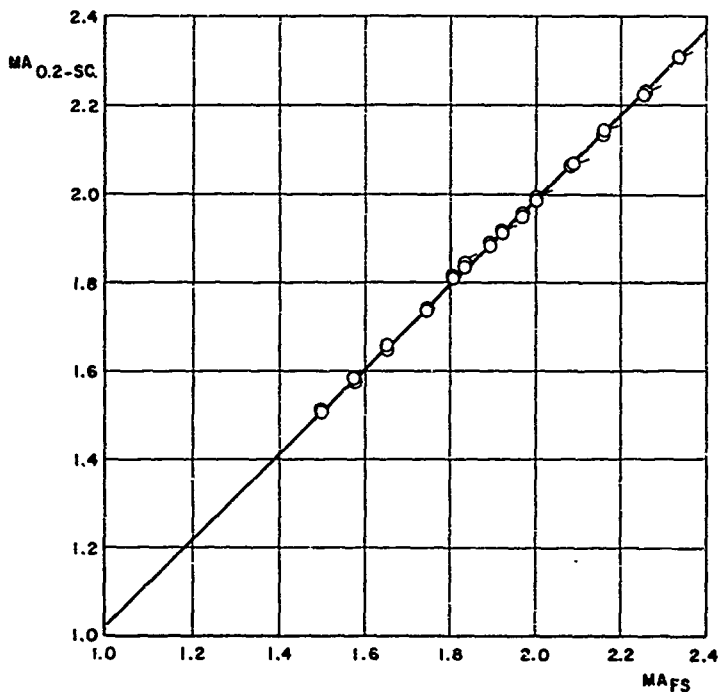


e. $M_0 = 1.4$
Figure 22. Continued.



f. $M0 = 1.2$
Figure 22. Concluded.

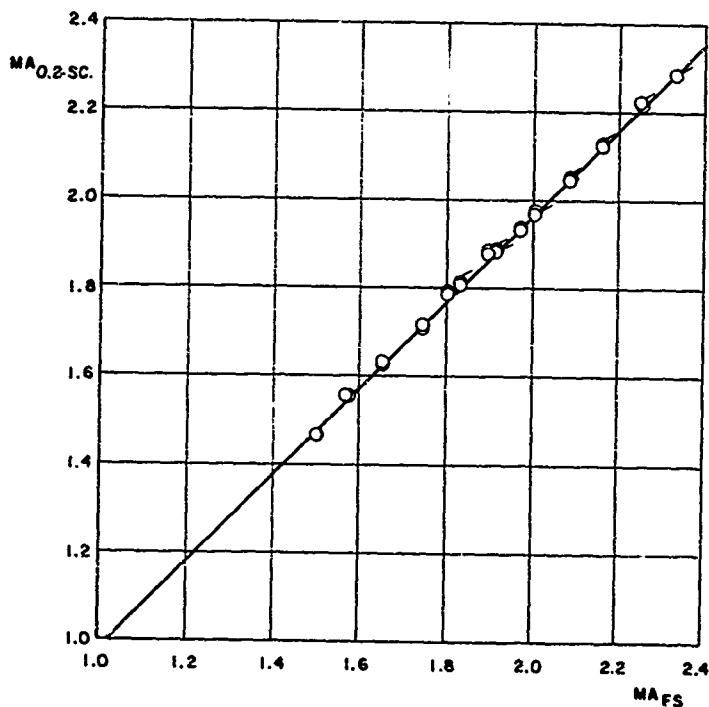
PLAIN SYM - DATA OBTAINED AT $M_0 = 1.8$
FLAGGED SYM - DATA OBTAINED AT $M_0 = 2.1$



a. Inboard inlet, ML probe

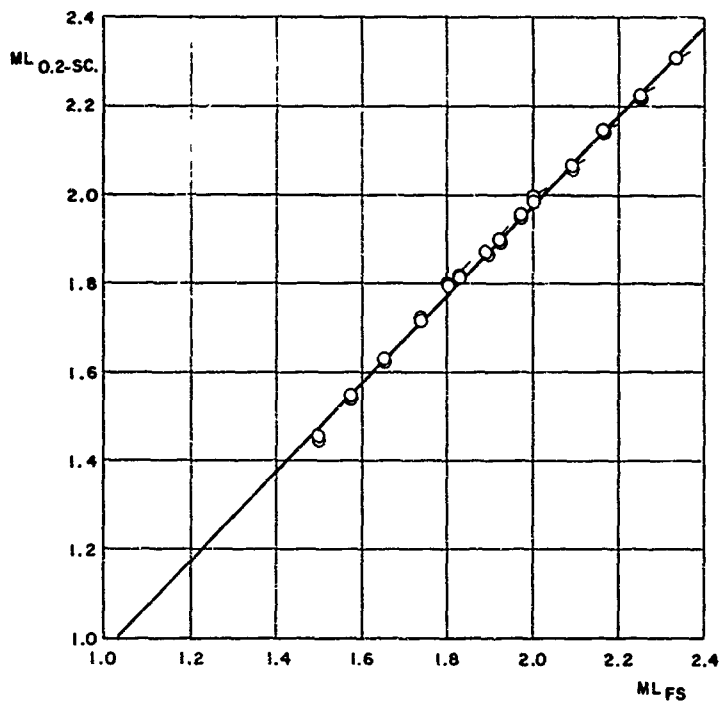
Figure 23. 0.2-scale/full-scale local Mach sensor correlation.

PLAIN SYM - DATA OBTAINED AT $MO = 1.8$
FLAGGED SYM - DATA OBTAINED AT $MO = 2.1$

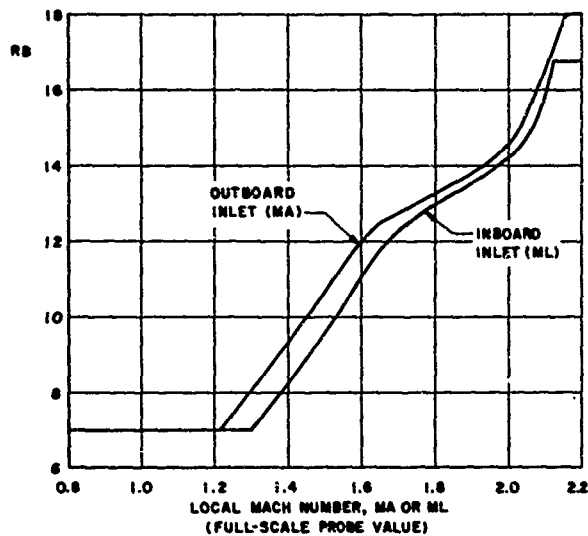


b. Outboard inlet, MA probe
Figure 23. Continued.

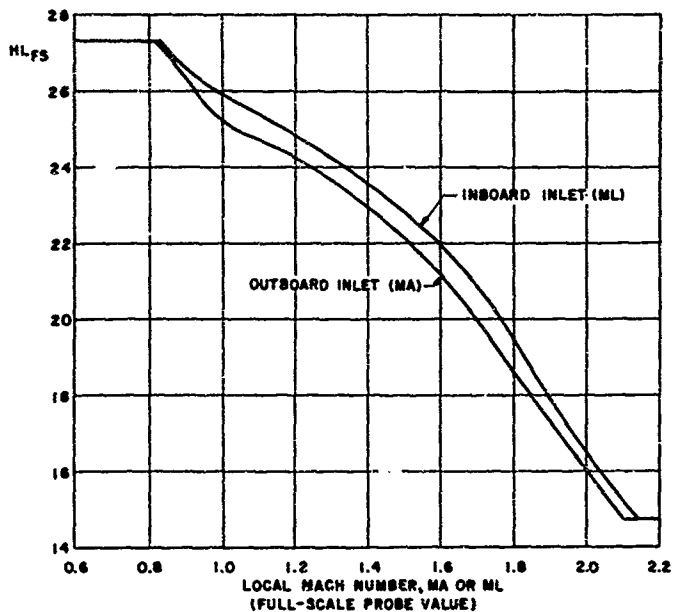
PLAIN SYM - DATA OBTAINED AT $MO = 1.8$
 FLAGGED SYM - DATA OBTAINED AT $MO = 2.1$



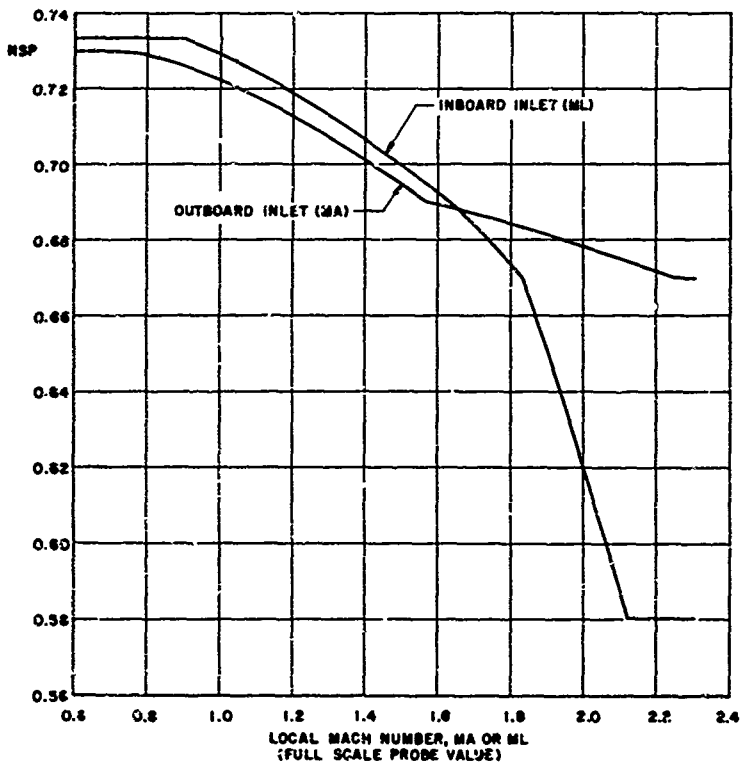
c. Outboard inlet, Ref. 1 MA probe
 Figure 23. Concluded.



a. Second ramp angle
Figure 24. Full-scale AICS schedules.



b. Lip height
Figure 24. Continued.



c. Normal shock parameter
Figure 24. Concluded.

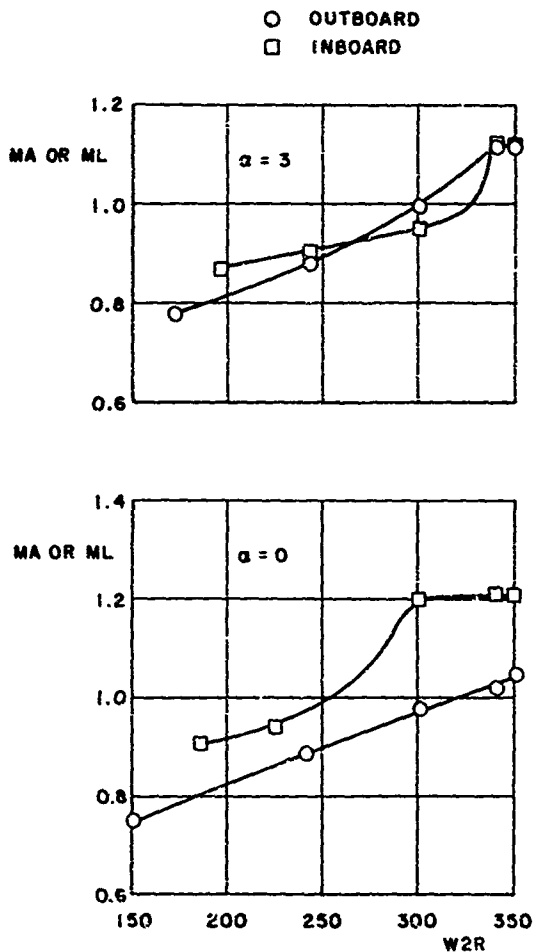


Figure 25. Effects of airflow on sensed local Mach numbers at $M_0 = 1.40$, $\psi = 0$.

SYMBOL	α	ϕ	RE	ML	GEOMETRY
□	2.5	0	7.4	5.45	SUBSONIC 2172
▲	2.5	0	15.0	3.46	MISPOSITIONED 2170
○	2.5	0	14.0	3.36	MO = 2.2 CRUISE 2084
◇	2.5	0	18.0	2.95	MAX SUPERSONIC 2168

FLAGGED SYM-STABILITY LIMIT

--- INTERMEDIATE POWER AIRFLOW, 36K II

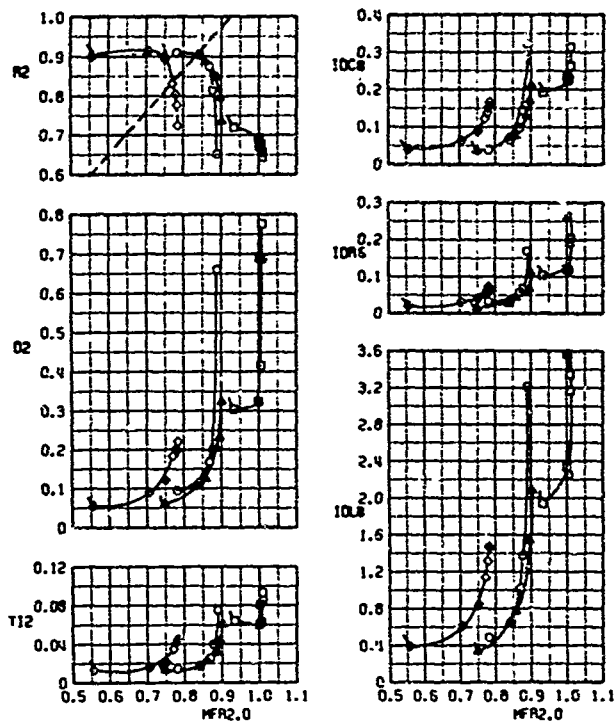
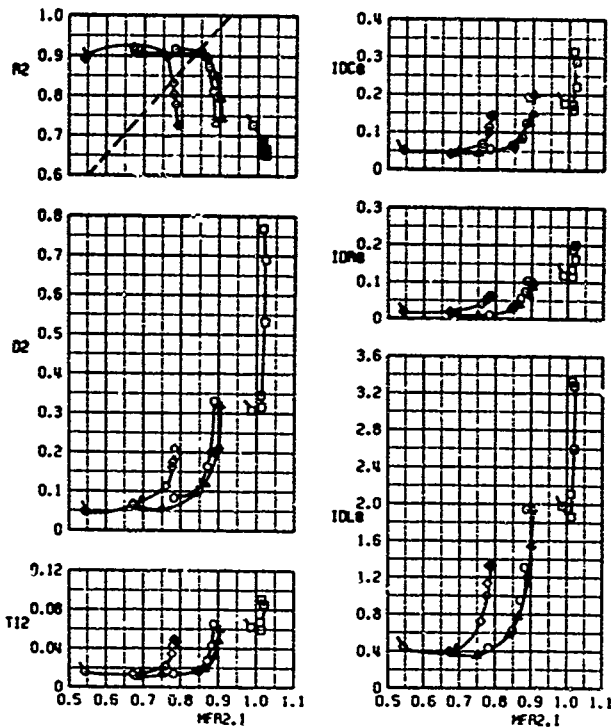
a. $MO = 2.2$, outboard

Figure 26. Inlet performance effects of extreme ramp geometry.

SYMBOL	α	ϕ	RS	HL	GEOMETRY
□	2.5	0	7.1	5.46	SUBSONIC 2172
△	2.5	0	14.9	3.46	MISPOSITIONED 2170
○	2.5	0	13.9	3.36	MO=2.2 CRUISE 2004
◇	2.5	0	18.0	2.94	MAX. SUPERSONIC 2169

FLAGGED SYM - STABILITY LIMIT

--- INTERMEDIATE POWER AIRFLOW, 36K II

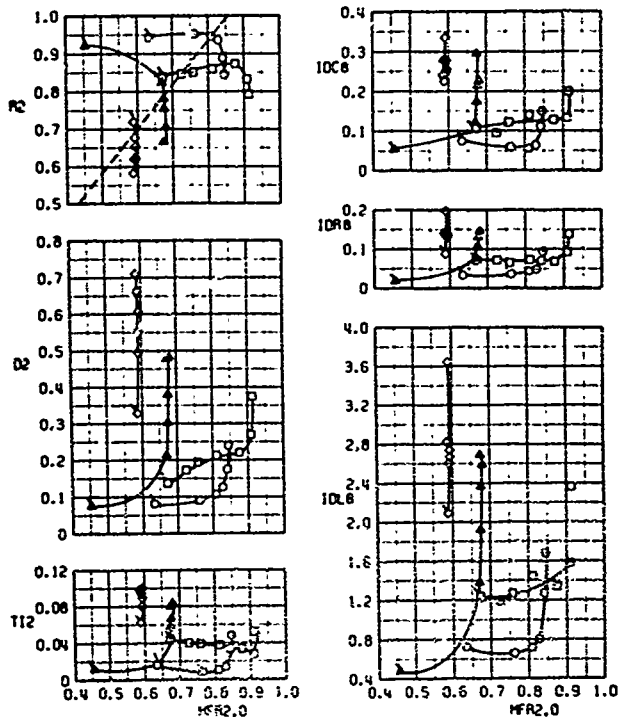


a. Concluded, inboard
Figure 26. Continued.

SYMBOL	α	ϕ	R_0	H_L	GEOMETRY	
\square	2.5	0	7.0	5.50	SUBSONIC	2119
\circ	2.5	0	11.4	4.34	MO = 1.8 CRUISE	2118
\triangle	2.5	0	14.0	3.36	MO = 2.2 CRUISE	2122
\diamond	2.5	0	18.0	2.95	MAX SUPERSONIC	2121

FLAGGED SYM-STABILITY LIMIT

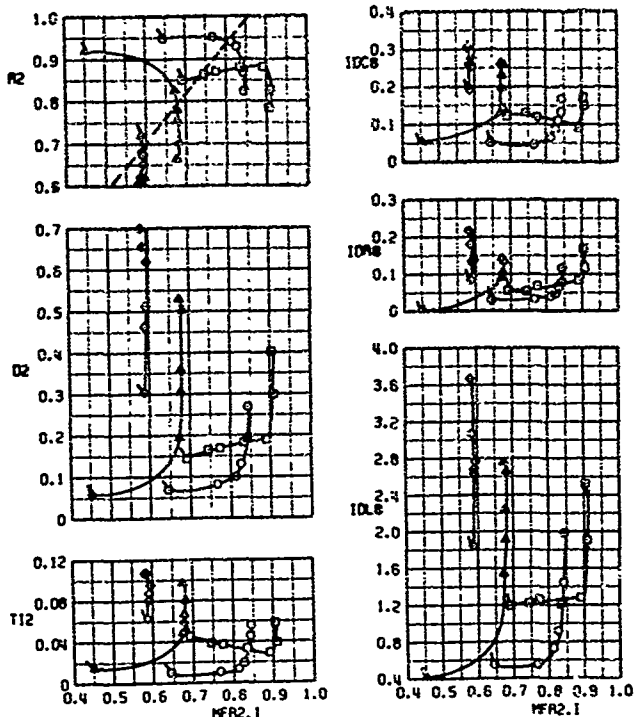
--- INTERMEDIATE POWER AIRFLOW, 35X II



b. $MO = 1.8$, outboard
Figure 26. Continued.

SYMBOL	α	ϕ	M_0	M_L	GEOMETRY	
\square	2.5	0	7.3	5.45	SUBSONIC	2119
\circ	2.5	0	11.4	4.34	NO = 1.8 CRUISE	2118
\triangle	2.5	0	13.9	3.26	NO = 2.2 CRUISE	2122
\diamond	2.5	G	18.0	2.94	MAX. SUPERSONIC	2121

FLANGED SYN STABILITY LIMIT
 --- INTERMEDIATE POWER AIRFLOW, 33K H

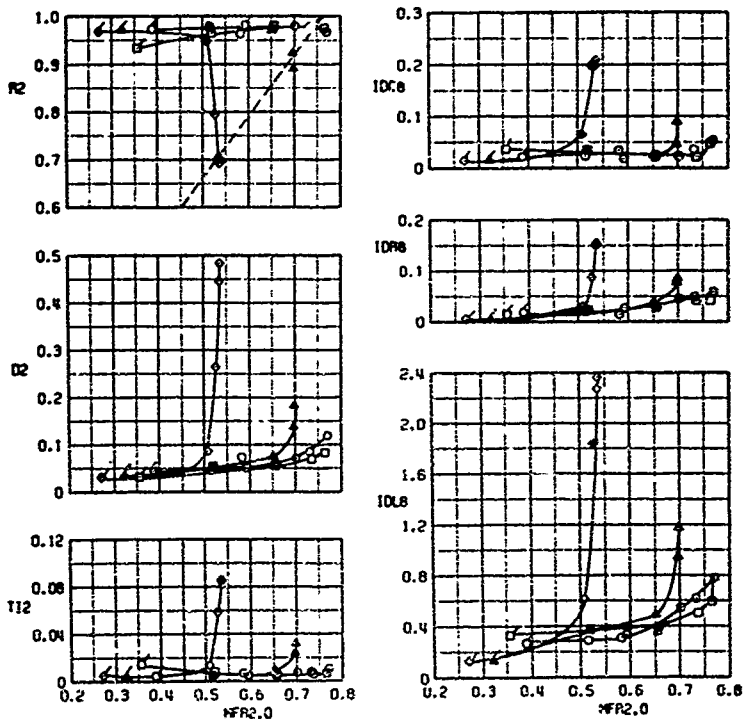


b. Concluded, inboard
 Figure 28. Continued.

SYMBOL	α	ϕ	RB	HL	GEOMETRY	
□	3.0	0.0	7.0	5.95	SUBSONIC	2699
△	3.0	0.0	7.0	4.91	MO = 1.4 CRUISE	2617
○	3.0	0.0	11.0	4.40	MO = 1.75 CRUISE	2614
◇	2.0	0.0	14.0	3.36	MO = 2.2 CRUISE	2615

FLAGGED SYM-STABILITY LIMIT

--- INTERMEDIATE POWER AIRFLOW, 36K II

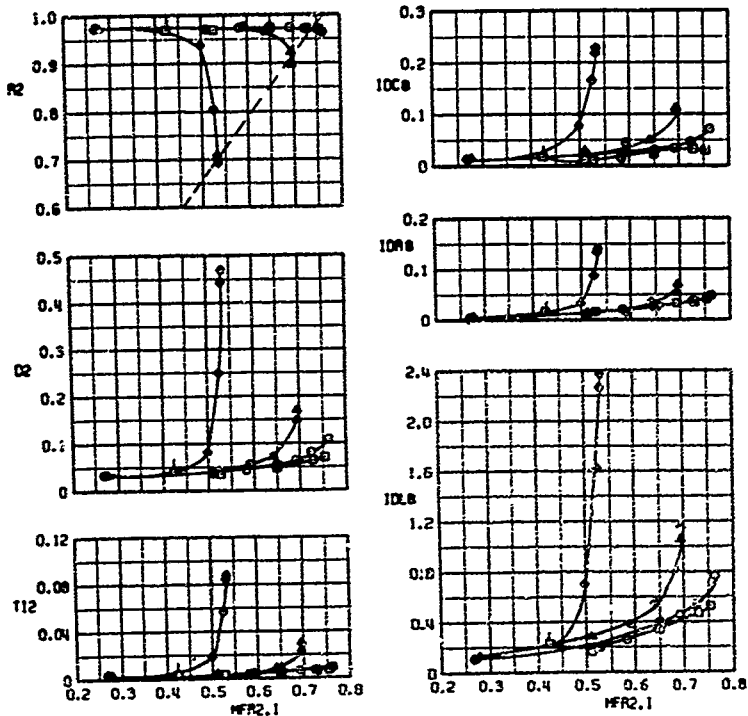


c. $M0 = 1.4$, outboard
Figure 26. Continued.

SYMBOL	α	ϕ	RB	HL	GEOMETRY	
O	3.0	0.0	7.0	5.96	SUBSONIC	2609
○	3.0	0.0	7.0	5.00	MO = 1.4 CRUISE	2617
△	3.0	0.0	11.0	4.40	MO = 1.75 CRUISE	2618
◆	3.0	0.0	14.0	3.36	MO = 2.2 CRUISE	2615

FLAGGED SYM - STABILITY LIMIT

--- INTERMEDIATE POWER AIRFLOW, 36K 11



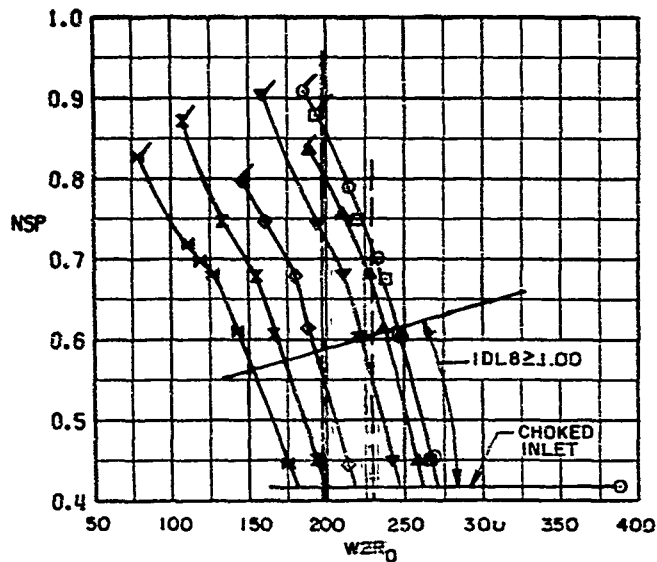
c. Concluded, inboard
Figure 26. Concluded.

SYMBOL	U
○	SEALED 2084
□	0 2184
△	5 2185
▽	10 2186
◇	20 2187
×	30 2188
⋈	52 2190

FLAGGED SYM-STABILITY LIMIT

--- INTERMEDIATE POWER, 36K ft

--- IDLE POWER, 36K ft

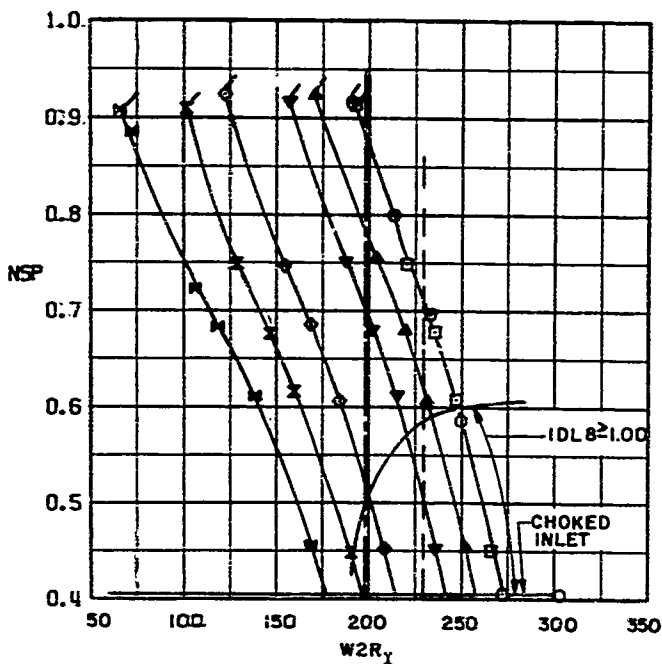
a. $M_0 = 2.2$, outboardFigure 27. Bypass door effectiveness at $c = 2.5$ deg, $\psi = 0$.

SYMBOL	U
○	SERLED 2084
□	0 2184
▲	5 2185
▼	10 2186
◇	20 2187
×	30 2188
✱	52 2190

FLAGGED SYM - STABILITY LIMIT

— INTERMEDIATE POWER, 36K ft

— IDLE POWER, 36K ft



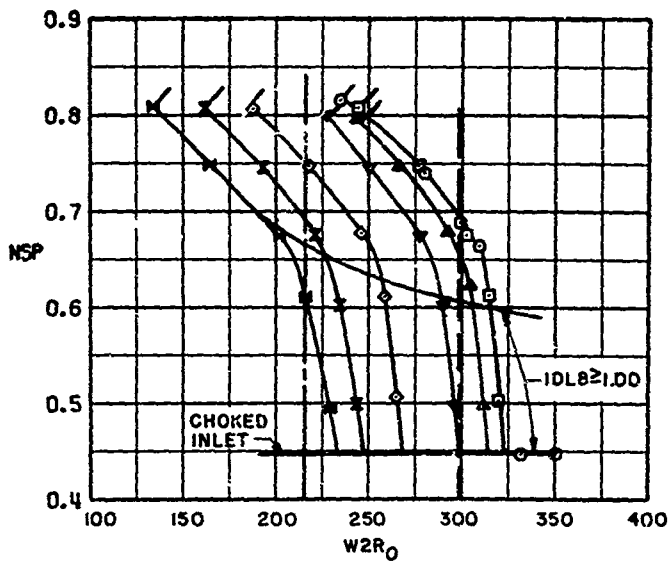
2. Concluded, inboard
Figure 27. Continued.

SYMBOL	U	
○	SEALED	2118
□	0	2211
△	5	2212
▽	10	2213
◇	20	2214
×	30	2215
■	50	2217

FLAGGED SYM - STABILITY LIMIT

--- INTERMEDIATE POWER, 36 K ft

--- IDLE POWER, 36 K ft

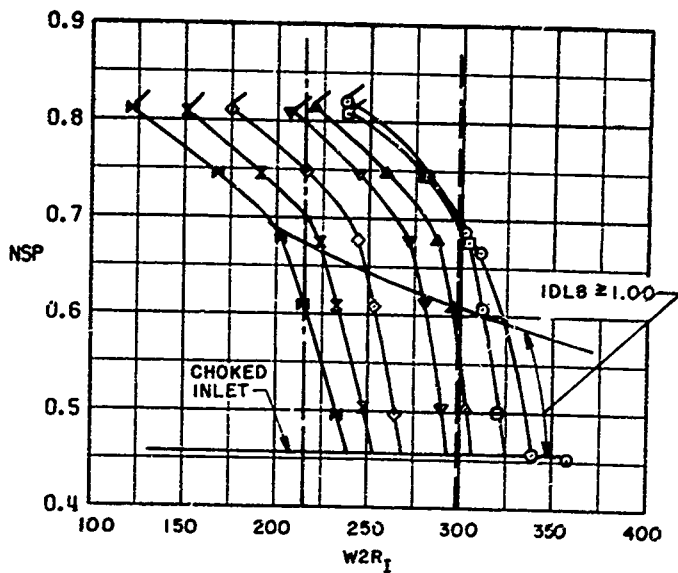


b. $M_0 = 1.8$, outboard
Figure 27. Continued.

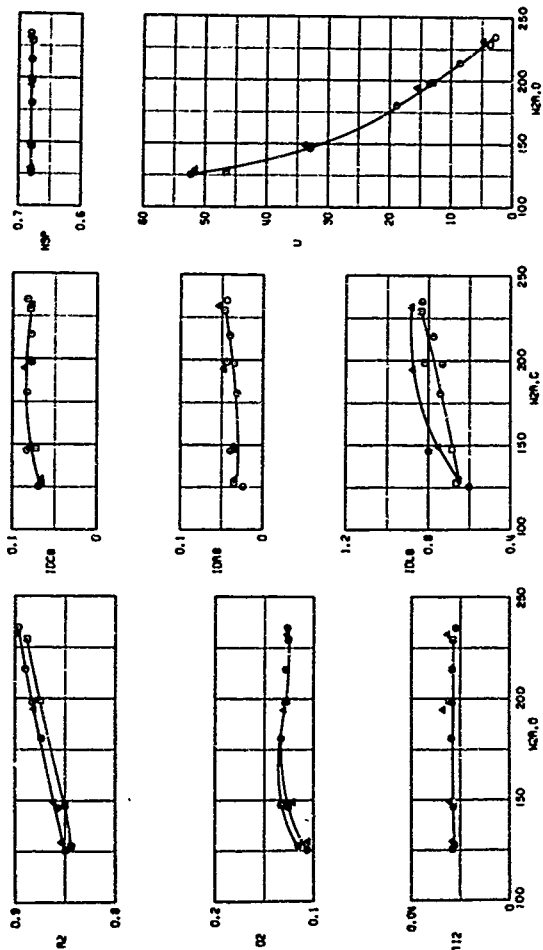
SYMBOL	U	
○	SEALED	2116
□	0	2211
△	5	2212
▽	10	2213
◇	20	2214
×	30	2215
M	50	2217

FLAGGED SYM - STABILITY LIMIT

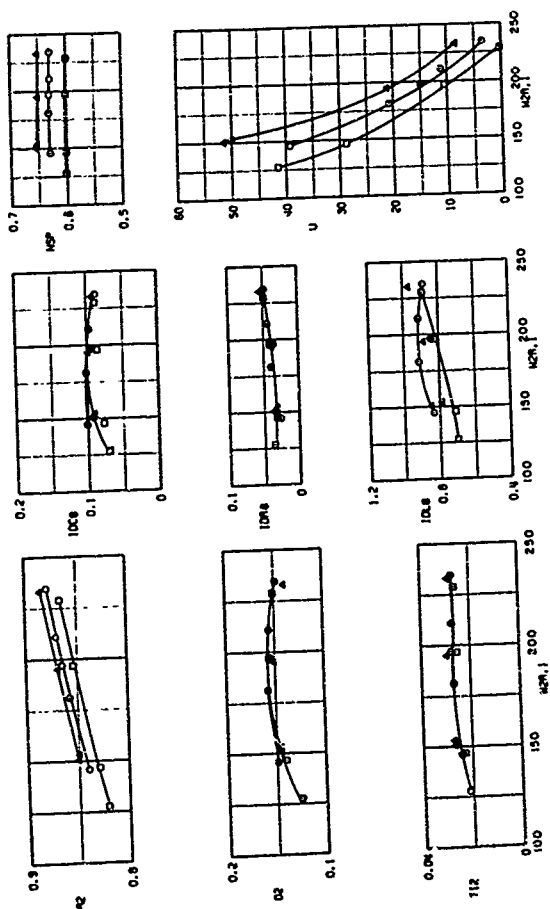
--- INTERMEDIATE POWER, 36K f1
 --- IDLE POWER, 36K f1



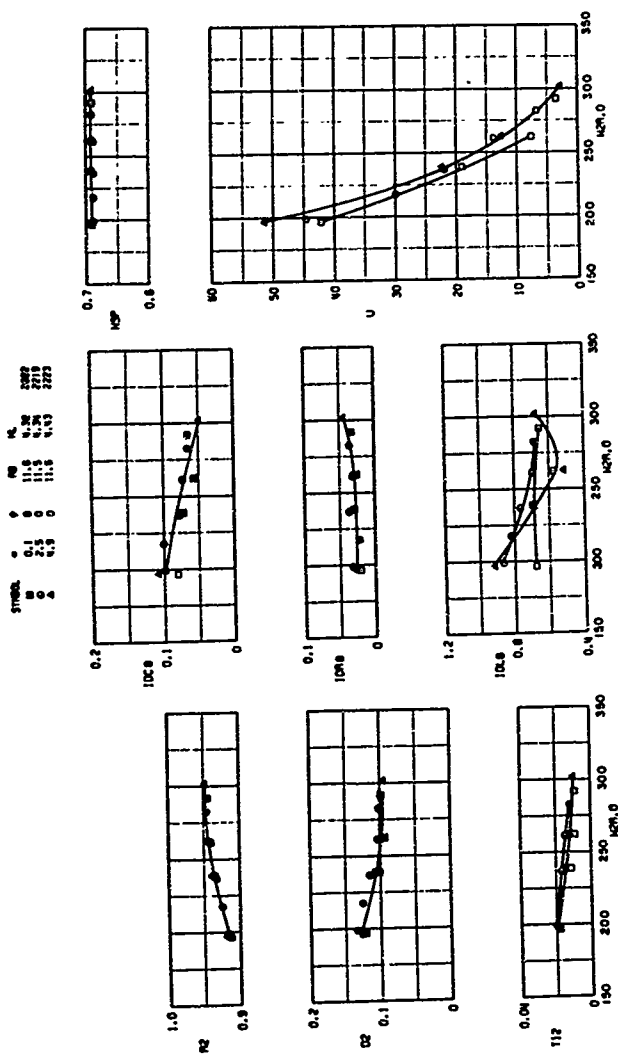
b. Concluded, inboard
 Figure 27. Concluded.

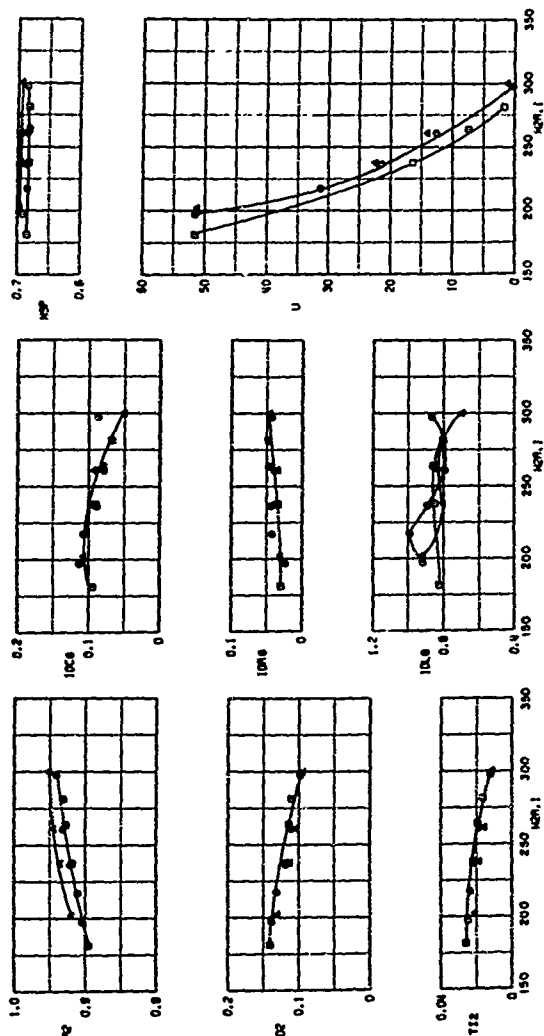


a. $M_0 = 2.2$, outboard

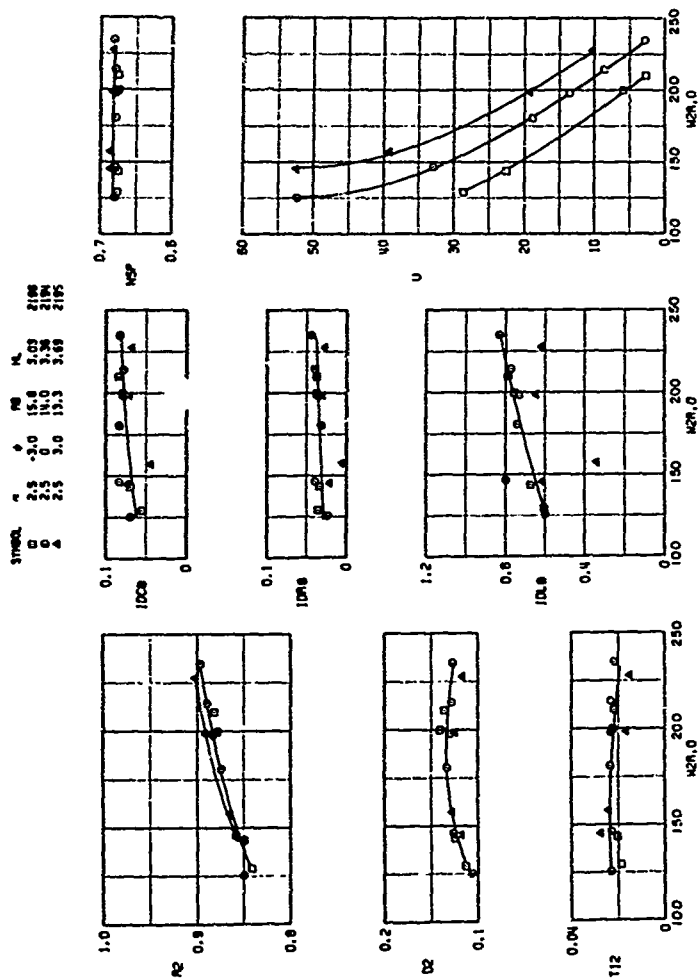


a. Concluded, inboard
Figure 28. Continued.

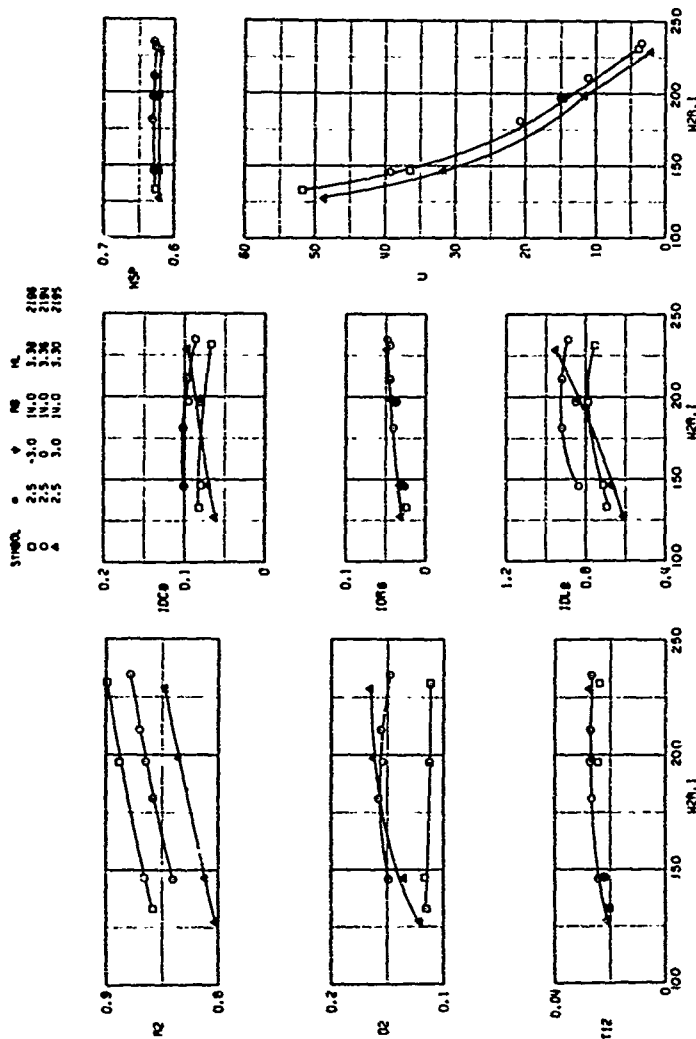




b. Concluded, inboard Figure 28. Concluded.

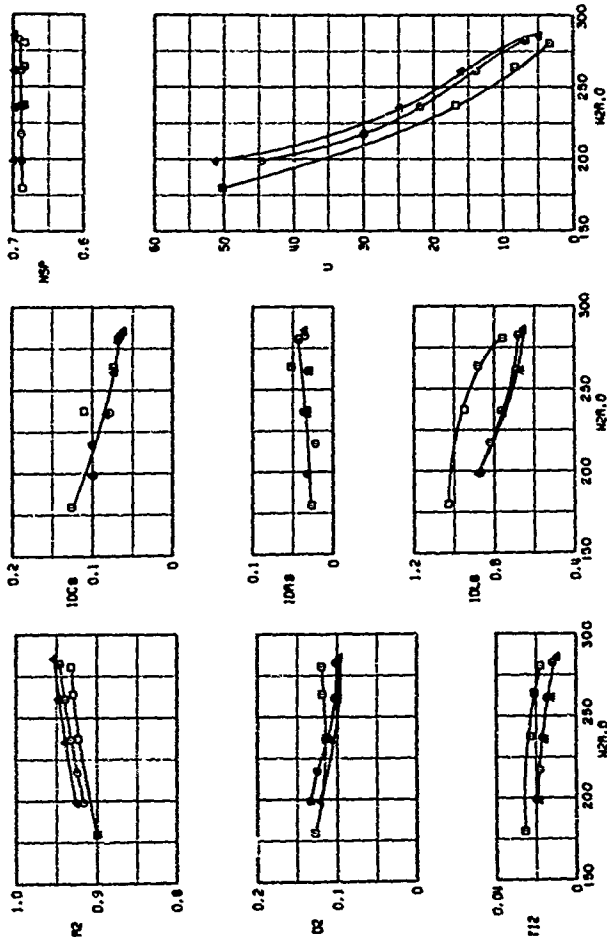


a. $M_0 = 2.2$, outboard
 Figure 29. Effects of airflow variations on inlet performance with inlet operated under simulated AICS control, $\alpha = 2.5^\circ$.

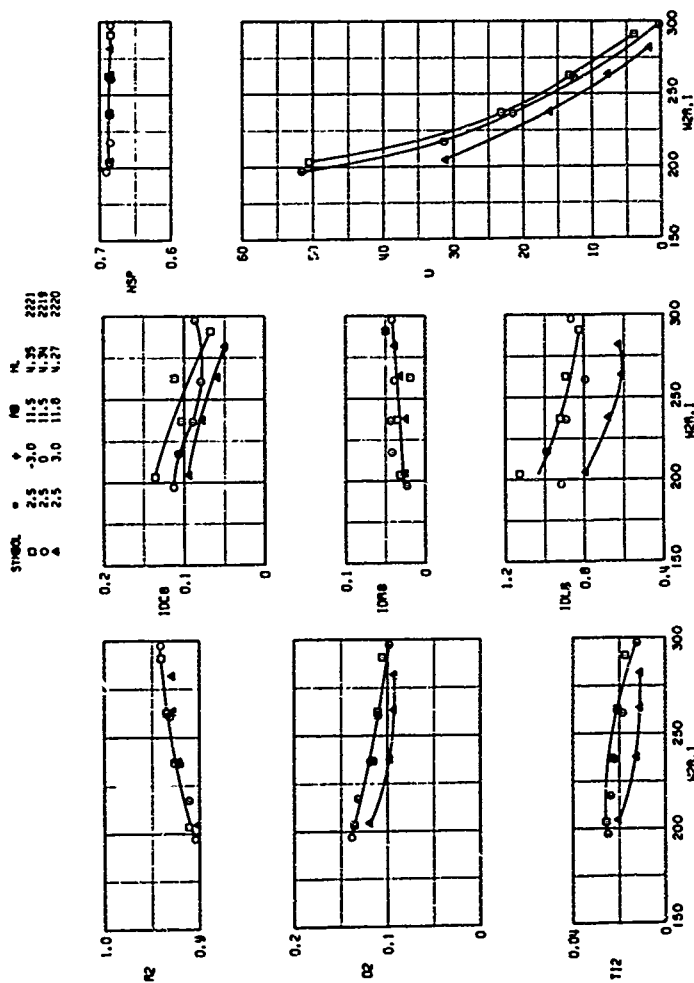


a. Concluded, inboard
Figure 29. Continued.

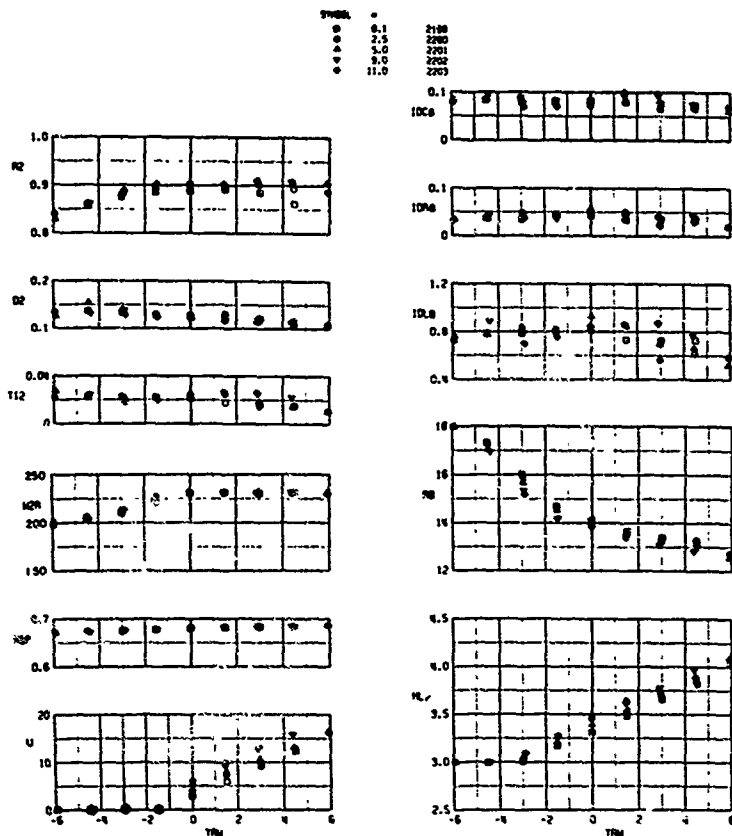
SYMBOL = γ M_0 M_L
 □ 2.5 -2.0 12.5 2221
 ○ 2.5 0 11.5 2218
 △ 2.5 5.0 10.0 2220



b. $M_0 = 1.8$, outboard
 Figure 29, Continued.



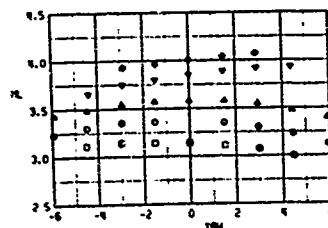
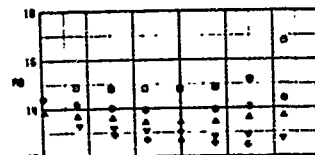
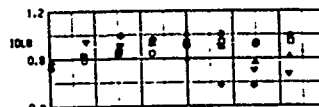
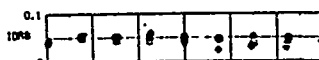
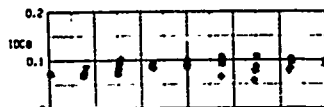
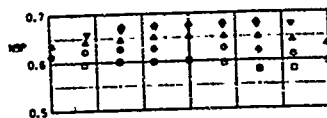
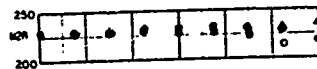
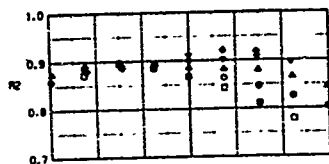
b. Concluded, inboard
Figure 29. Concluded.



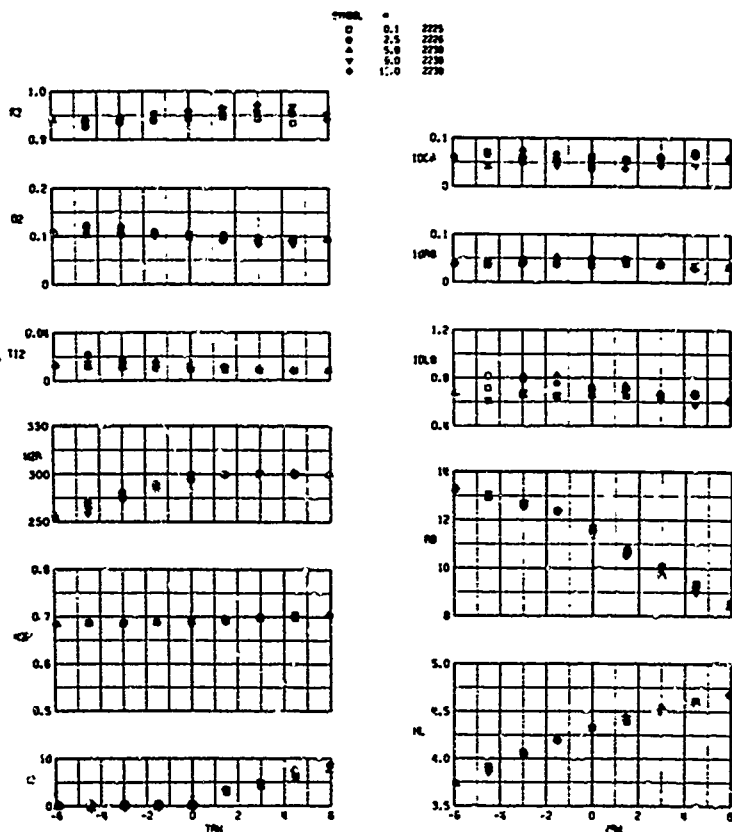
a. $M_0 = 2.2$, outboard

Figure 30. Inlet performance characteristics with inlet operated under simulated AICS control and at engine intermediate airflows.

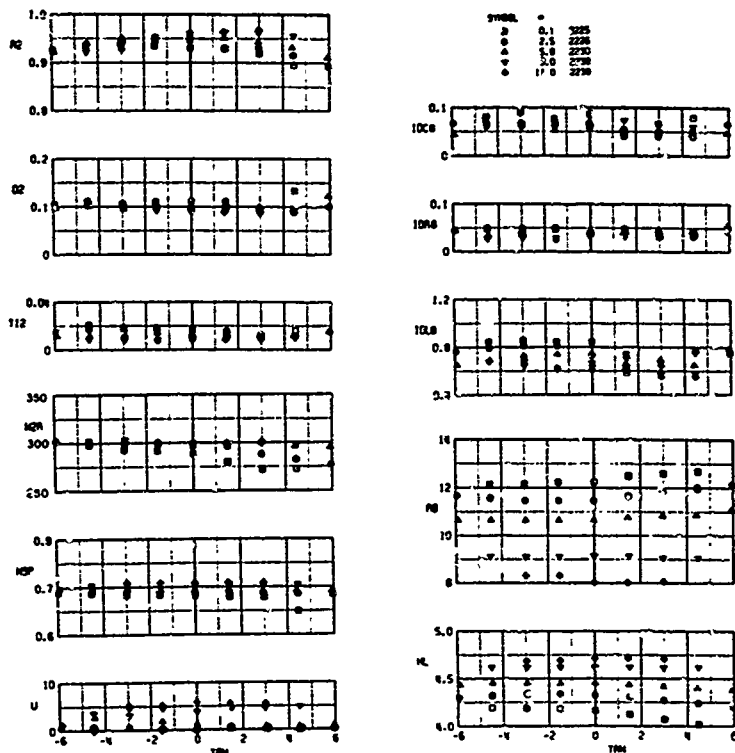
SYMBOL	α	
○	0.1	2198
□	2.5	2200
△	5.0	2201
▽	10.0	2202
●	111.0	2203



a. Concluded, inbound
Figure 30. Continued.



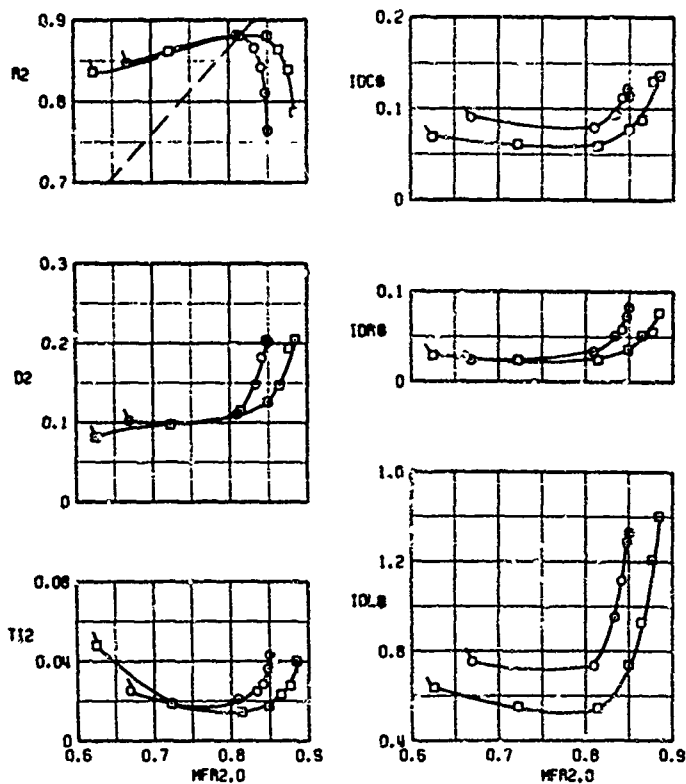
b. $M_0 = 7.8$, outboard
Figure 30. Continued.



b. Concluded, Inboard
Figure 30. Concluded.

STN00	=	ψ	PO	PL	
○	-2.0	0.0	14.2	3.22	SCHEDULED 2265
□	-2.0	0.0	13.7	3.49	Let FS > SCHEDULED 2281

FLAGGED SYM - STABILITY LIMIT
 --- INTERMEDIATE POWER AIRFLOW, 36K II

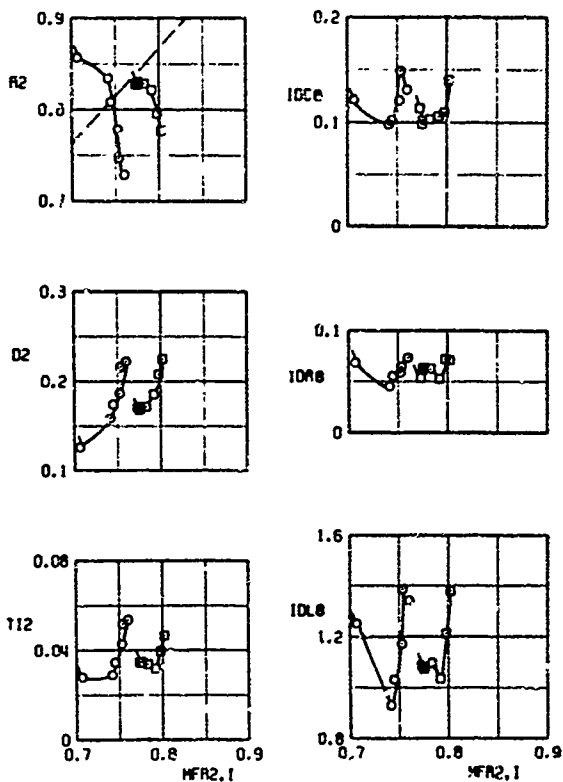


a. $\alpha = -2$ deg, $\psi = 0$, outboard

Figure 31. Effects of mispositioned inlet geometry on inlet performance at $M_0 = 2.2$.

SYMBOL	α	ψ	PS	HL		
O	-2.0	0.0	15.7	3.00	SCHEDULED	2265
□	-2.0	0.0	14.5	3.20	1-Hz. PS>SCHEDULED	2281

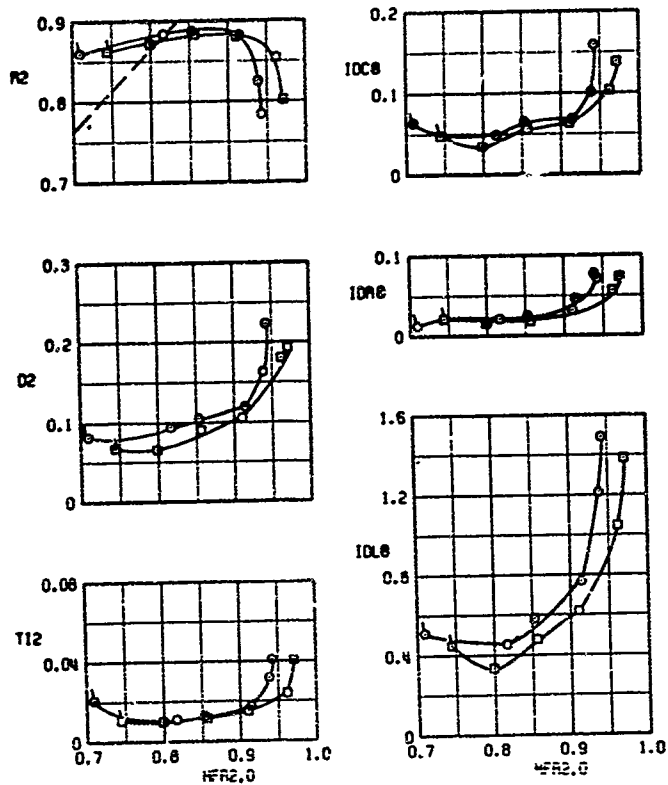
FLAGGED SYM - STABILITY LIMIT
 --- INTERMEDIATE POWER AIRFLOW, 36K II



a. Concluded, inboard
 Figure 31. Continued.

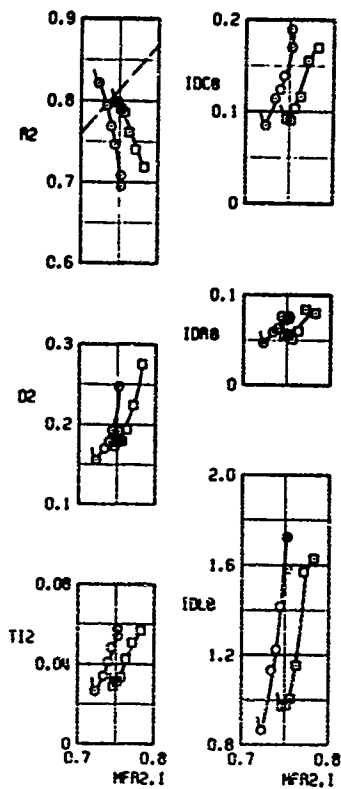
SYMBOL	α	ψ	R0	HL		
○	0.1	3.0	13.4	3.66	SCHEDULED	2299
□	0.1	3.0	13.0	3.86	1- α .FS>SCHEDULED	2204

FLAGGED SYM - STABILITY LIMIT
INTERMEDIATE POWER AIRFLOW, 36X II



$\alpha = 0.1$ deg. $\psi = 3$ deg. outboard
Figure 31 Continued.

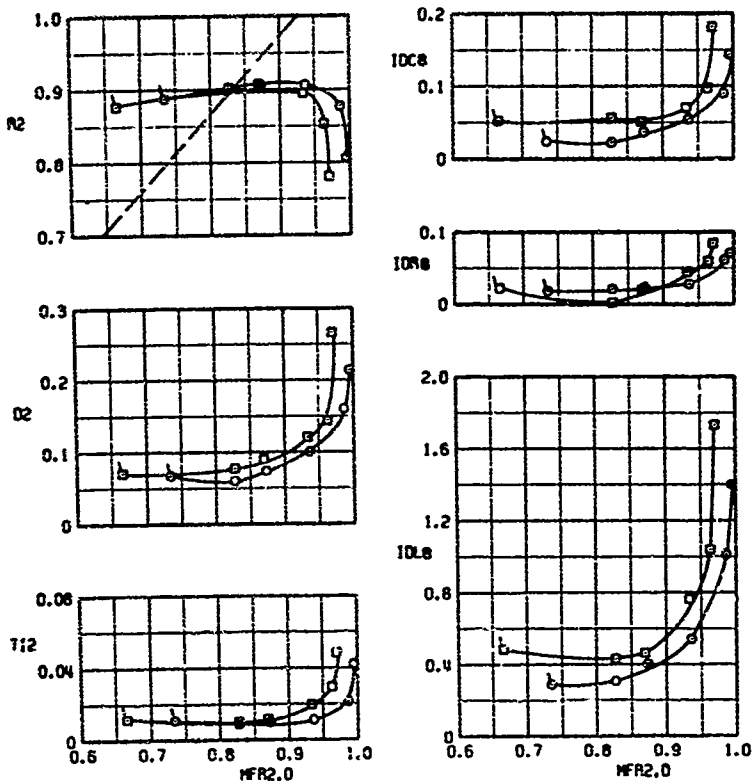
SYMBOL α ϕ P_0 M_∞
 ○ 0.1 3.0 15.2 3.07 SCHEDULED 2200
 □ 0.1 3.0 14.3 3.27 H₂ F₂ SCHEDULED 2200
 FLAGGED SYM - STABILITY LIMIT
 --- INTERMEDIATE POWER AIRFLOW, 36 K N



b. Concluded, inboard
 Figure 31. Continued.

SYMBOL	α	ψ	RE	HL		
○	2.5	4.5	13.3	3.85	SCHEDULED	2276
□	2.5	4.5	13.3	3.65	1/4a FS < SCHEDULED	2266

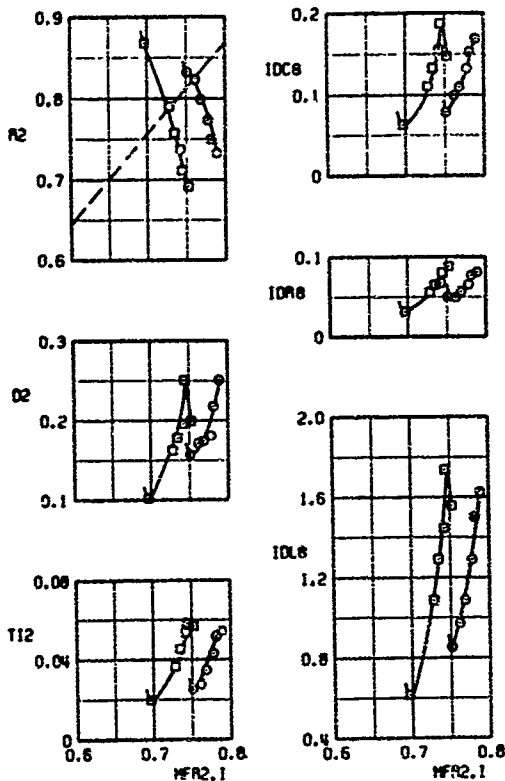
FLASSED SYM- STABILITY LIMIT
 ----- INTERMEDIATE POWER AIRFLOW, 36K ft



c. $\alpha = 2.5$ deg, $\psi = 4.5$ deg, outboard
 Figure 31. Continued.

SYMBOL	α	ϕ	PR	PL		
○	2.5	4.5	14.4	3.23	SCHEDULED	2276
□	2.5	4.5	16.4	3.03	1-in. FS<SCHEDULED	2296

FLAGGED SYM - STABILITY LIMIT
 --- INTERMEDIATE POWER AIRFLOW, 36K ft

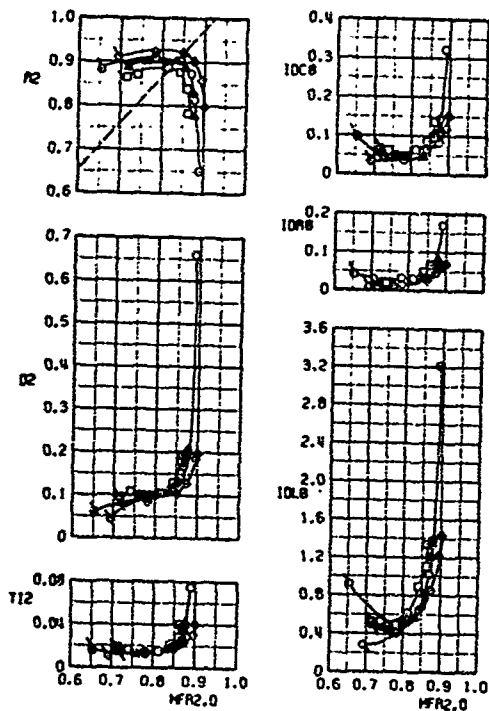


c. Concluded, inboard
 Figure 31. Concluded.

SYMBOL	α	ψ	NO	ML	
\square	-2.0	0.2	14.0	3.36	2150
\triangle	0.0	0.2	14.0	3.36	2152
\circ	2.5	0.0	14.0	3.36	2004
\diamond	9.0	0.0	14.0	3.36	2167

FLAGGED SYM - STABILITY LIMIT

--- INTERMEDIATE POWER AIRFLOW, 36K II

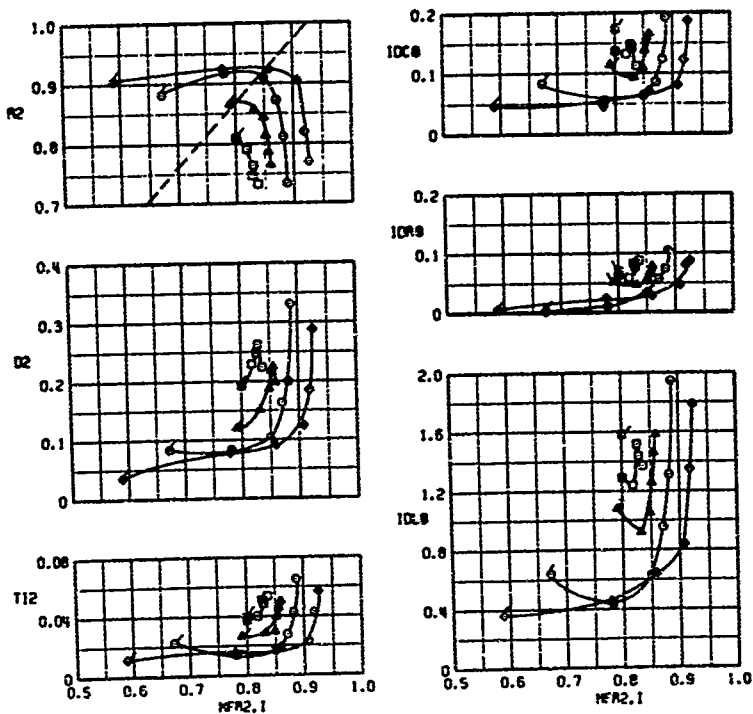


a. α = variable, ψ = variable, outboard
 Figure 32. Inlet performance characteristics with M0 scheduled geometry
 at M0 = 2.2.

SYMBOL	α	ϕ	RB	RL
□	-2.0	0.2	14.0	3.36
△	0.0	0.2	14.0	3.36
○	2.5	0.0	14.0	3.36
●	9.0	0.0	14.0	3.36

FLAGGED SYM - STABILITY LIMIT

--- INTERMEDIATE POWER AIRFLOW, 36K II

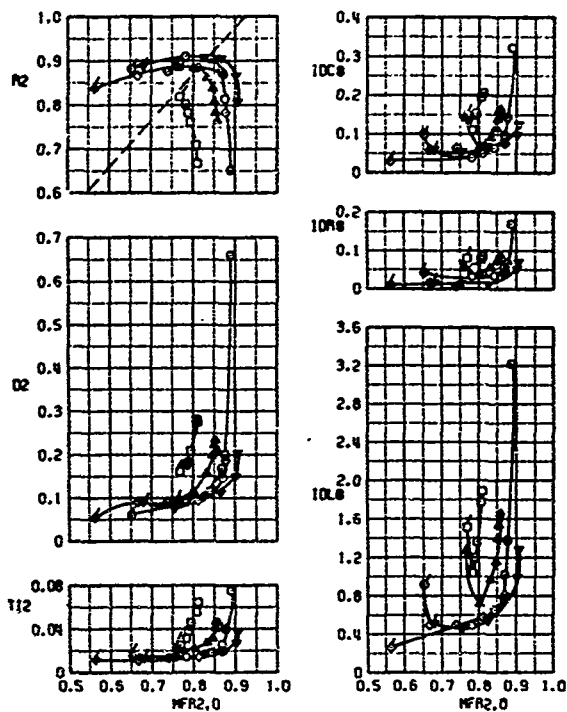


a. Concluded, inboard
Figure 32. Continued.

SYMBOL	α	ψ	M_2	M_L	
\square	2.5	-5.8	14.0	3.36	2157
\triangle	2.5	-2.8	14.0	3.36	2160
\circ	2.5	0.0	14.0	3.36	2204
∇	2.5	3.2	14.0	3.36	2161
\diamond	2.5	5.8	14.0	3.36	2164

FLAGGED SYM-STABILITY LIMIT

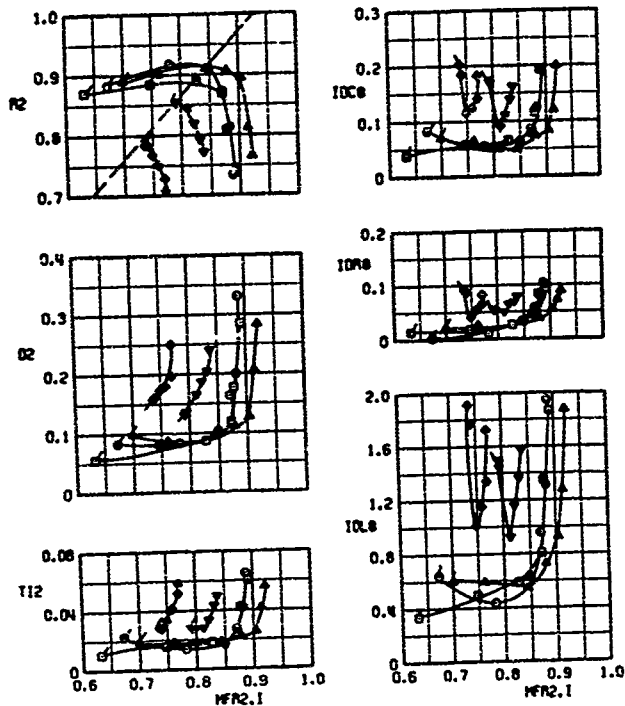
--- INTERMEDIATE POWER AIRFLOW, 36X 11



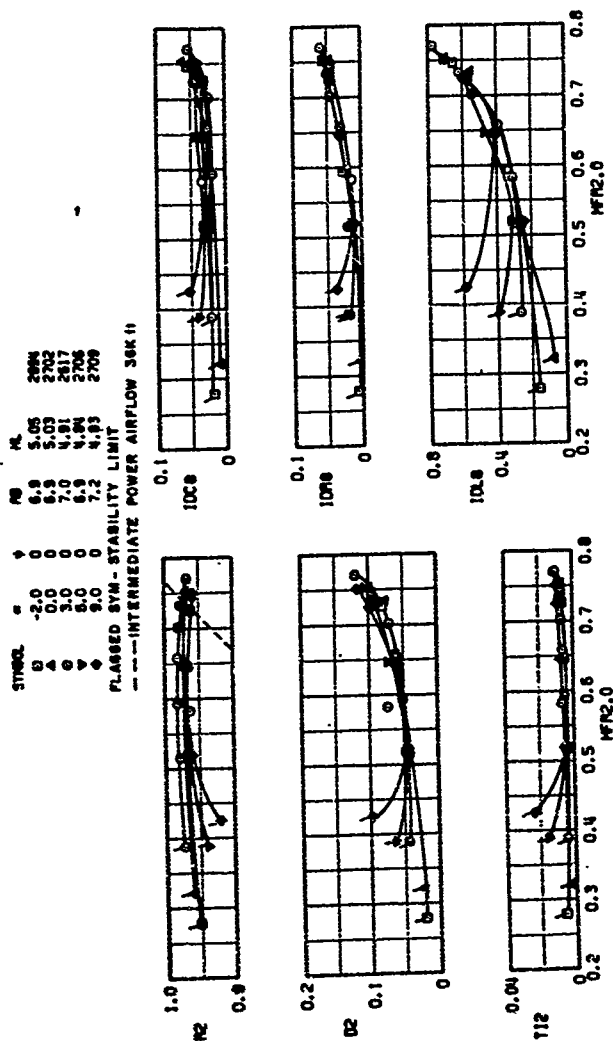
b. $\alpha = 2.5$ deg, ψ = variable, outboard
Figure 32. Continued.

SYMBOL	α	ϕ	RB	HL	
□	2.5	-5.0	14.0	3.36	2157
△	2.5	-2.0	14.0	3.36	2160
○	2.5	0.0	14.0	3.36	2004
◇	2.5	3.2	14.0	3.36	2161
▽	2.5	5.0	14.0	3.36	2164

FLAGGED SYM - STABILITY LIMIT
 --- INTERMEDIATE POWER AIRFLOW, 36K ft



b. Concluded, inboard
 Figure 32. Concluded.

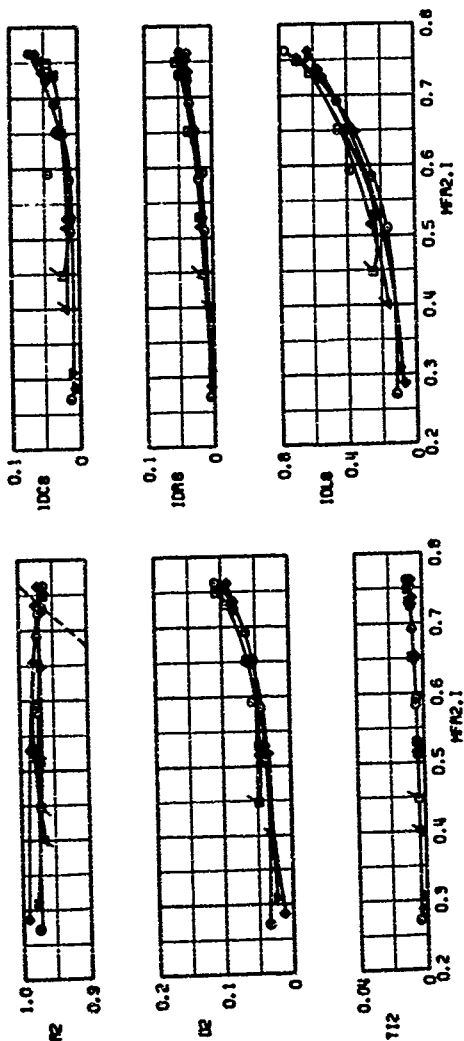


a. $M_0 = 1.4$, α = variable, outboard
 Figure 33. Transonic inlet performance characteristics at $\psi = 0$.

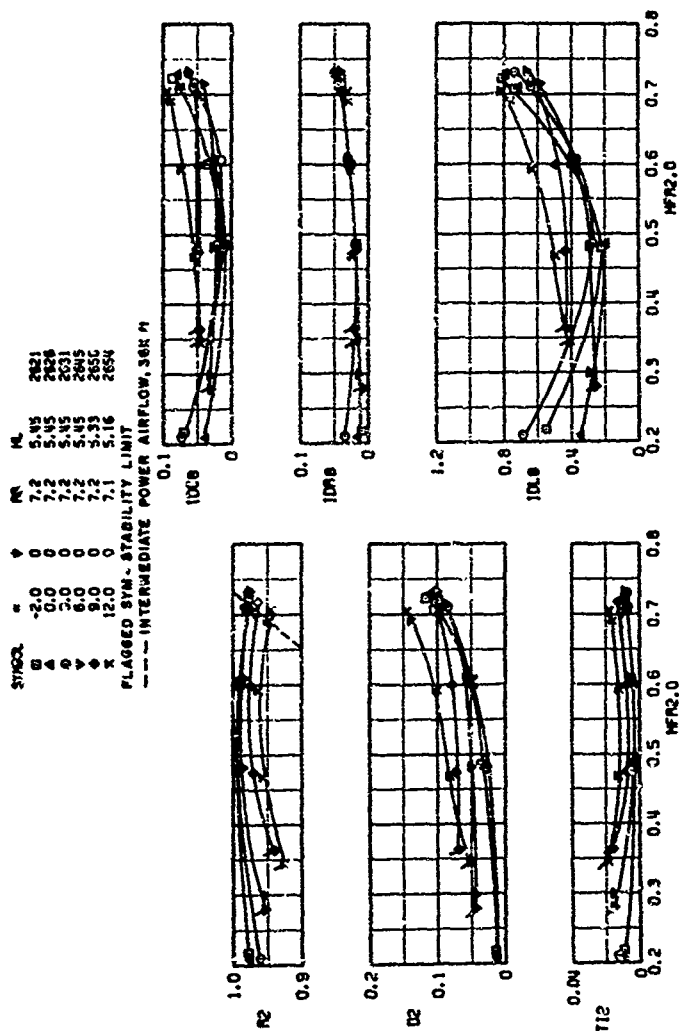
SYMBOL	α	β	PS	HL
20	-2.0	0	7.0	4.87
4	0.0	0	7.0	2094
4	0.0	0	7.0	4.81
4	2.0	0	7.0	2702
4	4.0	0	7.0	5.00
4	6.0	0	7.0	2717
4	8.0	0	7.0	5.09
4	9.0	0	7.0	2734
4	9.0	0	7.0	5.19
4	9.0	0	7.0	2709

FLAGGED SYM - STABILITY LIMIT

--- INTERMEDIATE POWER AIRFLOW 304 (1)



a. Concluded, inboard
Figure 33. Continued.

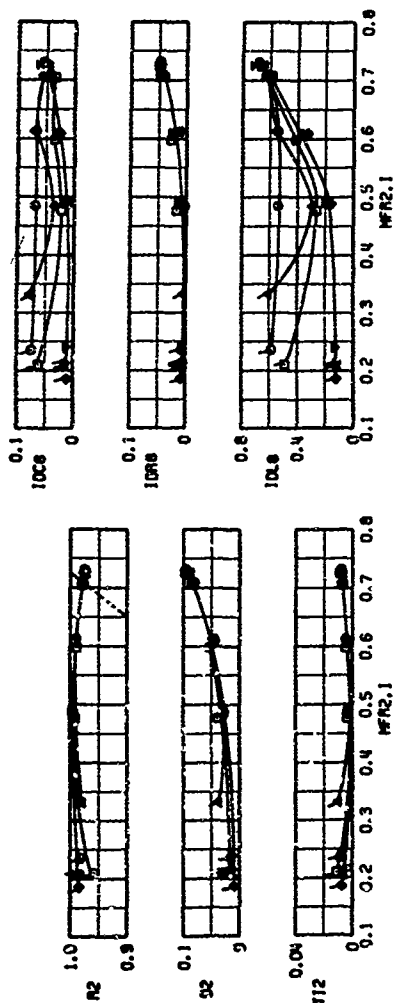


b. $M_0 = 0.85$, $\alpha = \text{variable}$, outboard
 Figure 33. Continued.

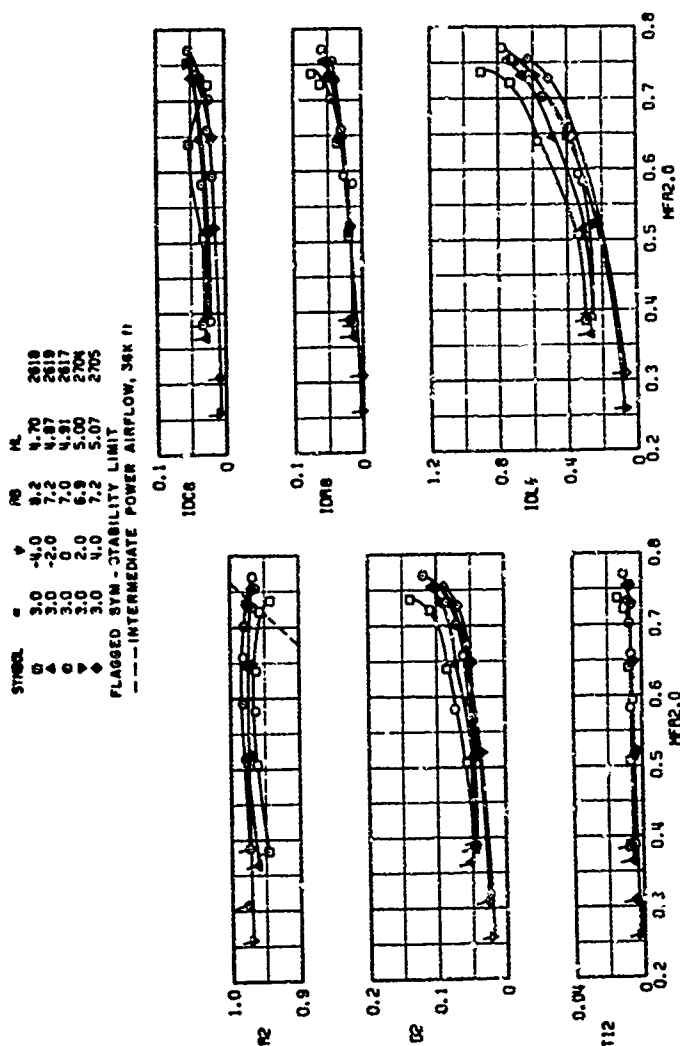
SYMBOL	"	↑	PS	HL	
□	-2.0	0	7.0	5.46	2821
△	0.0	0	7.0	5.46	2826
●	3.0	0	7.0	5.46	2831
▽	6.0	0	7.0	5.46	2845
+	9.0	0	7.0	5.46	2850
x	12.0	0	7.0	5.46	2854

FLAGGED SYM - STABILITY LIMIT

--- INTERMEDIATE POWER AIRFLOW, 30K II



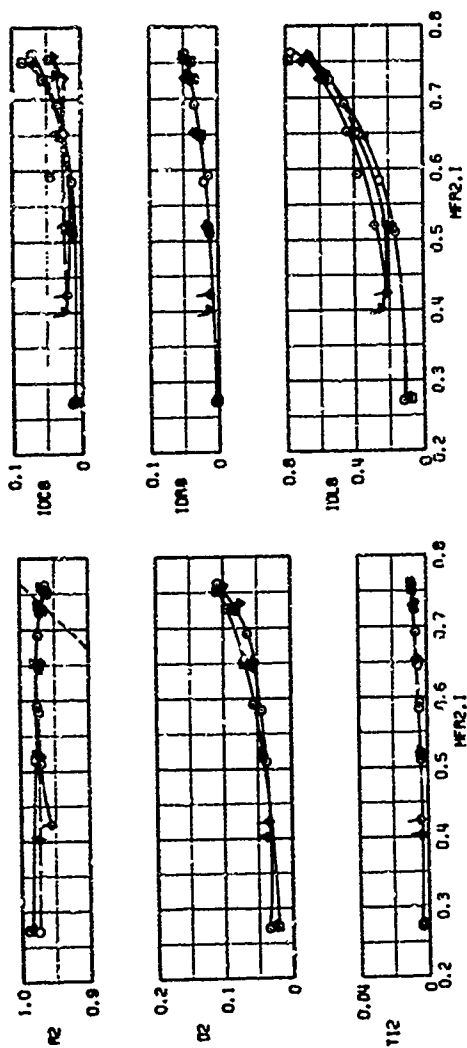
b. Concluded, Inboard
Figure 33. Concluded.



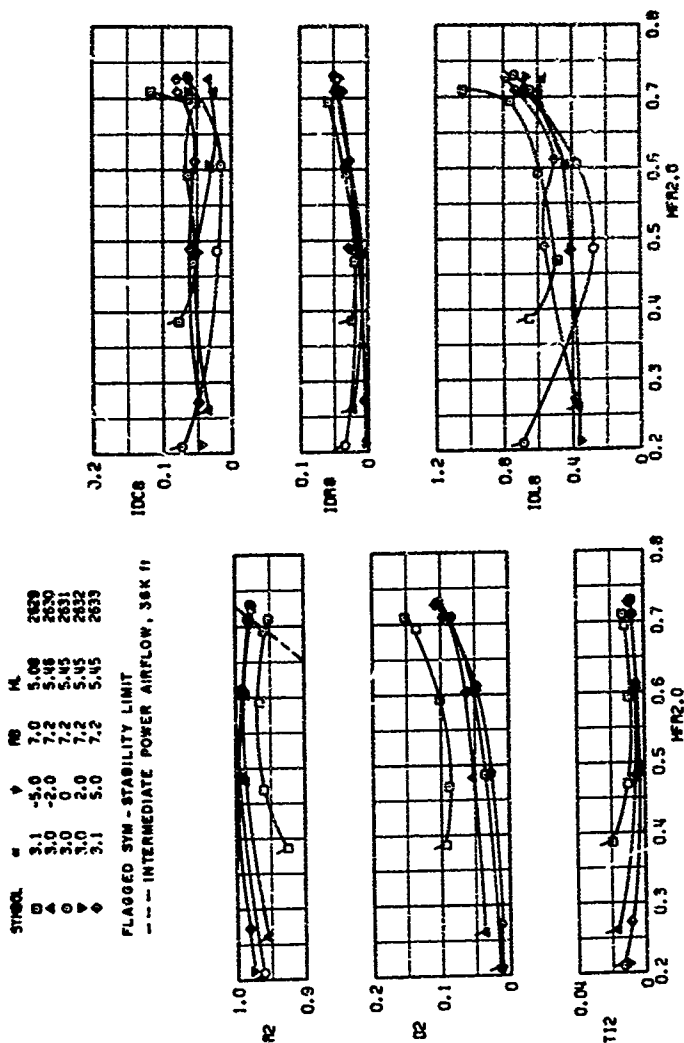
a. $M_0 = 1.4$, $\psi = \text{variable}$, outboard
 Figure 34. Transonic inlet performance characteristics at $\alpha = 3.0$ deg.

SYMBOL	α	β	MD	ML	20/8
□	3.0	-4.0	7.0	4.99	2618
△	3.0	-2.0	7.0	5.03	2619
○	3.0	0	7.0	5.00	2617
▽	3.0	2.0	7.0	4.99	2704
◇	3.0	4.0	7.0	4.99	2705

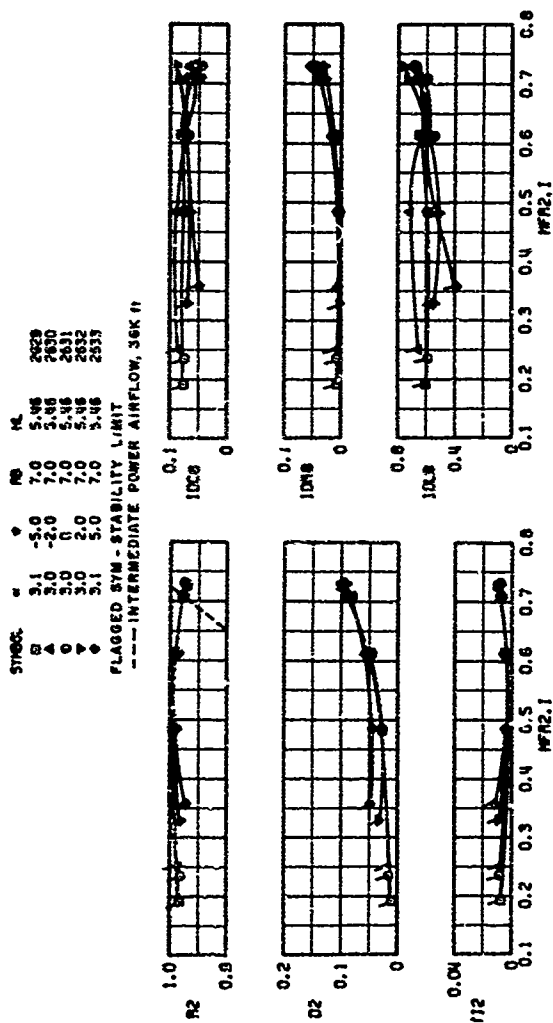
FLAGGED SYM - STABILITY LIMIT
 --- INTERMEDIATE POWER AIRFLOW, 36K II



a. Concluded, inboard
 Figure 34. Continued.



b. $MO = 0.85$, $\psi = \text{variable}$, outboard
 Figure 34. Continued.



b. Concluded, inboard
 Figure 3A. Concluded.

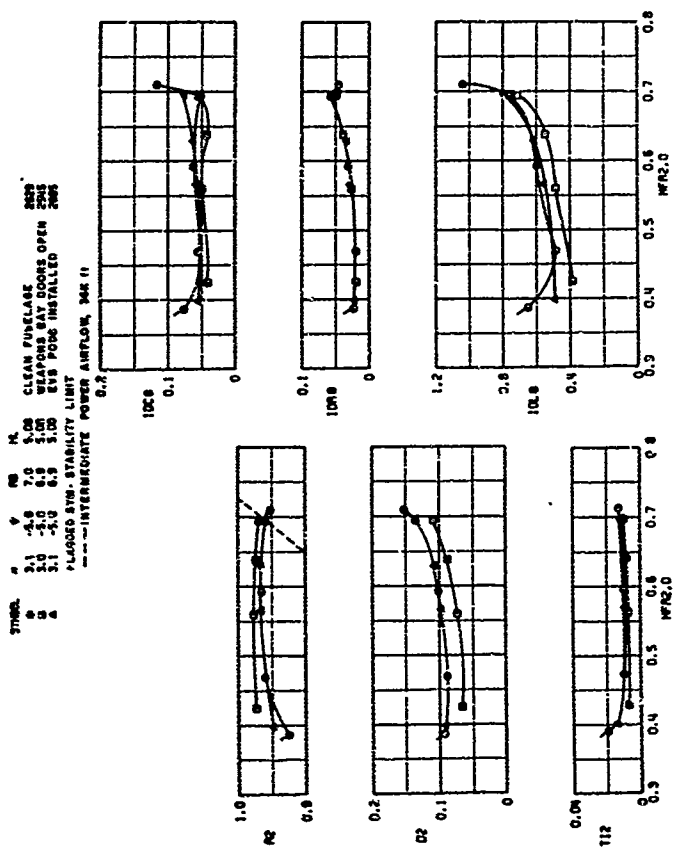
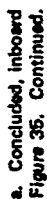
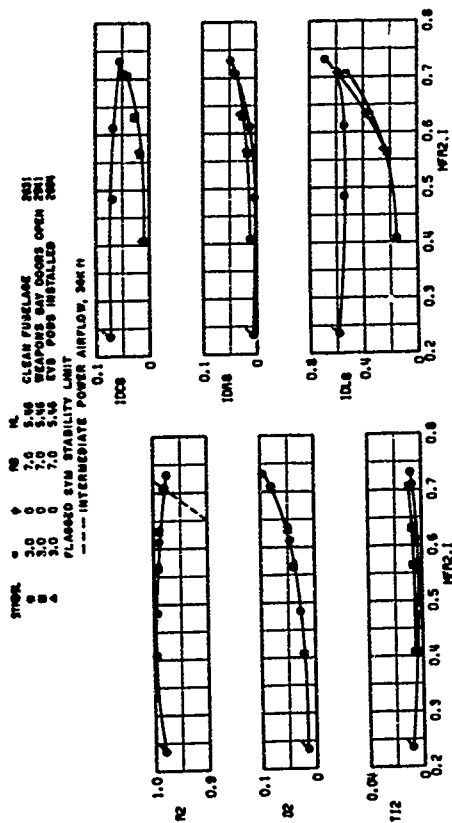
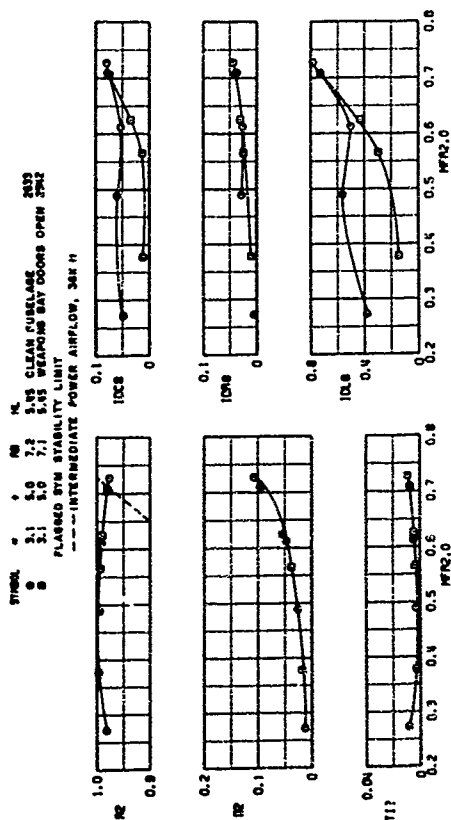


Figure 35. Effects of opened weapons bay doors and EVS pods at $M_0 = 0.85$.
 $\alpha, \psi = 15^\circ$ deg, outboard

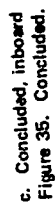


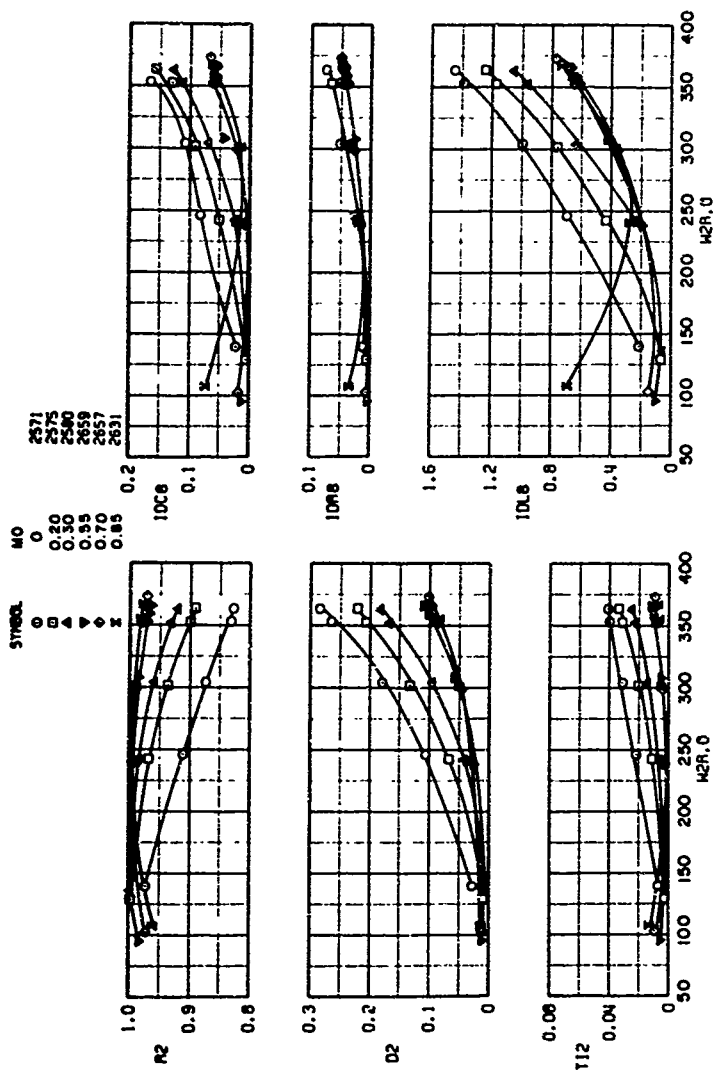


b. $\psi = 0$, outboard
 Figure 35. Continued.



$\phi, \psi = 5$ deg, outboard
Figure 35. Continued.





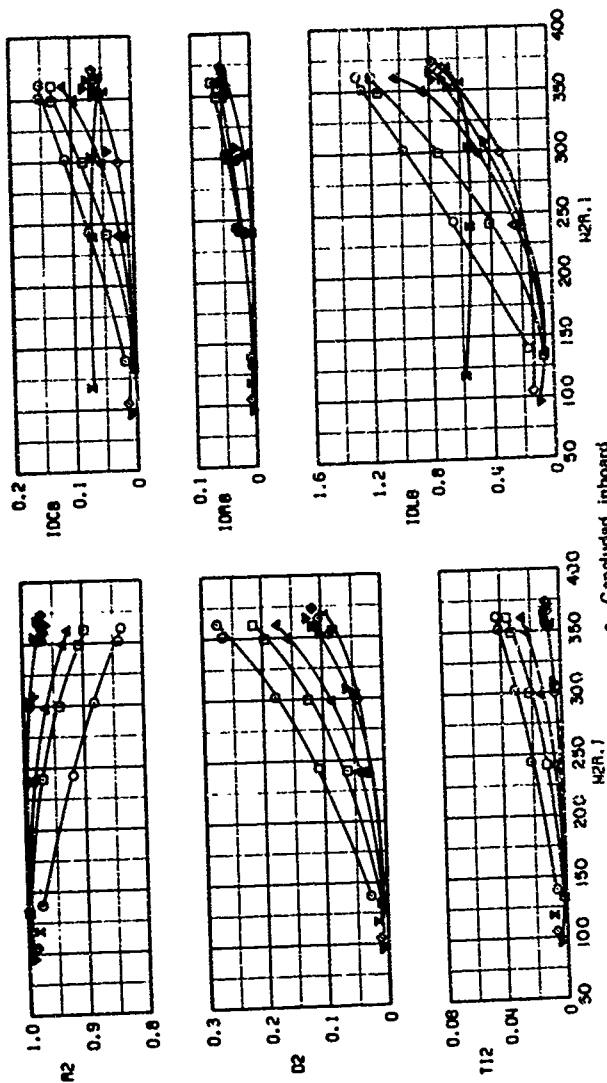
a. Cruise cowl, outboard

Figure 36. Effects of cruise and takeoff cowl lip positions on subsonic inlet performance.

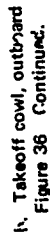
SYMBOL
 O
 □
 ▲
 ◆
 X

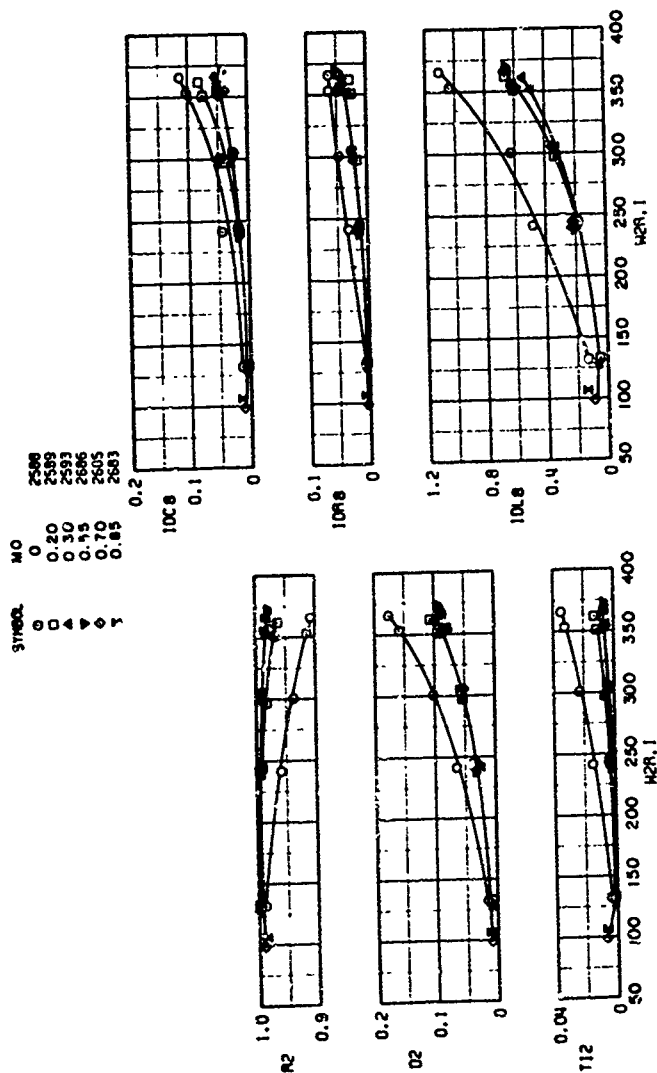
MO
 2571
 2575
 2580
 2659
 2657
 2631

FLAGGED SYM - STABILITY LIMIT

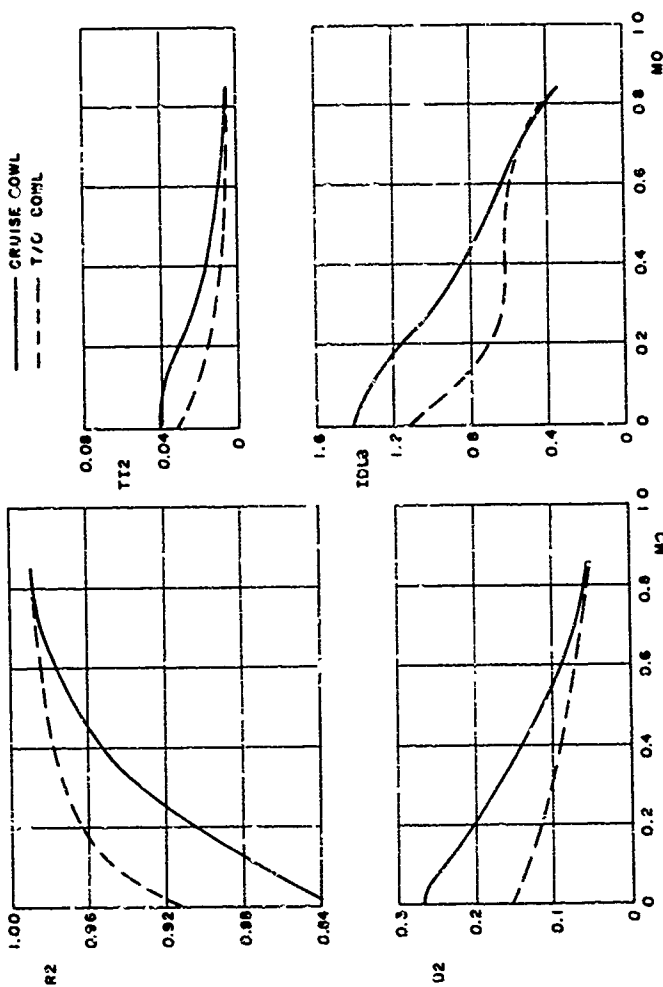


a. Concluded, inboard
 Figure 36. Continued.

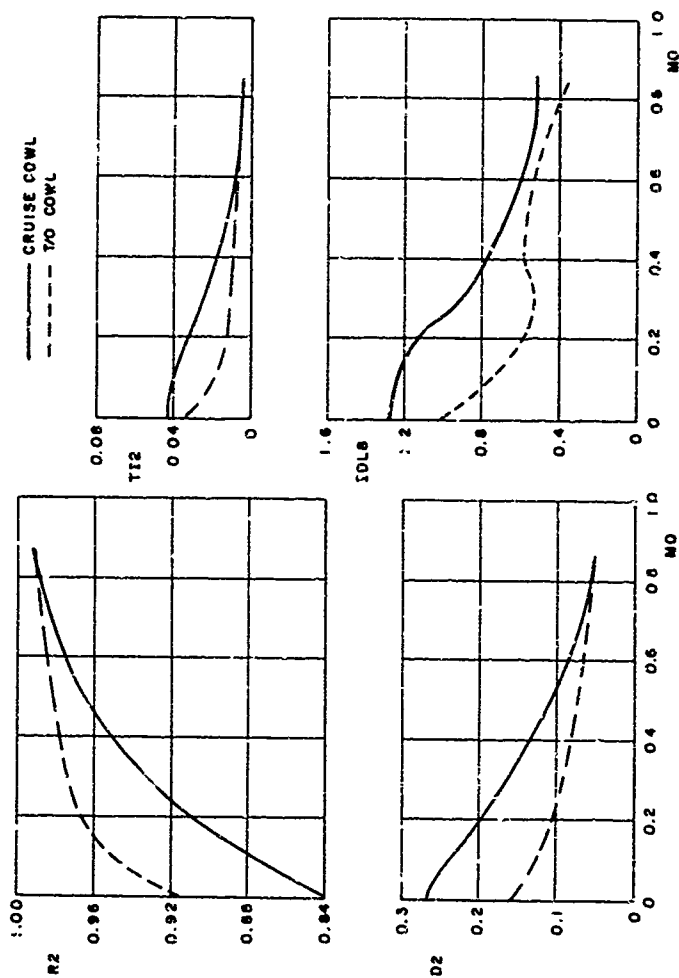




b. Concluded, inboard
Figure 36. Concluded.



a. Outboard
 Figure 37. Subsonic inlet performance characteristics as a function of Mach number.



b. Inboard

Figure 37. Concluded.

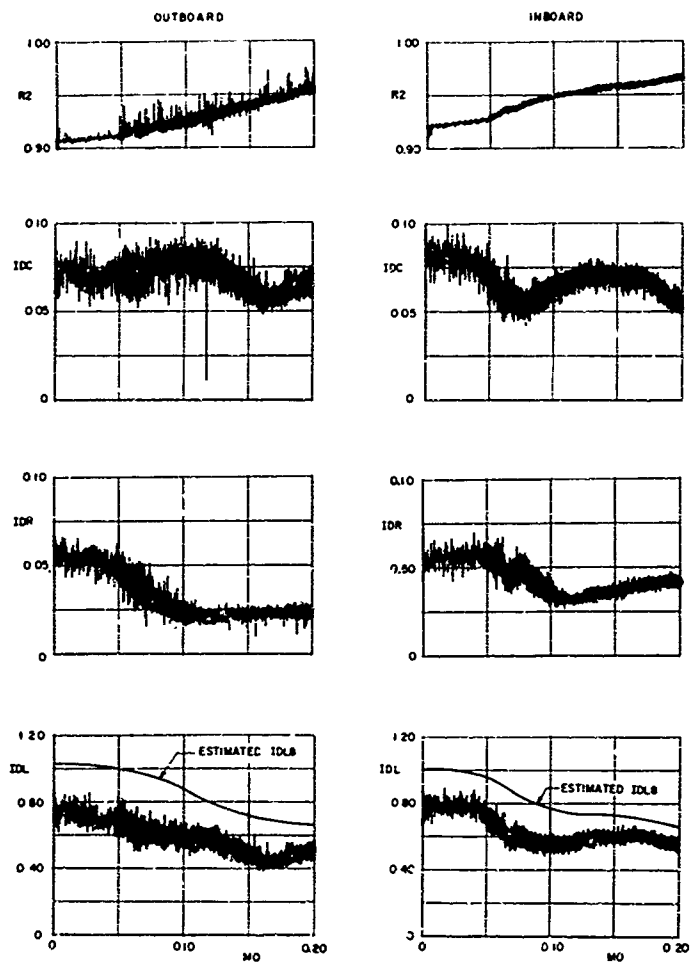
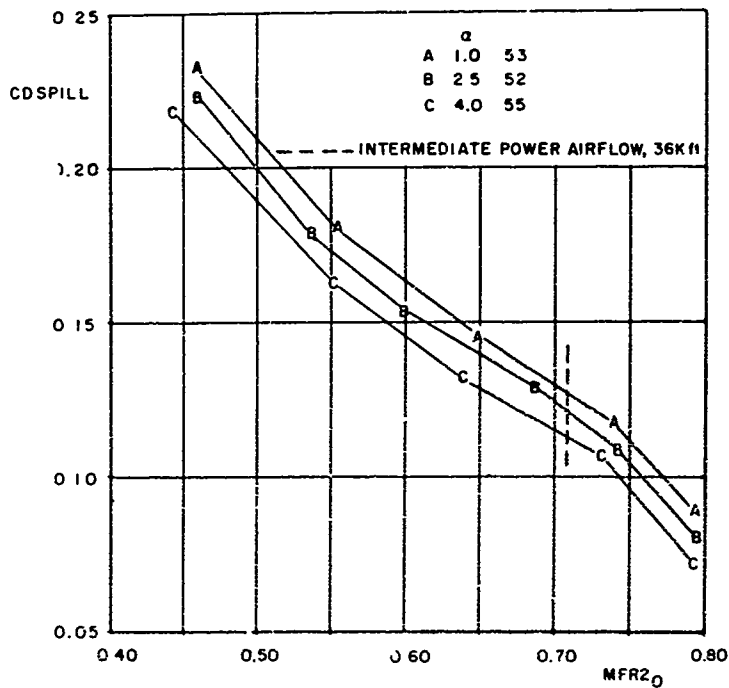
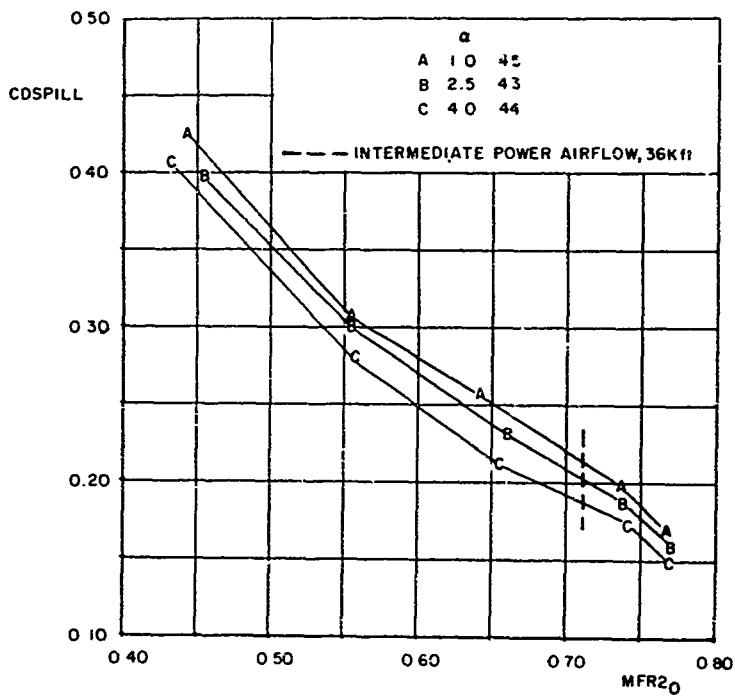


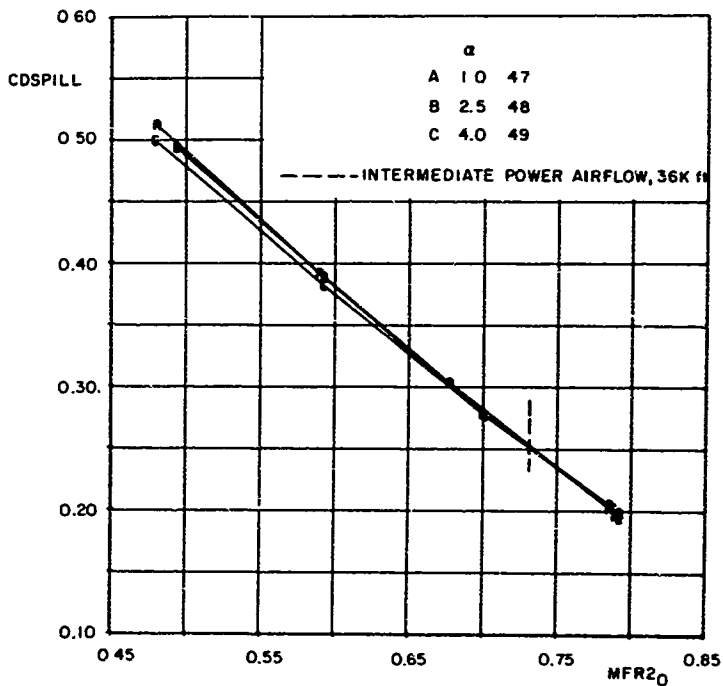
Figure 38. Simulated takeoff transient.



a. $MC = 0.85$
Figure Inlet spillage drag characteristics.



b. $M_0 = 1.20$
Figure 39. Continued.



c. $M_0 = 1.40$
Figure 39. Concluded.

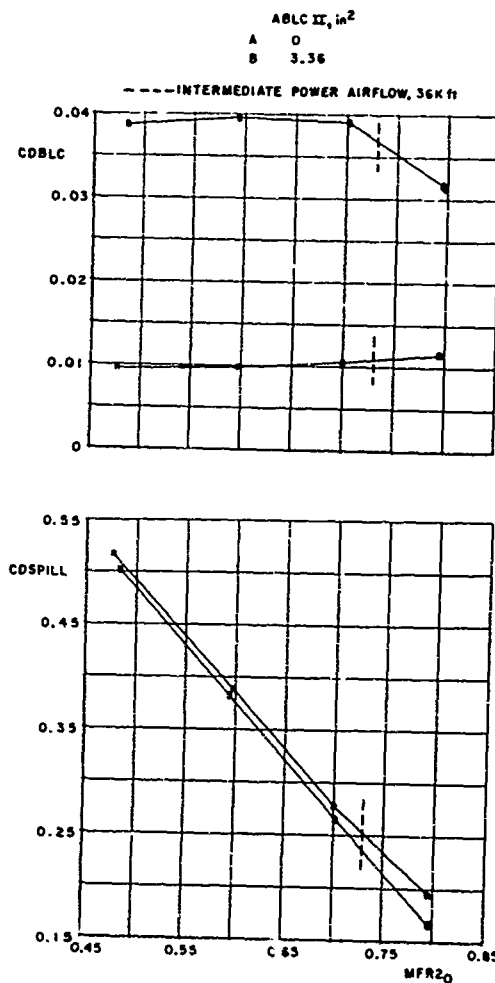


Figure 40. Effects of opened BLCII discharge doors on inlet drag characteristics at $M_0 = 1.40$, $\alpha = 2.5$ deg.

Table 1. Precision of Measurement

Test Conditions		Estimated Combined Error											
MO	Pto, psia	ΔMO	ΔPto, psf	ΔTto, °F	ΔHL, in	ΔRB, deg	Δα, deg	ΔU, deg					
2.20	1200	0.0157	5.31	5.0	0.015	0.13	0.04	0.60					
1.80	950	0.0131	5.18										
1.40	1300	0.0047	2.80										
0.85	1850	0.0044	3.35										
0.70	2300	0.0045	3.80										
0.30	2000	0.0061	3.50										
0.20	2000	0.0075	3.50										
0.00	2000	---	3.50										
MO	Pto, psia	ΔMFR	ΔW2R, lb/sec	ΔR2	ΔTDC8	ΔIDR8	ΔIDL8	ΔD2	ΔMA	ΔML	ΔNSP	ΔT12	
2.20	1200	0.008	1.15	0.0046	0.0121	0.0064	0.085	0.0014	0.0390	0.0396	0.0038	0.002	
1.80	950	0.007	1.38	0.0057	0.0153	0.0080	0.106	0.0018	0.0214	0.0214	0.0047		
1.40	1300	0.004	1.00	0.0025	0.0112	0.0058	0.077	0.0013	0.0080	0.0080	0.0041		
0.85	1850	0.004	0.83	0.0021	0.0078	0.0041	0.055	0.0009	0.0004	0.0004	0.0041		
0.70	2300	0.003	0.75	0.0020	0.0063	0.0034	0.045	0.0008	0.0002	0.0002	0.0042		
0.30	2000	0.008	0.80	0.0021	0.0073	0.0038	0.051	0.0009	---	---	0.0042		
0.20	2000	0.018	0.80	0.0021	0.0073	0.0038	0.051	0.0009	---	---	0.0042		
0.00	2000	---	0.80	0.0021	0.0073	0.0038	0.051	0.0009	---	---	0.0042		

APPENDIX A EQUATIONS FOR CALCULATING DISTORTION PARAMETERS: IDC, IDR, AND IDL

Circumferential Distortion on Individual Rings

$$IDC_i = (p_{t2ave_i} - p_{t2min_i}) / \bar{p}_{t2}$$

where

$$i = 1 \text{ to } 5 \text{ rings}$$

Hub Distortion

$$IDC_{12} = (IDC_1 + IDC_2) / 2$$

Tip Distortion

$$IDC_{45} = (IDC_4 + IDC_5) / 2$$

Total Circumferential Distortion

$$IDC = \text{Largest of } IDC_{12} \text{ or } IDC_{45}$$

Radial Distortion on Individual Rings

$$IDR_i = 1.0 - \frac{p_{t2ave_i}}{\bar{p}_{t2}}$$

Total Radial Distortion

$$IDR = \text{Largest of } IDR_1, IDR_2, IDR_4, \text{ or } IDR_5$$

Fan Stall Margin Ratio

$$IDL = b(KCIRC)IDC + (KRAD)IDR$$

where

$$b = \frac{IDR/IDC}{A+B (IDR/IDC)} + C$$

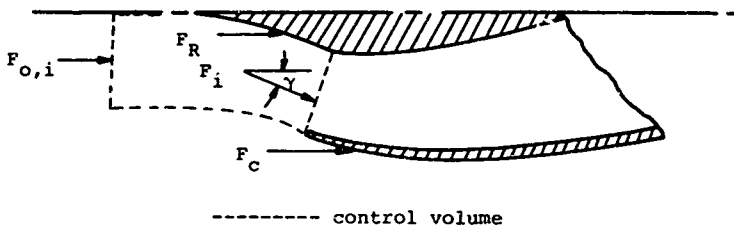
IDL CONSTANTS

(See Ref. 5)

H0	KCIRC	KRAD	Superposition Factor		
			A	B	C
2.2 2.1 2.0	7.69	11.75	-0.56	-0.92	1.0
1.8	7.69	13.33	-0.55	-0.71	1.0
1.4 1.2 0.85	7.69	12.83	-0.52	-0.644	1.0
0.7	7.69	12.92	-0.52	-0.644	1.0
0.55	7.69	12.28	-0.52	-0.644	1.0
0.3 0.2	7.69	11.76	-0.52	-0.643	1.0
0	7.93	12.41	-0.536	-0.951	1.0

APPENDIX B METHOD OF CALCULATION FOR INLET SPILLAGE AND BLEED DRAG TERMS

A. Spillage Drag



$$CD_{SPILL} = - \frac{F_{C,i}}{(QO)(AC)} + \frac{\cos \alpha}{(QO)(AC)} \left[F_R + F_i \cos \gamma + F_C \right]$$

where

F_C is the cowl axial force to nacelle station 26 as determined by pressure-area integration, lb

F_i is the inlet air momentum, lb

$F_{O,i}$ is the free-stream momentum of the air that enters the inlet, lb

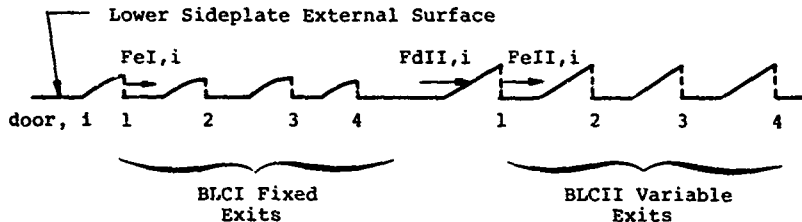
F_R is the ramp axial force as determined by pressure area integration, lbs

QO is the free-stream dynamic pressure, psi

γ is the angle of inclination of the average inlet airflow path from the model x-axis

$\left. \begin{matrix} AC \\ \alpha \end{matrix} \right\}$ see Nomenclature

B. Bleed Drag



$$CDBLCI = \frac{F_{o,I}}{(QO)(AC)} - \frac{\cos \alpha}{(QO)(AC)} \sum_{i=1}^4 F_{eI,i}$$

$$CDBLCII = \frac{F_{o,II}}{(QO)(AC)} - \frac{\cos \alpha}{(QO)(AC)} \left(\sum_{i=1}^4 F_{dII,i} + \sum_{i=1}^4 F_{eII,i} \right)$$

$$CDBLC = CDBLCI + CDBLCII$$

where

FdII is the BLCII exit door external axial force as determined by pressure-area integration, lb

FeI or II is the BLCI or II airflow exit momentum, lb

Fo, I or II is the free-stream momentum of the BLCI or II airflow, lb

CDBLCI or II is the BLCI or II drag coefficient

QO is the free-stream dynamic pressure, psi

AC
CDBLC } see Nomenclature
α }

NOMENCLATURE

ABLCI	Boundary-layer control bleed zone I exit area, in. ²
ABLCII	Boundary-layer control bleed zone II exit area, in. ²
AC	Inlet capture area, 58.54 in. ² (cruise cow!), 74.94 in. ² (takeoff cow!)
BLCI	Bleed zone I
BLCII	Bleed zone II
CDBLC	Bleed drag coefficient (see Appendix B)
CDSPIII	Spillage drag coefficient (see Appendix B)
D2	Compressor-face total-pressure distortion $(P_{t2_{max}} - P_{t2_{min}})/\bar{P}_{t2}$
FBL	Fuselage buttock line, in.
FS	Fuselage station, in.
FWL	Fuselage waterline, in.
HL	Inlet lip height, in.
IDC	Instantaneous circumferential total-pressure distortion factor
IDC8	Instantaneous circumferential total-pressure distortion factor at time of occurrence of IDL8
IDL	Instantaneous fan stall margin ratio (Appendix A)
IDL8	Peak value of instantaneous fan stall margin ratio
IDR	Instantaneous radial total-pressure distortion factor
IDR8	Instantaneous radial total-pressure distortion factor at time of occurrence of IDL8
M0	Free-stream Mach number
MA	Outboard inlet first ramp local Mach number

MFR2	Engine-face mass-flow ratio ratio of compressor-face station mass flow to inlet capture mass flow
ML	Inlet local Mach number exterior to inlet on surface of lower sideplates, used as control sensor for inboard inlet
NBL	Nacelle buttock line, in
NS	Nacelle station, in
NSP	Normal shock position parameter, inlet throat static to total-pressure ratio (see Section 3.1)
NWL	Nacelle waterline, in
p	Static pressure, psfa
P _{B1}	Bleed zone I plenum pressure, psfa
P _{B11}	Bleed zone II plenum pressure, psfa
\bar{P}_{rms}	Area-weighted average engine-face root-mean-square value of total pressure, psfa
P ₀	Free-stream total pressure, psfa
P ₁₂	Engine-face total pressure, psfa
\bar{P}_{12}	Area-weighted average engine-face total pressure, psfa
R2	Compressor-face total-pressure recovery average (area-weighted) compressor-face total pressure ratioed to free-stream total pressure, \bar{P}_{12}/P_0
RA	Inlet first ramp angle (7-deg fixed ramp), deg
RB	Inlet second ramp angle (first movable ramp), deg
RC	Inlet third ramp angle (second movable ramp), deg
RE	Free-stream unit Reynolds number, Re, ft ⁻¹ x 10 ⁶
T ₁₀	Free-stream total temperature, °R

T_{12}	Average compressor-face total temperature, °R
$TI2$	Turbulence index: average root-mean-square value of total-pressure oscillations at the compressor face normalized by the average compressor-face total pressure, p_{rms}/\bar{p}_{12}
U	Bypass door angle, referenced to nacelle surface, deg
W_a	Engine fan airflow, lb/sec
$W2R$	Engine fan airflow corrected to standard sea-level conditions for full-scale vehicle, $W_a\sqrt{\theta T2/\delta T2}$, lb/sec
α	Angle of attack, deg
$\delta T2$	$\bar{p}_{12}/2116$
$\theta T2$	$T_{12}/519$
ψ , or yaw	Model angle of yaw (angle between the plane of symmetry and the relative wind), nose right is positive, deg

SUBSCRIPTS

I	Inboard inlet
O	Outboard inlet
FS	Full scale
0.2-SC	0.2 scale